RECONNAISSANCE CENOZOIC VOLCANIC GEOLOGY OF THE LITTLE GOOSE CREEK AREA, NORHEASTERN ELKO COUNTY, NV WITH AN EMPHASIS ON THE JARBIDGE RHYOLITE

by

ANDREW INGALLS

B.S Environmental Science, Northeastern University, 2012

A THESIS

submitted in partial fulfillment of the requirements for the degree

MASTER OF SCIENCE

Department of Geology
College of Arts and Sciences

KANSAS STATE UNIVERSITY
Manhattan, Kansas

2014

Approved by:

Major Professor
Dr. Matthew Brueseke

Abstract

The Little Goose Creek area is located in Elko County, Nevada just south of the central Snake River Plain and in the northeastern Great Basin. During the Miocene, northeastern Nevada was characterized by volcanism as well as prevalent extension and basin development, including widespread occurrences of porphyritic quartz-phyric silicic lavas and domes (e.g., the Jarbidge Rhyolite), ash-flow tuffs, and basaltic volcanism. Recent workers (e.g., Colgan and Henry, 2010) have provided new constraints on the timing of extension in the northern Great Basin (U.S.A.) and indicate that much of it occurred in the mid-Miocene. Other recent work has provided new temporal and petrologic constraints on 16.1 to 15.0 Ma Jarbidge Rhyolite volcanism in the northern Great Basin west of our study area, and suggest that it is intimately linked (spatially and temporally) with the aforementioned extension. This study aims to: [1] understand the spatiotemporal link between the volcanism in the northeastern Nevada study area and potentially correlative volcanism regionally (e.g., Jarbidge Rhyolite and explosive deposits associated with the <13 Ma Bruneau-Jarbidge or Twin Falls eruptive centers); [2] determine if the sampled Jarbidge Rhyolite lavas are chemically similar to those in and around Jarbidge, Nevada. In the Goose Creek area, we report a new laser $^{40}Ar/^{39}Ar$ age for sanidine of 13.6 ± 0.03 Ma for a crystal-poor rhyolite lava (Rock Springs Rhyolite) and a Jarbidge Rhyolite lava (13.827±0.021 Ma) as well as an age on Jarbidge Rhyolite in Wells, NV (15.249±0.040 Ma) and West Wendover, NV (13.686±0.034 Ma). These lava samples, as well as sampled ash-flow tuffs from the Goose Creek region, plot within the A-type field on discrimination diagrams. The ash-flow tuffs are younger than the Rock Springs Rhyolite based on stratigraphic relationships and are sourced from both the Twin Falls eruptive center as well as the Bruneau Jarbidge eruptive center of the central Snake River Plain based on geochemical analysis. Also, a sequence of basaltic lavas crop out in the Goose Creek drainage; these basalts have ~43 wt.% silica and are chemically similar to <8 Ma olivine tholeiite basalts that crop out to the north, along the southwestern side of the Cassia Mountains, Idaho. These results, field relationships, and prior geological mapping suggest that the lavas and ash-flow tuffs erupted into active extensional basins.

Table of Contents

List of Figures

Brueseke et al. (2014) has extended further to the east via my own samples. The abbreviations are eruptive centers related to the Yellowstone hotspot (JM: Juniper Mountain, BJ: Bruneau-Jarbidge, TF: Twin Falls, P: Picabo, H: Heise, Y, Yellowstone). 120

List of Tables

Acknowledgements

Thank you to Dr. Matthew Brueseke for his unwavering patience as well as his numerous discussions about my thesis, general volcanology, igneous petrology, and funding. Also, for his encouragement to apply for the National Science Foundation fellowship and countless grants and conferences. Thanks to Dr. Jack Oviatt and Dr. Saugata Datta for being committee members and their encouragement and advice throughout the years, Dr. Willis Hames at Auburn University, Alabama for his role with geochronology, Dr. Stanley A. Mertzman at Franklin and Marshall College for his work with bulk and trace geochemistry of our data, a fellowship from the KSU GK-12 program during my 2013-2014 academic year, Robin Barker and Chad Hobson for their geologic discussions and help with my education, my girlfriend, Katy, for the countless pots of tea and backrubs, Kieran and Spencer for actually trying to read this thesis, my friends: Corey, Andy, and Ryan for making me take breaks to watch the bruins games, and last, but not least, my family, although they may not understand exactly what I study, they nonetheless supported me until the end.

Dedication

I would like to dedicate this thesis to rhyolites, without them, my work would not be possible. Don’t take them for granite.

Chapter 1 - Introduction

1.1 Purpose of Study

Elko County is located in northeastern Nevada, just south of the central Snake River Plain in the northeastern Great Basin (Figure 1.1). During the Miocene, northeastern Nevada was characterized by voluminous volcanism as well as prevalent extension and basin development, including widespread occurrences of porphyritic silicic lavas and domes (e.g., the Jarbidge Rhyolite), ash-flow tuffs, and basaltic volcanism (Figure 1.2). Recent workers (e.g., Colgan et al., 2008; Colgan and Henry, 2009; Henry et al., 2011) have provided new constraints on the timing of widespread extension in the northern Great Basin (U.S.A.) and indicate that much of it occurred in the mid-Miocene. Other recent work by Callicoat (2010) and Brueseke et al. (2014) have provided new temporal (16.1 to 15.0 Ma) and petrologic constraints on rhyolite magmatism in the northern Great Basin (e.g., the Jarbidge Rhyolite) that is coeval and likely intimately linked (spatially and temporally) with the aforementioned extension (Figure 1.3). The purpose of this study was to investigate Cenozoic geology in northeastern Nevada with a focus on the Jarbidge Rhyolite within the Little Goose Creek Drainage area (Figure 1.4) to: [1] understand the spatiotemporal link between the volcanism in the NE NV study area and potentially correlative volcanism regionally (e.g., the Jarbidge Rhyolite and 13-5.5 Ma explosive deposits associated with the Bruneau-Jarbidge or Twin Falls eruptive centers); [2] determine whether the sampled Jarbidge Rhyolite lavas are chemically similar to those in and around Jarbidge, NV documented by Brueseke et al. (2014).

Using physical, bulk chemical, and temporal data from the northeastern bodies mapped by Coats (1987) as Jarbidge Rhyolite, I am able to establish constraints on what appears to be the oldest mid-Miocene volcanic event in the study area. Using the stratigraphic relationship of this volcanic event, the potential onset of "modern" Basin and Range extension in the study area is able to be determined (Colgan et al., 2008; Henry et al., 2011; Brueseke et al 2014). By constraining the tertiary ash-flow tuffs from my study to either the Bruneau-Jarbidge or Twin Falls eruptive center via physical and bulk chemical constraints, correlative techniques can be used to further confine the potential onset of "modern" Basin and Range extension in the study area. These constraints will help to address the relationship between the Jarbidge Rhyolite volcanism and the regional contemporaneous tectonomagmatic processes.

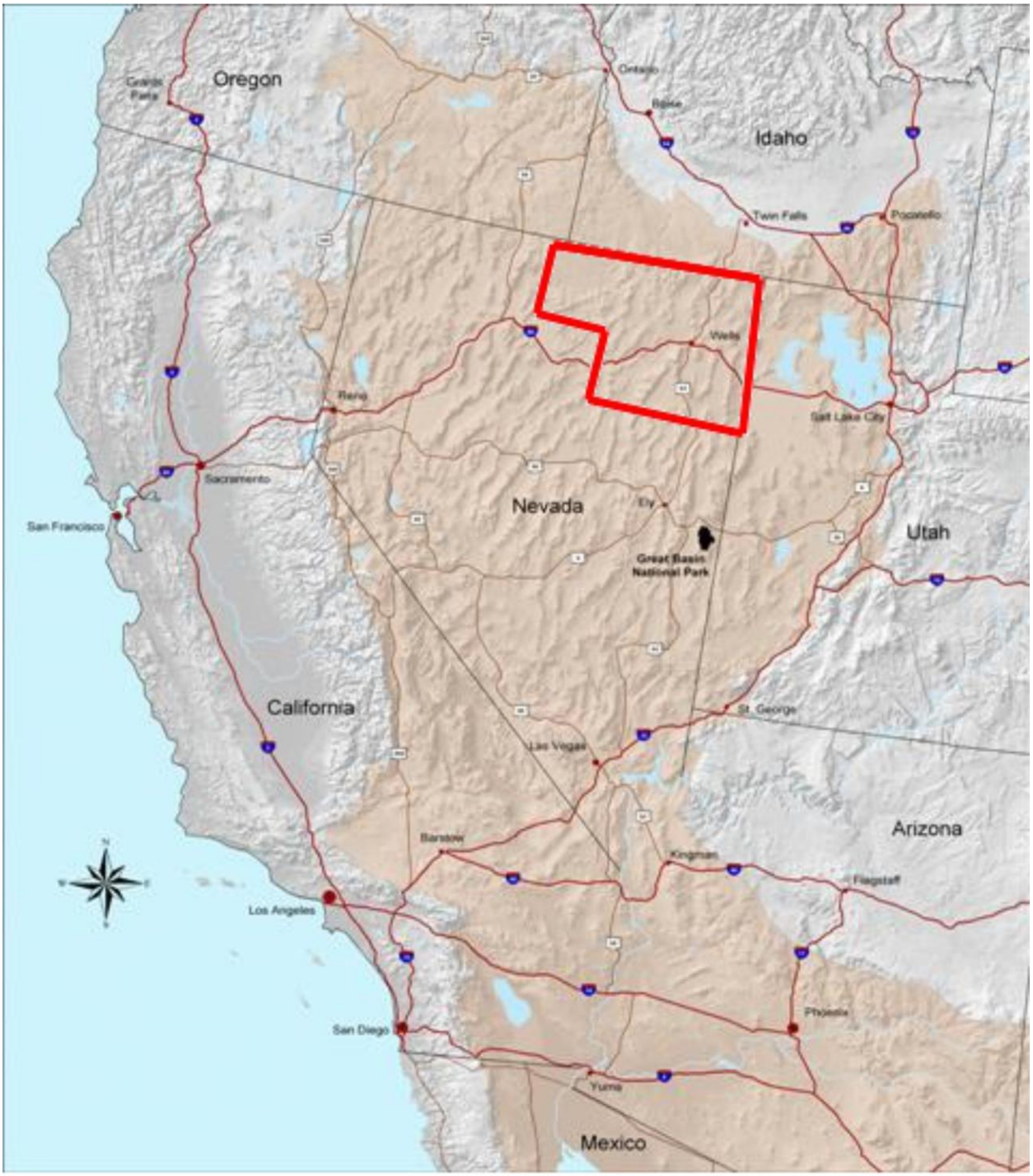

Figure 1.1: Map of the extent of the Great Basin (shown in tan). The red outline depicts Elko County in northeastern Nevada in Figure 1.4. ***Figure adapted from United States. National Park Service.***

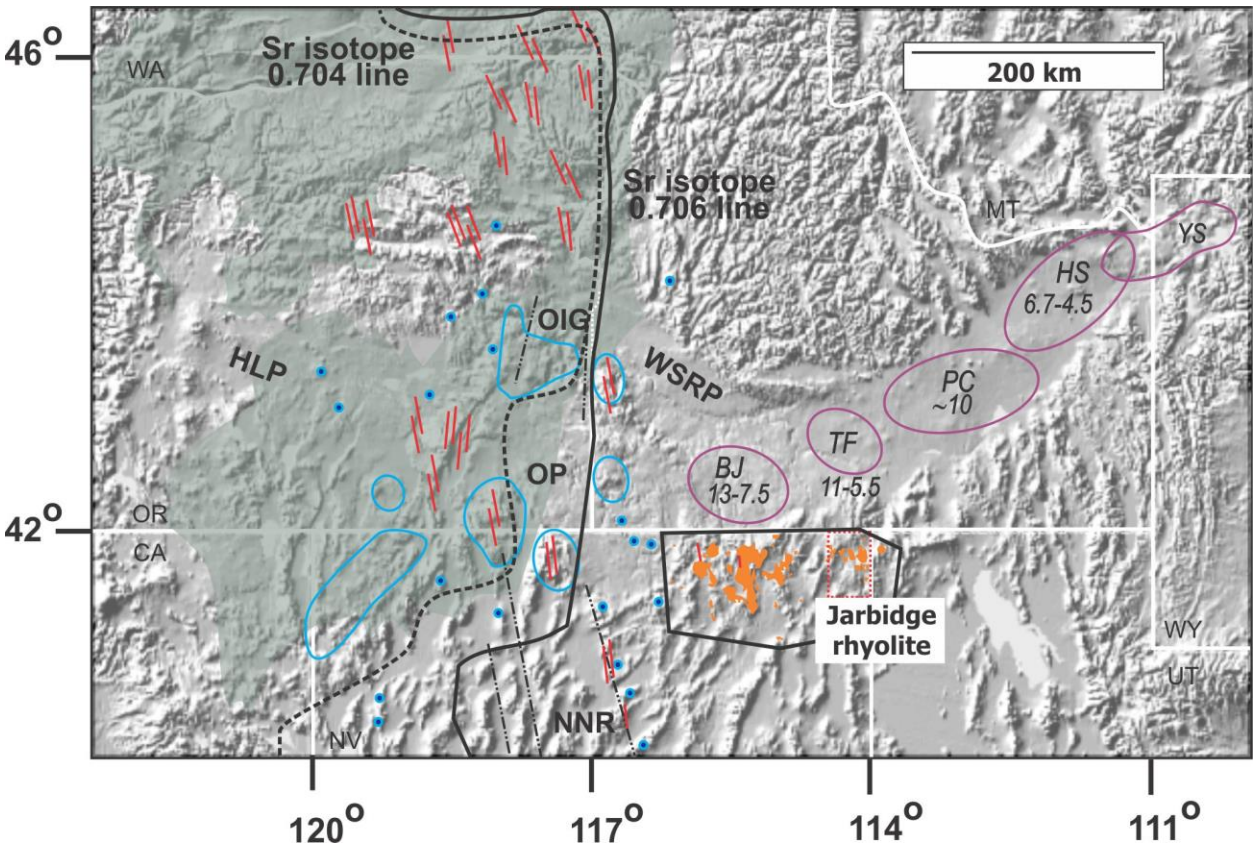

Figure 1.2: ***Adapted from Brueseke et al. (2014).*** **Blue ovals and circles are mid-Miocene felsic eruptive centers and volcanic fields. The purple ovals are the felsic volcanic fields of the Snake River Plain. (BJ, Bruneau-Jarbidge; TF, Twin Falls; PC, Picabo; HS, Heise; YS, Yellowstone). The numbers associated with the purple circles are their ages in millions of years. The orange bodies are mapped Jarbidge Rhyolite (Coats, 1987). The red lines represent mid-Miocene flood basalt eruptive loci and the shaded green region represents flood basalt extent. The black lines (solid and dashed) trending north-south represent the $^{87}Sr/^{86}Sr$ isopleths, 0.706 and 0.704, which denote the western edge of the Pre-Cambrian North American craton and the Mesozoic accreted terrains to the west respectively. These are shown through the $^{87}Sr/^{86}Sr$, 0.706 and 0.704, isopleths. Abbreviations are: northern Nevada Rift (NNR), Owyhee Plateau (OP), Oregon-Idaho Graben (OIG), western Snake River Plain (WSRP), High Lava Plains (HLP).**

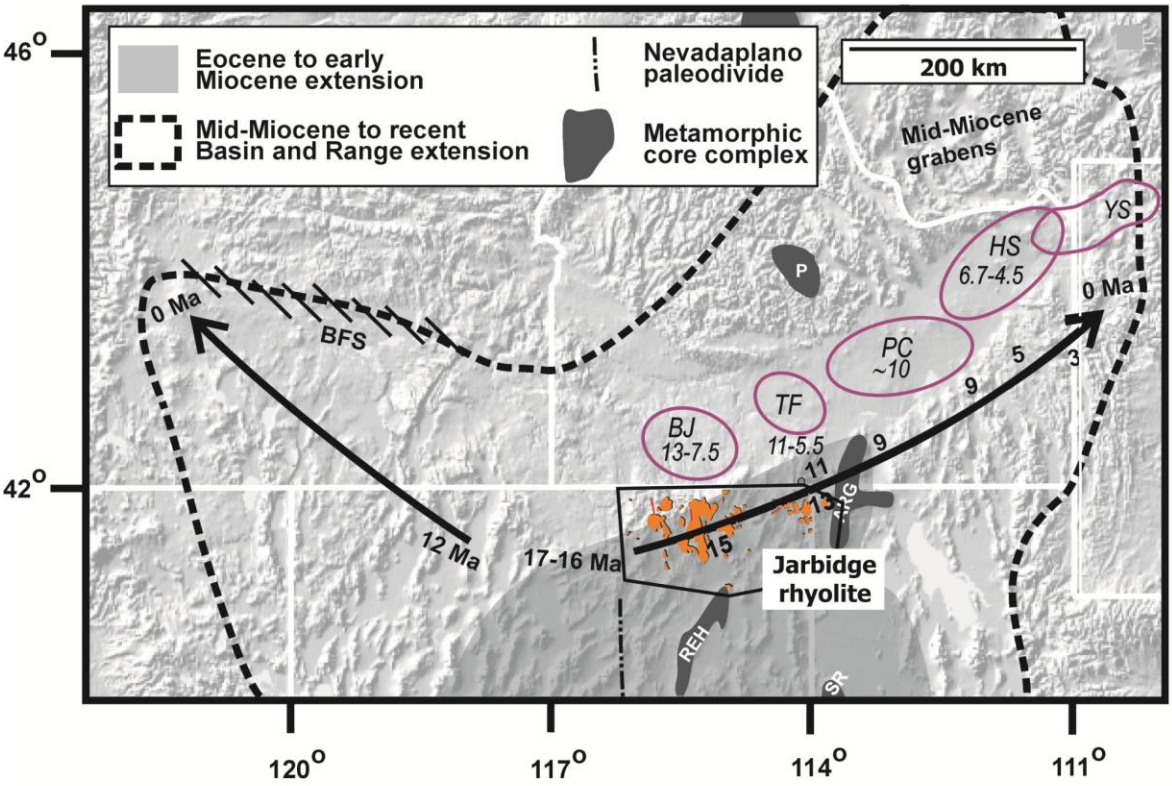

Figure 1.3: ***Adapted from Brueseke et al. (2014).*** **Map depicting important extensional and temporal features of the northern Great Basin. The ages trending to the northeast are compiled from Rodgers et al. (1990) and Perkins et al. (1995), for extensional basin formation along the southern margin of the Snake River Plain. The ages and arrow represent the northwestern-trending extension compiled from Colgan et al. (2006) and Scarberry et al. (2009). Mapped Jarbidge Rhyolite depicted in orange and the purple ovals show felsic volcanic systems of the Snake River Plain, as in Figure 1.2 (BJ, Bruneau-Jarbidge; TF, Twin Falls; PC, Picabo; HS, Heise; YS, Yellowstone). Abbreviations are: northern Nevada Rift (NNR), Owyhee Plateau (OP), Oregon-Idaho Graben (OIG), western Snake River Plain (WSRP), High Lava Plains (HLP); P, Pioneer Mountains; ARG, Albion-Raft River-Grouse Creek; REH, Ruby-East Humboldt; SR, Snake Range; BFS, Brothers fault zone.**

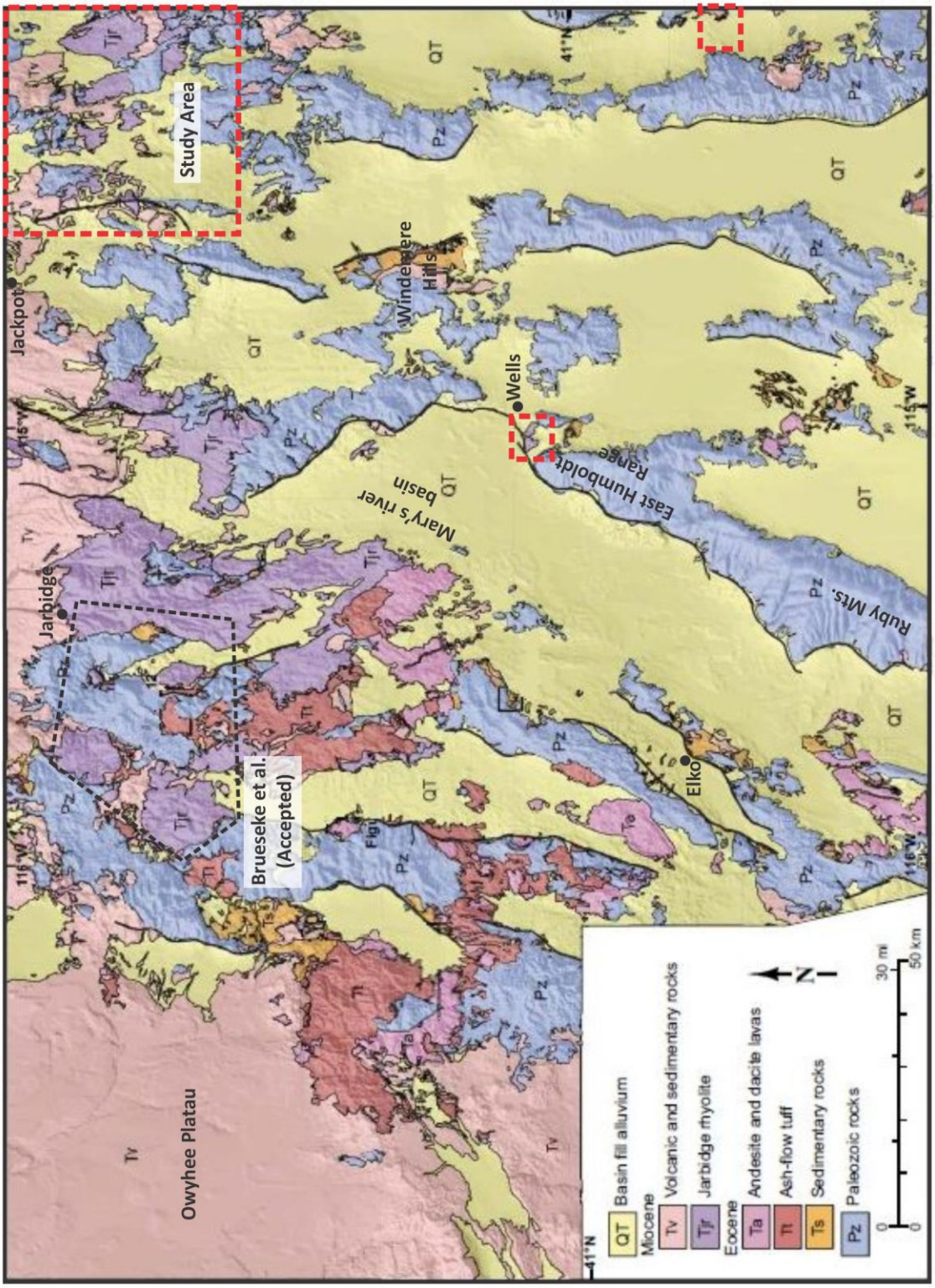

Figure 1.4: Modified geologic map of Elko County, NV (Henry, 2008; simplified from Coats, 1987). The black dashed outline represents previous work done by Brueseke et al. (2014). The red dashed lines represent approximate study areas of this thesis.

1.2 Regional Geology

The geology of the northern Great Basin is complex and lithologies consist of a series of Paleozoic sedimentary rocks (mostly quartzite, chert, limestone, and siltstone), Triassic marine sandstone and shale, Jurassic diorite, and Tertiary volcanic rocks ranging in composition from rhyolite to basalt (Burchfiel et al., 1992; Coats, 1977; Crafford, 2008; Henry, 2008). There are Quaternary sedimentary strata deposits filling the basins, including alluvial, colluvium, and landslide deposits related to the extensional basin-fill of the Cenozoic (Coats 1977). This long history and complex rock types are due to the interaction between the continent-ocean lithospheric boundaries to the west along the margin of continental North America (Burchfiel et al., 1992). This interplay between continent-ocean lithospheric interaction caused major tectonic activity during the Paleozoic, and continuous activity during both the Mesozoic and Cenozoic (Burchfiel et al., 1992). This tectonic activity includes both compressional (Antler, Sevier, and Laramide orogenies) and extensional (Proterozoic rifting and "modern" Basin and Range extension) events that contribute to the complex geological formations of the Great Basin.

1.2.1 Paleozoic

Prior to the Paleozoic Era there was a series of extensional events that resulted from late Proterozoic widespread rifting and mafic volcanic activity, which led to continental separation and ocean-floor spreading approximately 600 Ma (Burchfiel et al., 1992). This caused the formation of a shallow sea and the deposition of continental shelf sedimentary strata (limestones and shales) in the region that is now Elko county, Nevada, known as the Windermere Sequence. The lower Paleozoic shelf domain (Crafford, 2008), comprised of Cambrian through Devonian carbonate shelf facies rocks, underlies the central-southern portion of Elko county. In northern Elko county, the slope facies domain occurs as outcrops, where Ordovician to lower Mississippian shale, calcareous shale, siltstone, chert, quartzite, greenstone, platy limestone, dolomite, graywacke, conglomerate, and limestone are present (Crafford, 2008; Burchfiel et al., 1992). Mafic volcanism occurred coevally with the Antler strata formation to the west of the study area. As indicated by Burchfiel et al. (1992), these lavas are predominantly of alkalic origin. This volcanic depositional period lasted until the late Devonian when the Antler volcanic arc was thrusted 200-km onto miogeoclinal rocks of the North American slope and shelf (Figure 1.5) (Burchfiel, 1992; Henry, 2008). Although not a contributor to the later Cordilleran Rocky

Mountain building tectonics involving the subduction of the Farallon plate (Laramide and Sevier orogenies), it builds the Cordilleran crust, through the subduction of the Laurentia plate and accretion of the antler formation wedge, that is involved later in Cordilleran mountain building. As the orogeny continued, a thick, clastic wedge was deposited in front of the thrust belt (Henry, 2008). This orogeny lasted until the early Mississippian, where the Carlin Unconformity was formed at the collision zone (NE Nevada), deforming the sediments deposited during the Paleozoic extension.

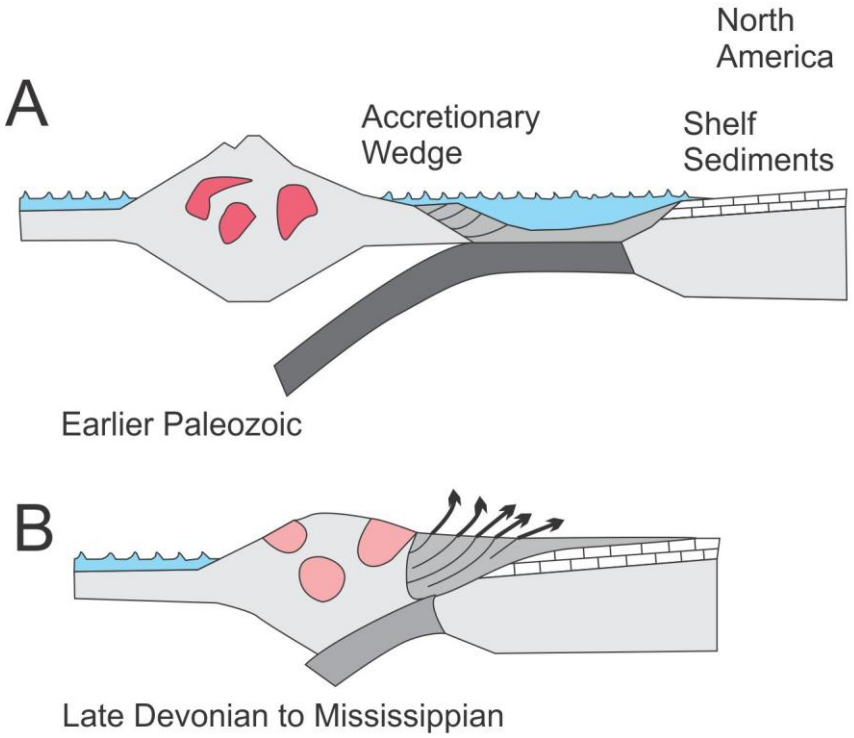

Figure 1.5: Depictions of the formation of the Antler Orogeny. (A) is pre-orogeny. The Antler arc is experiencing volcanic activity (red amorphous shapes). (B) is post orogeny during the late Devonian-Mississippian. This shows the formation of the Robert Mountain thrust and associated other compressional structures above the shelf sediments (Dorsey, 2007).

1.2.2 Mesozoic

During the Mesozoic, crustal shortening events initiated in eastern Nevada in the late Jurassic and continued until the Eocene (Henry, 2008). These periods of compression were known as the Sevier and Laramide orogenies. In northern Elko county, Jurassic and Cretaceous plutons associated with these orogenies are widespread. These plutons are found throughout the Ruby Mountain-East Humboldt Range and according to isotopic data are considered to contain a significant mantle component (Wright et al., 1993). Their compositions range from diorite to granodiorite, with the Jurassic plutons being generally smaller and more mafic in composition (Coats, 1977).

The Sevier orogeny (140-80 Ma) was the beginning of the Cordilleran mountain building event. As the subduction of the Farallon plate initiated under the North American plate, the fold-thrust belt "plowed" its way to the eastern edge of Nevada/western Utah (Humphreys et al., 2003). The beginning of major deformation along the Sevier fold-thrust belt initiated due to reduced lithospheric strength, which was caused by several factors: an increase in Farallon-North American plate-convergence rate, enhanced vigor of arc magmatism, and an increase in subduction-induced conductive heating of hinterland crust (Livaccari, 1991). Between 90 and 70 Ma, the peak of metamorphism occurred for the Sevier fold-thrust belt. The Sevier orogeny is known as a "thin-skinned" thrusting event, where associated forelands are composed of weaker sedimentary bedding from the Paleozoic and early Mesozoic; this thrusting does not involve the Precambrian basement in the deformation process. As the angle of the subducting slab and compression stresses began to steepen, a transition was made in the Late Cretaceous, approximately 70 Ma, to the Laramide orogeny (Robinson Robert et al., 1995). The Laramide orogeny is referred to as a "thick skinned" orogeny due to the deformation of the Precambrian basement rock as well as the overlying Paleozoic and Mesozoic strata (Figure 1.6).

These orogenies resulted in a 3-km topographic high across the present day Great Basin known as the Nevadaplano (Henry, 2011; Figure 1.7). By the end of the Cretaceous, the compression events had notably thickened the crust to approximately 45-70 km (Figure 1.8) between the Cenozoic Cascades volcanic arc (located in western North America that extends from southwestern British Columbia through Northern California) and the Sevier thrust belt in western Utah (Brueseke et al, 2014) (Figure 1.7). Colgan and Henry (2009), Henry (2008), and Henry et al. (2011) assert that during this time of compression, central-eastern Nevada was

characterized by low-relief terrain crosscut by paleovalleys <1.5-km-deep that were initiated through the compressional uplift.

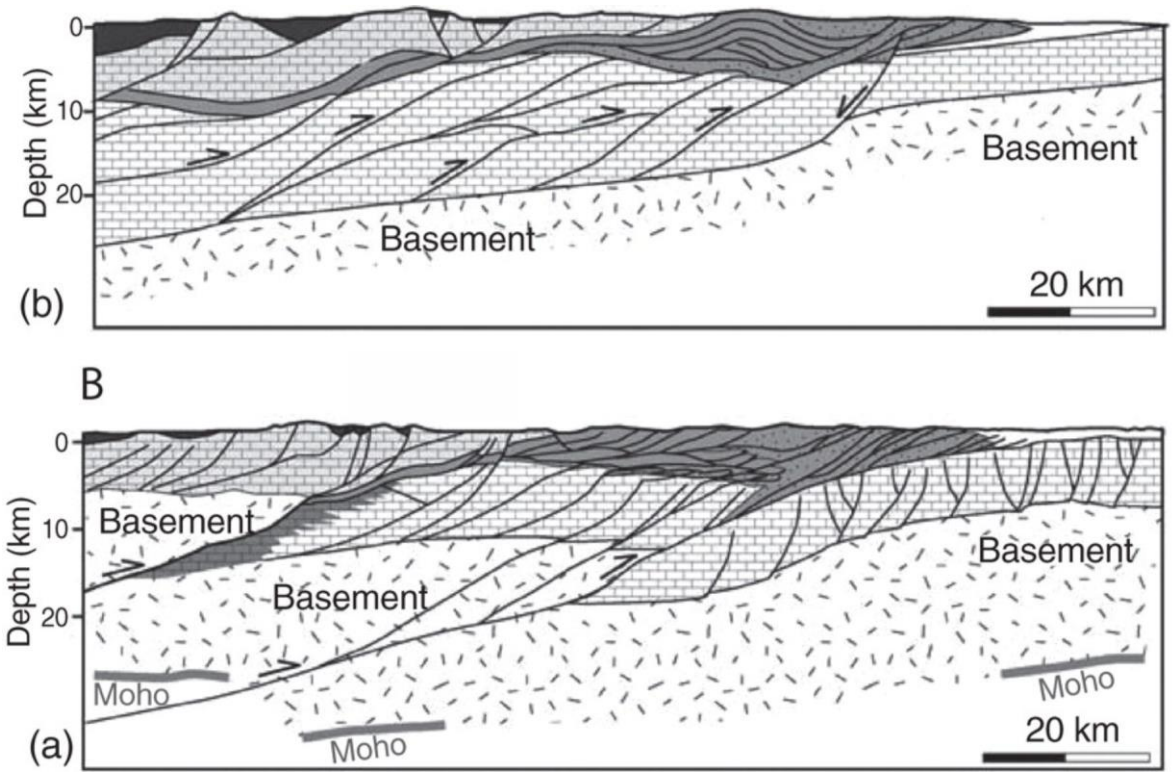

Figure 1.6: ***Adapted from Steckler et al. (2008*****). A representation of the difference between "thick and thin-skinned" thrusting in the North American Cordillera. (A) refers to "thin-skinned", where only the relatively horizontal Paleozoic sedimentary strata were involved during the Sevier orogeny. (B) refers to "thick-skinned" thrusting, when the angle of the fault steepens and the crystalline basement rock becomes deformed; this type of faulting occurred during the Laramide orogeny.**

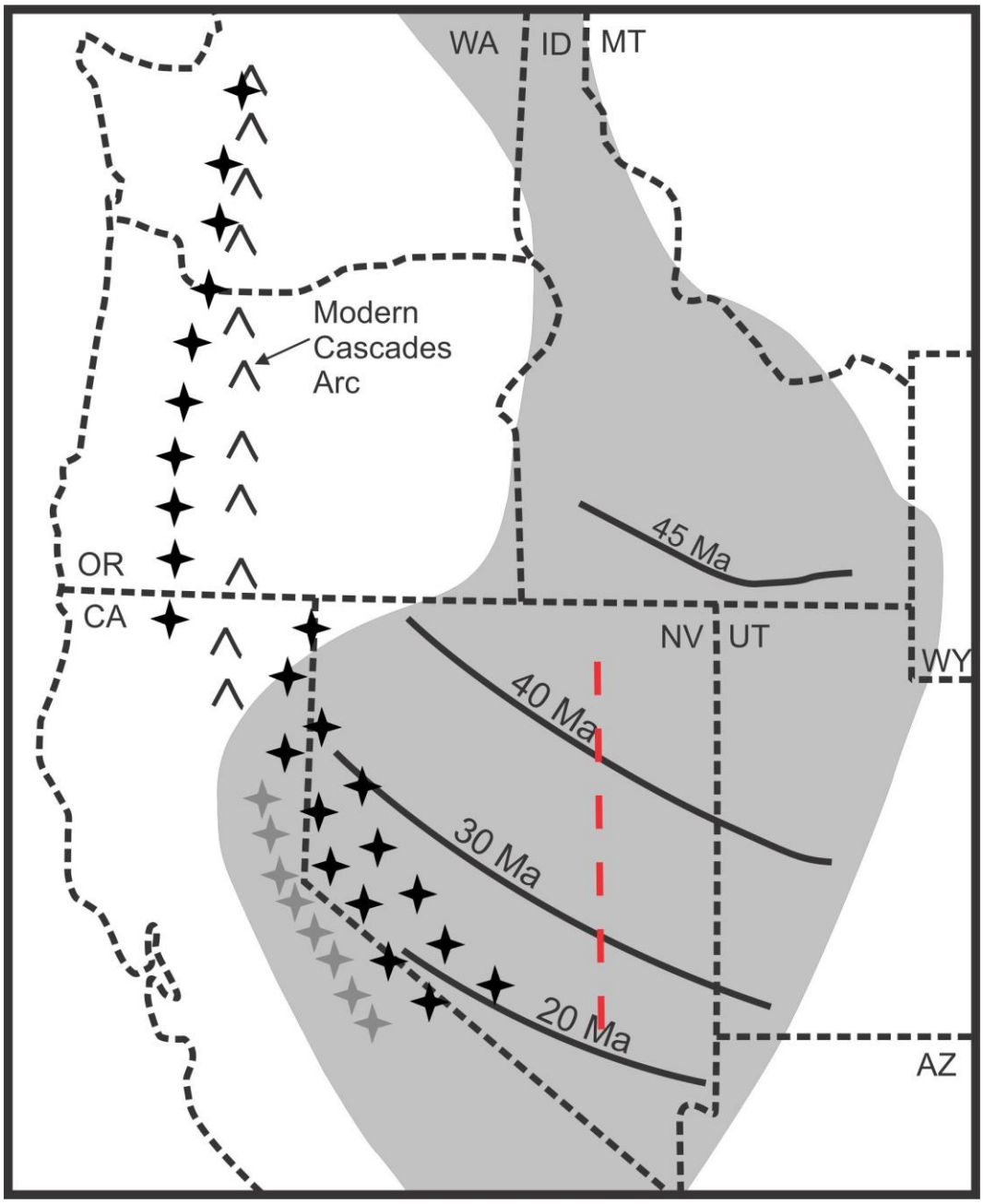

Figure 1.7: ***Adapted from Brueseke et al. (2014)*****. Depiction of the western USA illustrating the location of the Nevadaplano and Cenozoic volcanic arcs. Black solid lines labeled from 45-20 Ma refer to the southward sweep of subduction related to volcanism (e.g., "ignimbrite flare-up") due to slab rollback and steepening. Red dash is the paleodivide of the Nevadaplano. Eastern approximation of Nevadaplano (grey shaded region) corresponds to the eastern edge of the Sevier fold and thrust belt (Colgan and Henry, 2009; Brueseke et al., 2014; Busby, 2013; Dickinson, 2013).**

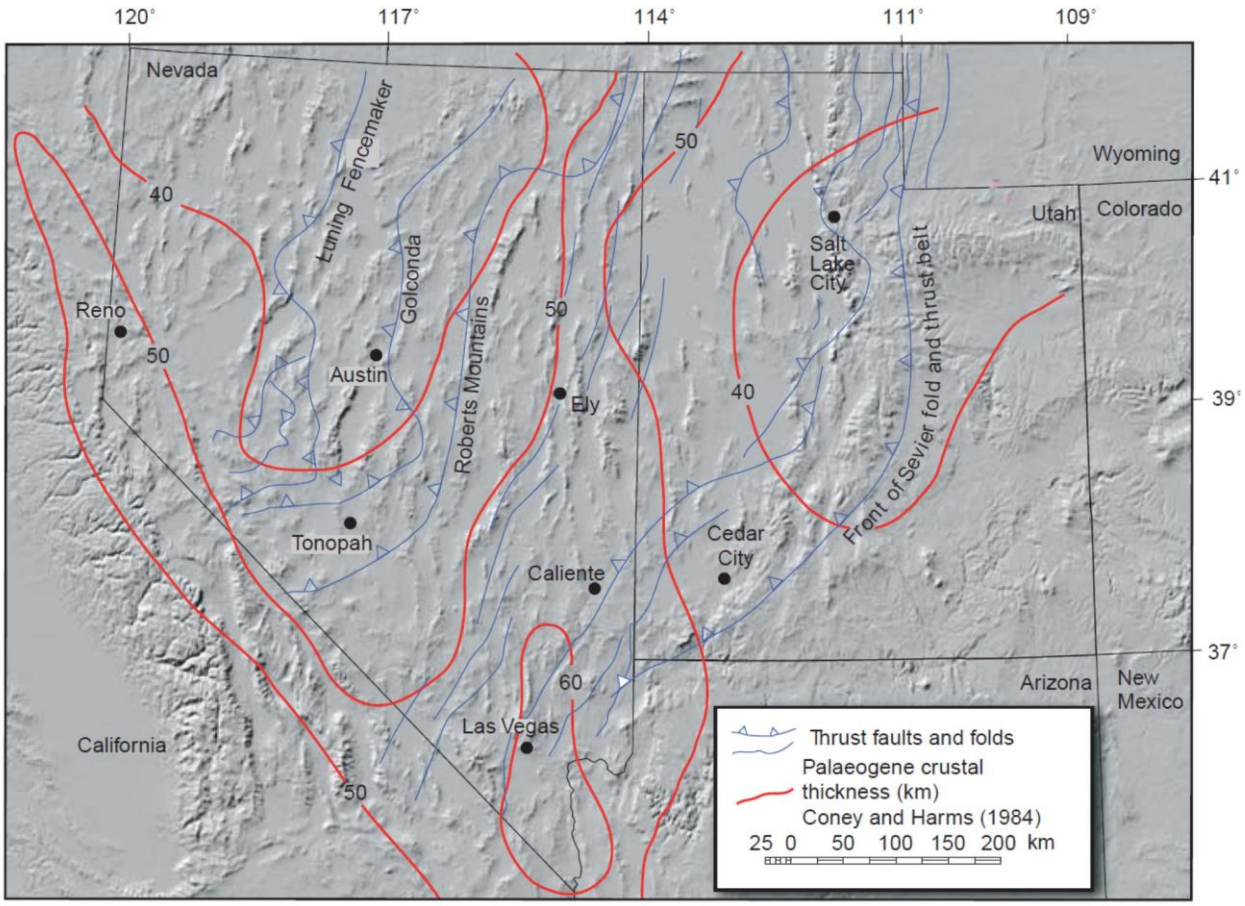

Figure 1.8: The hypothetical contours (in km) of the Nevadaplano crustal thickness as well as major thrust faults and fold belts in the Great Basin of Nevada and Utah (Best et al., 2009).

1.2.3 Cenozoic

1.2.3.1 Mesozoic to Oligocene

After the formation of the Nevadaplano, there was an increase in widespread volcanism that occurred immediately after the Laramide orogeny at about 45 Ma. During this time, the "roll back" of the previously subducted "shallow-dipping" slab brought hotter asthenosphere into contact with lithosphere, initiating voluminous magma generation in the overlying thickened crust (Best et al., 2009) (Figure 1.9). The flare-up of magmatism over 45-20 Ma (Henry, 2008), produced over 500,000 km^3 of intermediate to felsic ash flow tuffs, and may have produced up to 5,000,000 km^3 of intermediate to silicic volcanism associated with this explosive volcanism (Johnson, 1991). This large-scale event was known as the "ignimbrite flare-up" and the end

result was the production of numerous calderas that erupted tuffs which flowed down the central-east trending paleovalleys across Nevada (Figure 1.10). Henry (2008) documented that these valleys were as much as 1.5 km deep and 10-km wide. This increase in volcanism during the Eocene is not associated with major extension of the region. However, Eocene-Oligocene extension did occur across the northern Great Basin in relatively restricted locations (Henry et al., 2011). This period of magmatism was short-lived, and by 35 Ma, the majority of the early Cenozoic magmatism in northeastern Nevada had ceased with the exception of the Ruby Mountain core complex sills at 29 Ma (Henry, 2008).

1.2.3.2 Mid-Miocene

Compositionally bimodal basalt-rhyolite volcanism in the mid-Miocene occurred contemporaneously with the inception of "modern" Basin and Range extension, at approximately 17-15 Ma, as well as the collapse of the Nevadaplano (Colgan and Henry, 2009). Although the cause of the collapse is debated, more recent studies (Henry, 2008; Colgan and Henry, 2009) have suggested that the northern Great Basin underwent minor extension until the mid-Miocene (~17 Ma to 15 Ma). Coney (1987) suggests that this collapse was caused by gravitational collapse due to the Nevadaplano being over 3 km in height. However, more recent work (Best and Christiansen, 1991; Snoke et al., 1997; Colgan et al., 2008; Henry, 2008; Colgan and Henry, 2009) indicates that gravitational collapse would be insufficient to drive major Basin and Range extension, unless extension was restricted to the lower and middle crust. It is more likely that the model provided by Humphreys et al. (1995), which involves upwelling of asthenosphere, was the driving factor in the lithospheric weakening. The northeastward trend of this major extension started across northeastern Nevada *ca.* 14 to 10 Ma (Perkins et al., 1995) to its current region of termination in northwestern Wyoming (e.g., Jackson Hole area) (Figure 1.3) (Colgan et al., 2004; Brueseke et al., 2014). The bimodal basalt-rhyolite volcanism produced in the mid-Miocene, which occurred roughly coevally with the onset of this major extension, produced both voluminous flood basalt and widespread silicic magmatism. The origin of this voluminous magmatism (e.g., Columbia River Basalt Group and Oregon Plateau/northern Great Basin silicic volcanism, potentially including the Jarbidge Rhyolite), is still debated.

The controversy centers on whether the catalyst for the inception of the magmatism is related to a mantle plume (e.g., a lower mantle-sourced Yellowstone hotspot; Pierce and Morgan, 1992; Camp and Ross, 2004; Coble and Mahood, 2012), or to tectonic processes in the upper

mantle (Carlson and Hart, 1987; Dickinson, 1997; Christiansen et al., 2002; James et al., 2011; Fouch, 2012; Brueseke et al., 2014). However, regardless of the origin of the magmatism, the clear spatiotemporal relationship between the voluminous magmatism (including the Jarbidge Rhyolite), the mid-Miocene inception of Basin and Range extension in northeastern Nevada, and the collapse of the Nevadaplano (Colgan and Henry, 2009) suggest a common origin (Colgan and Henry, 2009; Brueseke et al., 2014).

Recent work (Callicoat, 2010; Brueseke et al., 2014) has identified the wide-spread volcanism (e.g., Jarbidge Rhyolite) in the northeastern Nevada as roughly coeval with that of the mid-Miocene inception of the Basin and Range extension. The Jarbidge Rhyolite (16.1 to 15.0 Ma) as studied by Brueseke et al. (2014) and Callicoat (2010) is located directly south of the Bruneau-Jarbidge eruptive center and east of the Owyhee Plateau. Previous work on the Jarbidge Rhyolite includes: Schrader, 1912; Coats, 1964, 1987; Christiansen et al. 1983, 1986; Bernt, 1998; Wallace et al., 2008; Henry et al. 2011. The Jarbidge Rhyolite was originally described by Schrader (1912) as quartz-phyric lava, but it wasn't until later when Coats (1964, 1987) mapped this unit consisting of quartz-phyric lavas, flow-dome complexes, minor pyroclastic deposits, and sparse interbedded sedimentary strata, that it was named Jarbidge Rhyolite. The "main body" and largest mapped area of Jarbidge Rhyolite occurs in the town of Jarbidge, Nevada, the Jarbidge mining district, the Jarbidge Mountains, and areas to the south. Brueseke et al. (2014) determined volume estimates for the four major bodies of Jarbidge Rhyolite (Mahoganies, Wild Horse Reservoir, Peak 7201, and the "Main Body") (Figure 1.11). These volume estimates for the four bodies range from 0.93 to 405 km^3, with a total of 509 km^3. Using an extrusive: intrusive ratio of 1:2 (Leeman et al., 2008) and 1:5 (de Silva and Gosnold, 2001), the range of total Jarbidge Rhyolite magma as calculated by Brueseke et al. (2014) is ~1,500 to 3,000 km^3.

According to Christiansen (1986) and Brueseke et al. (2014), the Jarbidge Rhyolite lavas are chemically similar to Topaz rhyolites across the Basin and Range that are intimately linked to localized extension and Jarbidge Rhyolite volcanism is coeval with the unroofing of the Ruby-East Humboldt Range ca ~16 Ma (Henry et al., 2011). Topaz rhyolites are characterized by an association with Cenozoic extension and Precambrian crust (Christiansen, 1986). They are formed through the process of partial melting of continental crust hybridized by upwelling basalt, accompanied by fractional crystallization (Christiansen et al., 1983,1986, 2007)

According to prior work by Brueseke et al. (2014) and Callicoat (2010), the Jarbidge Rhyolite has a smoky quartz-phyric texture with a high quantity (20 to 40 modal %) of phenocrysts. The main mineral phases include quartz, sanidine, and plagioclase. Other phenocrysts include locally oxidized clinopyroxene, orthopyroxene, and rare pseudomorphs of biotite and amphiboles. Accessory Fe-Ti oxides, apatite, and zircon are common. Callicoat (2010) and Brueseke et al. (2014) have made detailed descriptions of the mineralogy of the Jarbidge Rhyolite.

Quartz phenocrysts have an average modal abundance of 11% with a range of 4.4 to 16.7% by volume. They are euhedral to anhedral and vary in size from microcrystalline to 5.4 mm. Textures include embayments, ocelli, chessboard extinction, broken crystals, and granophyre and graphic granite textures. Sanidine crystal modal abundance varies from 1.6 to 16.5 % by volume, with an average of 9.6 modal %. They are commonly anhedral to subhedral and contain textures including embayments, anti-rapakivi, skeletal, spongy, inclusion rims and boxy textures. Plagioclase crystals are subhedral to anhedral and range modally from 2.5 to 14.1 % by volume, with an average of 7.0 modal %. The textures include skeletal, embayed, boxy, and spongy crystals. The compositional range is An_{10-40}. Garnet has been found as anhedral to subhedral, oxidized, and within or near crystal "clots" of plagioclase and oxides. It is suggested from Brueseke et al. (2014) that these garnets "clots" are xenocrysts/xenoliths derived from Cretaceous granitoid and associated contact aureole(s).

Roughly coeval with the mid-Miocene Basin and Range extension, the Snake River Plain underwent major and widespread volcanism related to the Yellowstone hotspot (e.g., Bruneau Jarbidge and Twin Falls eruptive center) (Figure 1.2). The resulting hotspot track is represented by a northeast-trending linear belt of silicic, caldera-forming volcanism that arrived at Yellowstone ~2 Ma and started near the Nevada-Oregon-Idaho border region at ~16-17 Ma (Pierce and Morgan 1992). There are two phases of the hot-spot track: 17 to 10 Ma and 10 to 0 Ma. The first phase of this trend has increasingly more dispersed loci from the primary track versus the younger, more track-centered, defined caldera-forming volcanism. According to Pierce and Morgan (1992) this major change at 10 Ma is most likely due to a transition from a larger plume head prior to 10 Ma, to a much narrower "chimney" plume tail after 10 Ma. The Yellowstone track has produced bimodal rhyolite-basalt volcanism over the 16 to 0 Ma, including periods of explosive silicic volcanism and flood basalts. Specific to this study, the

Bruneau-Jarbidge and Twin Falls eruptive centers are some of the earliest locations of the Yellowstone hotspot track (13 to 5.5 Ma) (Wright 2002; Bonnichsen et al., 2008; Ellis et al., 2010; Brueseke et al., 2014).

1.2.3.2 Late Miocene

Although the eruptive loci are found in southern Idaho, outflow from the two major central Snake River Plain silicic eruptive systems, the Twin Falls volcanic field and the Bruneau-Jarbidge eruptive centers are found in Elko County (Figure 1.12)(Coats, 1987). Ash-flow tuffs from these volcanic fields are thought to be representative of "Snake River-(SR) type" volcanism (Ellis et al., 2010). SR-type ash-flow tuffs are characterized by an alternation of intensely welded (lava-like) and non-welded deposits, where the dominant form is intensely welded. They are also void of pumice and lithic clasts. Branney et al. (2008) provide a detailed account of the regional, large-volume SR-type rhyolite lavas. They are extensive (10s of km) and voluminous (>10 km^3), with some lavas exceeding 200 km^3 (e.g., Sheep Creek Rhyolite) (Bonnichsen, 1982). The physical characteristics of all SR-type rhyolite lavas are similar. Branney et al. (2008) describe them as blocky with thick (> 5m) marginal and upper carapace autobreccias. The central zones of the lavas are microcrystalline, massive or flow-banded, and dominated by steep columnar jointing, as well as close-spaced sheeting joints. Spherulites and lithophysae are common near the base of the lithoidal zone. These rhyolites are typically A-type and contain plagioclase, Ca pyroxene, opaque oxide phenocrysts and nearly all contain pigeonite. Many units contain quartz, while some contain sanidine (Bonnichsen 1982). The central Snake River Plains (CSRP) rhyolite lavas differ from eastern Snake River Plains rhyolite (ESRP) lavas geochemically in that they have lower silica (~71.9 to 76 wt. %), Na_2O (2.52 to 3.40 wt. %), and total alkalis, while having higher TiO_2 (0.15 to 0.64 wt. %), FeO (1.30 to 4.42 wt. %), and CaO/Al_2O_3 (Hughes and McCurry, 2002). Bonnichsen et al. (2008) estimate the cumulative volume of all CSRP units to be at least 7000 km^3, most of which erupted between (12.7 to 10.5 Ma).

The Bruneau-Jarbidge eruptive center (BJEC) is located in eastern Owyhee County, southwestern Idaho (Bonnichsen, 1982) and extends into Twin Falls County to the east (Bonnichsen, 2008) (Figure 1.12). According to Bonnichsen et al. (2008), the BJEC was characterized by two major stages with differing eruptive styles: [1] a high temperature, caldera-forming ash-flow tuff-dominated stage that is associated with eruptions of the Cougar Point Tuff and [2] a less voluminous, rifting stage dominated by lavas. The more voluminous ash-flow tuff

stage has been dated by Bonnichsen et al. (2008) as 12.7 to 9.5 Ma. There are nine highly welded ash-flow tuff units mapped as the Cougar Point Tuff that occurred during this stage. According to Bonnichsen et al. (1982), the mineralogy of these units is homogeneous. Quartz appears from euhedral to rounded and is nearly always between 0.05 to 0.3 mm across. Sanidine occurs as euhedral to subhedral with minor zoning and ranges from 0.5 to 3 mm in diameter. There are abundant plagioclase crystals ranging from An_{30} to An_{55} (Bonnichsen et al., 1982). They range from 0.5 to 2 mm long and form subhedral tablets or laths. Some of the plagioclase phenocrysts include anhedral clots of pyroxene and sanidine, suggesting refractory protolithic material that was not fully melted when the magma was generated or magma chamber cumulates (Bonnichsen et al., 1982; Ellis et al., 2014). Both augite and pigeonite occur throughout, although relative proportions vary. Individual crystals range from 0.1 to 0.75 mm long and are typically subhedral prismatic to anhedral. Lastly, opaque oxides occur in all of the Cougar Point Tuff units and these are either magnetite and/or ilmenite (Bonnichsen, 1982). The geochemistry of the Cougar Point Tuff is very typical of the BJEC, predominantly A-type rhyolite with typically higher silica values (~73-77 wt. %) (Bonnichsen, 2008). The second stage of the BJEC occurred from 9.5 to 5.5 Ma and is associated with coeval basaltic eruptions. There are eight to twelve large rhyolite lavas connected with this volcanic field (Bonnichsen, 1982). The lavas average ~100–km-thick and 10 km^3 in volume, with the largest of the lavas (Sheep Creek Rhyolite) being upwards of 250-km-thick and over 200 km^3 (Bonnichsen, 1982). The mineralogy of these lavas is very similar to that of the Cougar Point Tuff and will not be discussed further.

The 11 to 5.5 Ma Twin Falls (TF) volcanic field is located in the south-central Idaho region. Ellis et al. (2010) describes the ash-flow tuffs of Cassia Mountain as intensely welded rhyolitic exposures, which produce steep cliff outcrops. The volcanic field erupted at least six distinct Miocene rhyolitic tuff Members in and around the Cassia Mountains, Idaho (Figure 1.12): Magpie Basin Member (~11.3 Ma), Big Bluff Member (10.98±0.07 Ma), Steer Basin Member (10.63±0.07 Ma), Deadeye Member, the Wooden Shoe Butte Member (10.13±0.03 Ma), and the McMullen Creek Member (8.94±0.07 Ma) ($^{40}Ar/^{39}Ar$ ages from Perkins and Nash, 2002; Nash et al., 2006; Bonnichsen et al., 2008; Ellis, 2009; Ellis et al., 2010). Ellis et al. (2010) showed that the Members sampled consist of 3-15% phenocrysts and documented samples from the Cassia Mountains to contain euhedral clinopyroxene. The younger Members contain both pigeonite and augite, while Magpie Basin and Big Bluff Members only contain augite. Feldspars

are found commonly as euhedral crystals up to 5 mm in length. All units contain plagioclase, while the Big Bluff Member contains sanidine intergrown with quartz in a myrmekitic texture (Ellis et al., 2010). As the units get younger, the plagioclase changes from oligoclase (An_{21} to An_{30}) to andesine (An_{32} to An_{43}). Magnetite is present throughout as the Fe-Ti oxide phase; ilmenite is much less common. As estimated by Nash et al. (2006), the McMullen Creek Tuff erupted from 9.14 to 8.6 Ma. The McMullen Creek Tuff has 10-20% phenocryst and has a very homogeneous mineralogy. Pumice is rare in these samples. Plagioclase appears as subhedral to euhedral, from 0.5 to 2 mm and contains inclusions of pigeonite, augite, Fe-Ti oxides, apatite, zircon, or glass. Pigeonite and ferroaugite are subhedral to euhedral, range from 0.5 to 3 mm, and appear as prismatic, individual grains. This unit also contains common inclusions of Fe-Ti oxides as well as apatite within the plagioclase and quartz (Wright, 2002). Due to the lack of mineralogical diversity between the six Members, these two Members are described in detail to represent the mineralogy of the entire Cassia Mountain Tuff complex.

Shortly following these events (1 to 3 m.y.), a series of basaltic eruptions began in the central Snake River plain. The early phase, which occurred from ~10 to 5 Ma, formed mainly sub-aerial olivine tholeiite eruptions (e.g., Snake River olivine tholeiites; SROT). These basalts now cover much of the central Snake River Plain (Bonnichsen, 2002). Phenocrysts from these lavas are olivine and plagioclase. Olivine ranges from Fo_{35} to $Fo_{60,}$ while plagioclase ranges from An_{80} to An_{60} (Bonnichsen, 2002). SROT lavas have an iron-rich olivine and sodic (An_5) plagioclase groundmass (Leeman, 1982). There have been two distinct groups of SROT studied on the Snake River Plain. Group I has a relatively higher range for K_2O (0.61 wt. %), P_2O_5 (0.58 wt. %), and TiO_2 (2.70 wt. %) and have a tendency to be enriched in iron (13.51 wt. % FeO). Group II has lower contents of K_2O (0.17 wt. %), P_2O_5 (0.18 wt. %), and TiO_2 (1.07 wt. %), while having a raised CaO (12.34 wt. %) and Al_2O_3 (16.35 wt. %) (Leeman, 1982). In addition, Group II is separated from Group I SROT by trace element contents. Group II contains relatively high Cr/Ni (3.77) ratios as well as lower contents of Rb (~4 ppm), Zr (~84 ppm) (magmaphile trace elements), and Ba (~162 ppm) (Leeman, 1982). Group I contains high concentrations of those trace elements: Ba (~399 ppm), Rb (~10 ppm), and Zr (~255 ppm), while maintaining a lower Cr/Ni ratio (2.23) (Leeman, 1982). CIPW normatives for both groups (I and II) of lavas contain both olivine and hypersthene, while none contain quartz and a few Group I SROT contain nepheline (Leeman, 1982). According to McCurry et al. (2008), the western margins of the

Cassia Mountains contain a number of SROTs, one of significance to this thesis is the Deadline Ridge basalt. The significance to this thesis will be detailed below. These basalts have also been classified as SROT via physical and geochemical analysis. They have been dated via $^{40}Ar/^{39}Ar$ geochronology as ranging from 9 Ma to 7 Ma. Hughes (unpub.) also studied late Miocene SROT in southern Idaho similar to those in the Cassia Mountains. There is a distinct chemical difference between the late Miocene SROT as described by Hughes (unpub.) and McCurry (unpub.) versus the much younger (Pleistocene) SROT, a.k.a McKinney Basalt (and other eruptive units), as studied by Leeman (1982). This difference will be used below in this thesis to correlate my mafic samples and to infer an age of either late Miocene or Pleistocene.

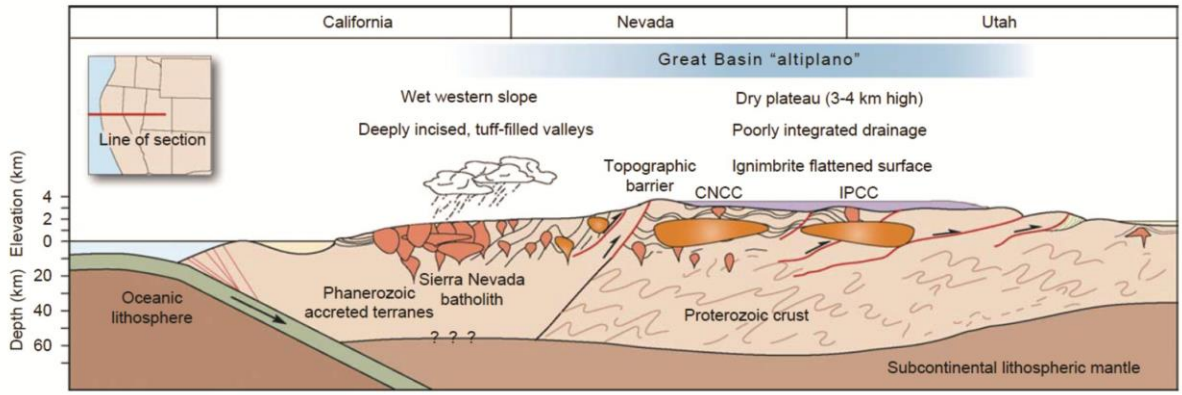

Figure 1.9: West-east cross-section of the Nevadaplano prior to it "collapsing" and during the "ignimbrite flare-up" as depicted by Best et al. (2009). The topographic barrier is represented in Figure 1.10 as the dark black line that outlines geologic units perpendicular to the paleovalleys. It is labeled as the paleodivide.

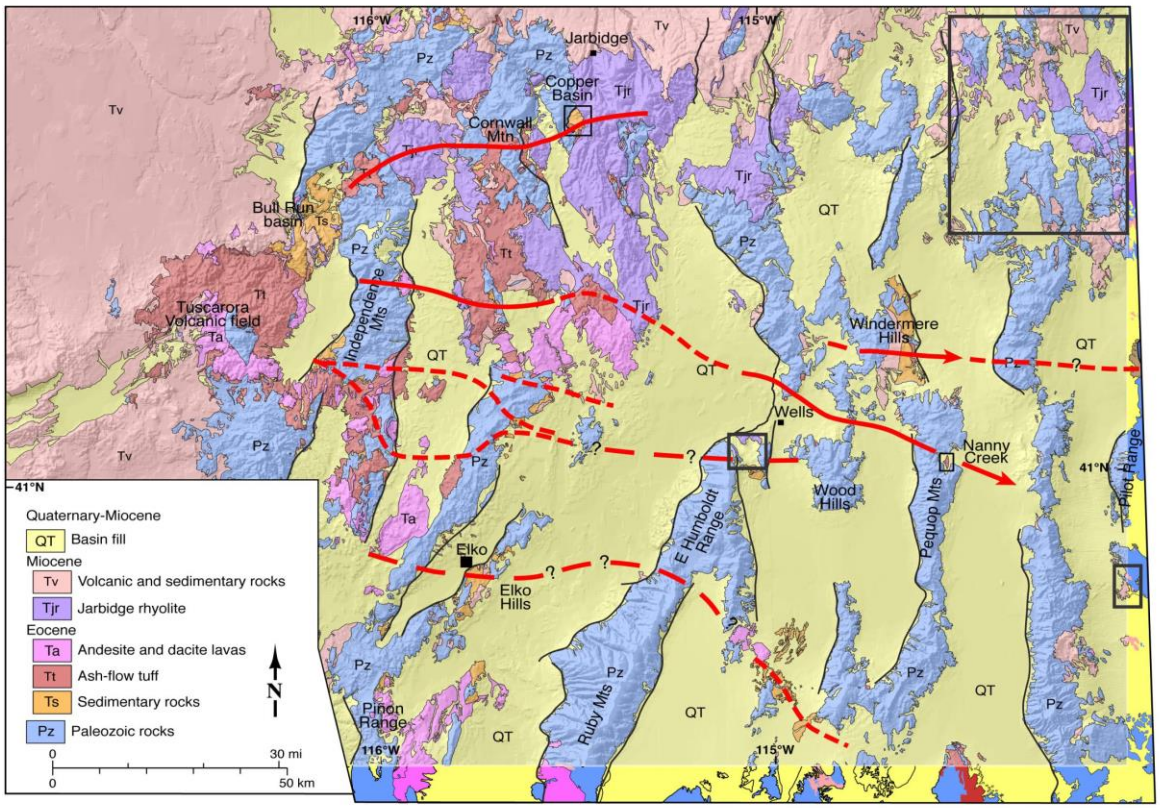

Figure 1.10: ***Adapted from Henry et al. (2011).*** **A depiction of extent of the Eocene paleovalleys. Solid red lines are documented paleovalleys. Dashed red lines are predicted extension(s) of the confirmed paleovalleys. Solid black boxes outline my study areas.**

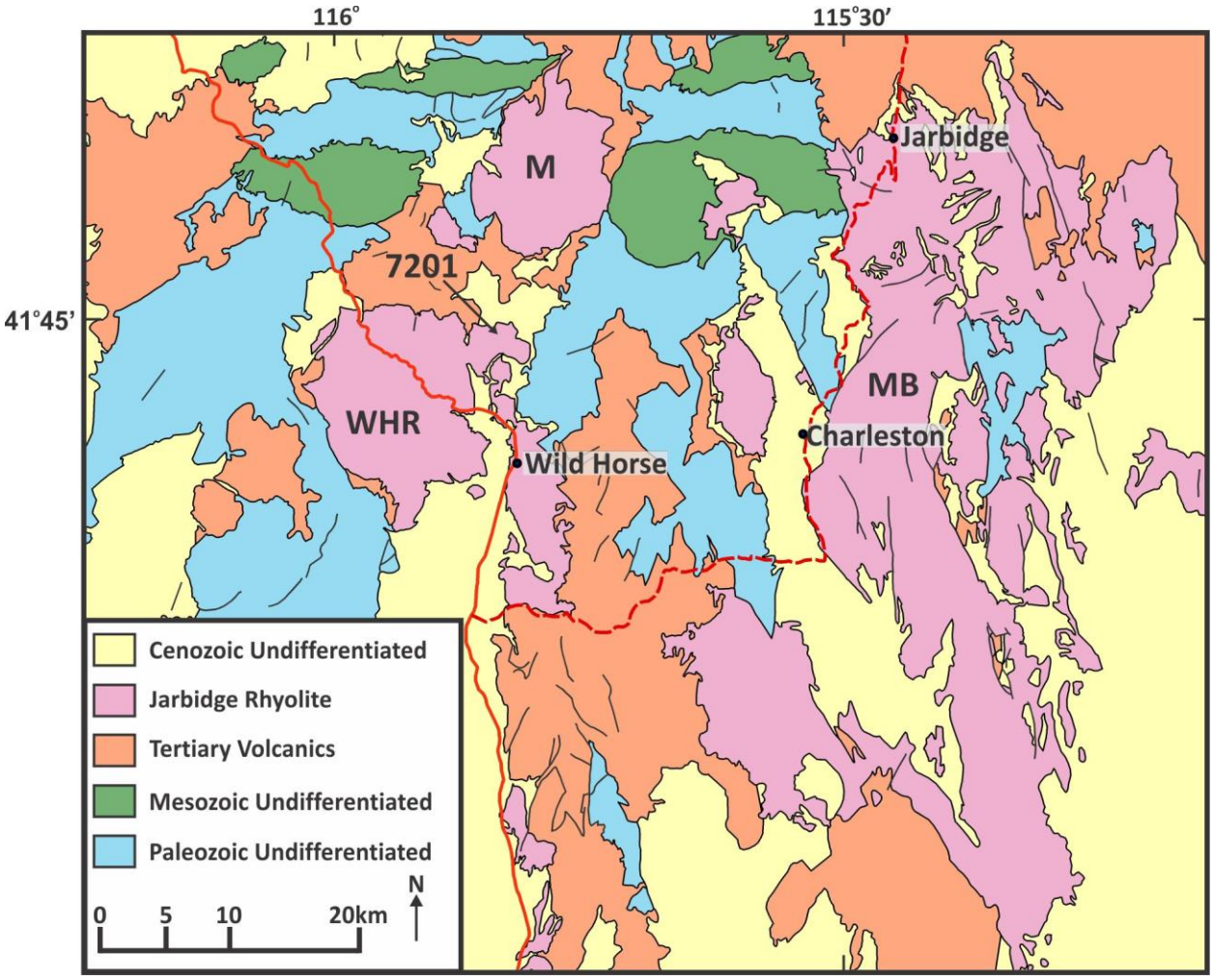

Figure 1.11: Main bodies in northwestern Elko County, NV. Abbreviations are as follows: M, Mahoganies; MB, Main Body; WHR, Wild Horse Reservoir; 7201, Peak 7201.

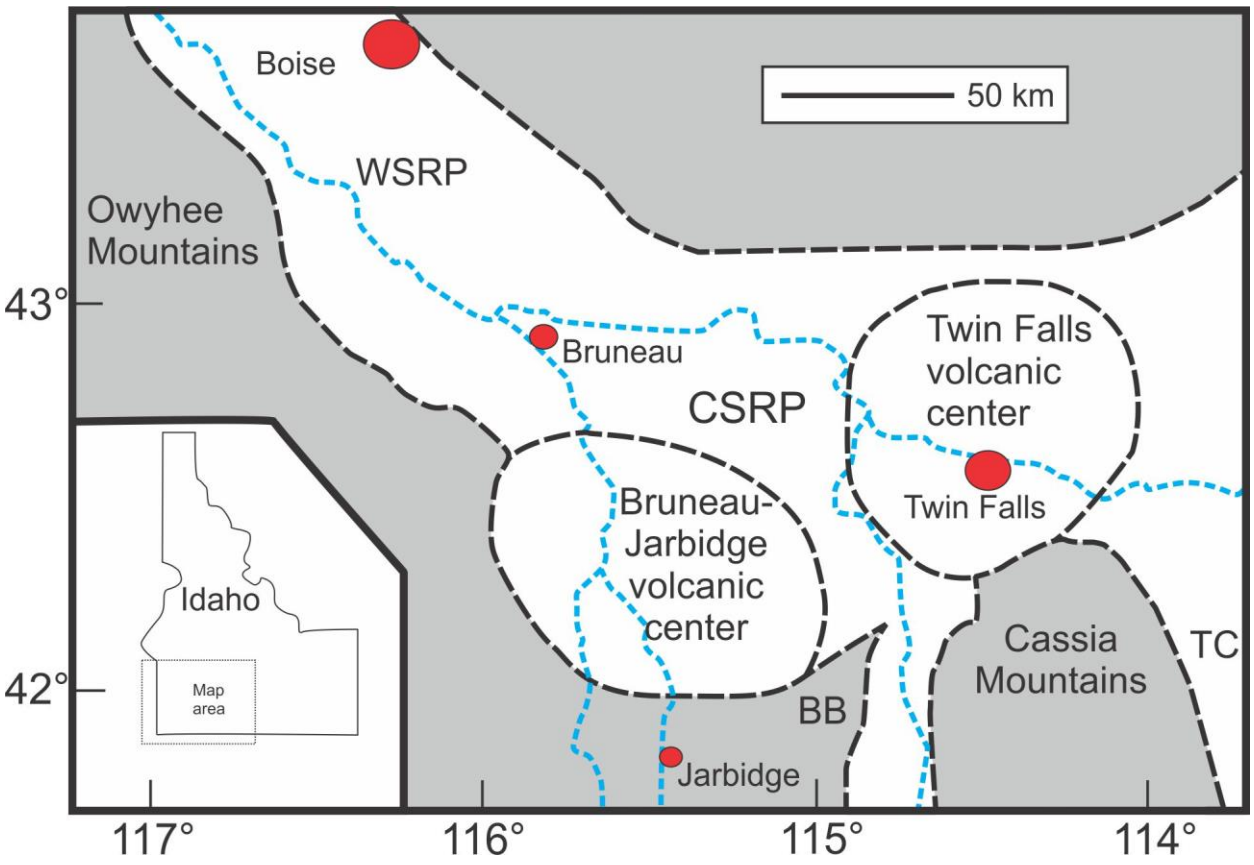

Figure 1.12: ***Adapted from Bonnichsen, 2008.*** **Blue dashed line represents the Snake River. Red circles represent city and sizes of cities. Black dashed circles represent individual volcanic centers. Abbreviations are as follows: BB, Browns Bench; TC, Trapper Creek; WSRP, Western Snake River Plain; CSRP, Central Snake River Plain.**

1.3 Local Geology

Little work has been done in the primary northeastern Nevada study area in and adjacent to the Little Goose Creek drainage (Figure 1.13) aside from the large scale mapping done by Coats (1987). While not a focus of this work, the oldest exposed rocks in the region are Permian limestones, cherts, and shales (Coats, 1987). These Permian sedimentary strata are cross-cut by numerous faults and are overlapped by a diverse Cenozoic volcanic and volcaniclastic assemblage. These relationships, as mapped by Coats (1987), are of major importance to constraining the Tertiary geologic history of my study area. Jarbidge Rhyolite exposures that are mapped by Coats (1987) in the study area also crop out throughout Elko county. Due to the distance from these widespread and voluminous Jarbidge Rhyolite exposures (Figure 1.13), it is presumed they are sourced from local vents in and adjacent to my study areas.

Some lavas in NE Nevada that have been mapped as the Jarbidge Rhyolite, as well as younger rhyolites, have been dated by K-Ar and $^{40}Ar/^{39}Ar$ methods (McKee et al., 1975; Armstrong, 1970; Evans & Brown, 1981; Compton, 1983; Henry, 2008; Brueseke et al., 2014). Specific to my study area, McKee et al. (1975) dated a tridymite rhyolite lava in West Wendover, NV, using K-Ar to 11.6 Ma. This unit is mapped and, based on geomorphology, corresponds to a Jarbidge Rhyolite unit I sampled in West Wendover, NV. Initial K-Ar dating of the Jarbidge Rhyolite ("main body") west of my study area in Little Goose Creek, as studied by McKee et al. (1975), provides a preliminary timing on the inception of the main body of Jarbidge Rhyolite volcanism at ~16.8-15.4 Ma. As well, Henry (2008) dated a Jarbidge Rhyolite lava using $^{40}Ar/^{39}Ar$, south of Bull Run Basin, to 16.2 Ma. More recent studies by Brueseke et al. (2014) show a range of 16.1 to 15.0 Ma using more accurate $^{40}Ar/^{39}Ar$ geochronology. Armstrong (1970) reported a whole-rock radiometric age of 15 Ma for a rhyolite within Palisade Canyon, east of the Humboldt-Ruby range. This rhyolite is not a Jarbidge Rhyolite, but still fits with the age progression of magmatism. Miller et al. (2012) has correlated rhyolite lava units in the Grouse Creek quadrangle of Utah, specifically in the Grouse Creek Valley (Tr) directly adjacent to my study area to the Jarbidge Rhyolite lavas mapped by Coats (1987). K-Ar sanidine ages of approximately 12.2 to 11.7 Ma have been measured by Compton (1983) and Evans and Brown (1981) for these rhyolites. They have been described by Miller et al. (2012) as gray to purple, porphyritic, high-silica rhyolite flows, domes, and intrusions interbedded with the Salt Lake Formation (Ts). They contain abundant phenocrysts of smoky or pink quartz and feldspar;

sparse biotite and hornblende present in some flows. This description is essentially identical to the Jarbidge Rhyolite I have studied in NE Elko County, NV and those studied by Brueseke et al. (2014). The magnitude of distance between the Jarbidge Rhyolite lava fields (Jarbidge, NV; Wells, NV; West Wendover, NV; Goose Creek, NV; and Grouse Creek, UT) indicate individual localized eruptions.

Adjacent to and surrounding the exposures of the Jarbidge Rhyolite and the other lavas are widespread exposures of the Humboldt formation (Ts_3; Coats, 1987), which is known as the Salt Lake Formation in Utah (Ts; Miller et al., 2012). As in other areas across Elko County, NV, local exposures of the Humboldt formation contain lacustrine, fluvial, and alluvial sedimentary strata, interbedded with air-fall tuffs and ash-flow tuffs. These strata formed and were deposited primarily in extensional basins and basins formed by damming of drainages by volcanism in northeast Nevada (Henry, 2008; Wallace, 2008). The lower sections are typically more ash-rich and the upper sections are dominated by conglomerate and sandstones, as the basins likely filled due to a cessation of extension (Coats, 1987). Regionally, Humboldt Formation exposures typically record a depositional (e.g., extensional origin; Wallace, 2008; Colgan and Henry, 2009) period from ~16 to 10 Ma (Sharp, 1939; Coats, 1987; Wallace, 2008; Colgan et al., 2010; Henry et al., 2011), overlapping with Jarbidge Rhyolite volcanism. Perkins et al. (1995) have provided $^{40}Ar/^{39}Ar$ age constraints on tuffs of the Trapper Creek area, southeastern Idaho, just west of the lower Goose Creek Reservoir ranging from 13.74±0.04 Ma to 10.02±0.03 Ma. This constrains the local basin extensional deposition to roughly that time period. The Humboldt Formation extends into the Grouse Creek quadrangle, UT and has been mapped by Miller et al. (2012) as the Salt Lake Formation. Miller et al.(2013) has dated, using $^{40}Ar/^{39}Ar$ geochronology, similar rhyolites to the east of my study (Grouse Creek, Utah) in Pole Creek to 12.92 Ma.

Outside of the Little Goose Creek Basin, I studied two exposures of Miocene rhyolite, one at Wells and the other at West Wendover, NV. They are included in the thesis because they are Jarbidge or "Jarbidge type" Rhyolite that are far from the most extensive Jarbidge Rhyolite exposures. The Wells, NV outcrops have been mapped by Coats (1987) as two small Jarbidge bodies just southwest of Wells, NV. Mueller and Snoke (1993) used K-Ar dating to date these bodies of rhyolite, which they named Willow Creek Rhyolite, as ranging between 14.8 to 13.4 Ma. The West Wendover, NV sample has been mapped by Coats (1987) as Tr_3, which he describes as phenorhyolites, just like the Rock Springs rhyolite was mapped. However, unlike

the Rock Springs Rhyolite, the West Wendover sample is nearly identical in phenocryst abundance and groundmass texture to that of the Jarbidge Rhyolite. McKee et al. (1976) has provided a K-Ar age on the same body as sampled by myself and places it at 11.6 Ma.

There are other Miocene units in the area that are inferred to be younger than the Jarbidge Rhyolite. Coats (1987) has mapped younger rhyolites within my study area as T_{r3}. These rhyolites, both mapped at Rock Springs and West Wendover, NV are brown or reddish brown. In hand sample, phenocrysts include sanidine, quartz, biotite, and pigeonite. A small outcrop of what Coats (1987) describes as "Tertiary Ignimbrites" is also located within my study area near Goose Creek. This unit has been correlated by Coats (1987) to more widespread ash-flow tuff units (e.g., the Cougar Point Tuff and the Idavada volcanics). The youngest volcanic unit in the quadrangle is what appears to be a flow-field of late Miocene olivine basalt, labeled by Coats (1987) as (Tb). In most locations they are uncut by faults (Coats, 1987). According to McKee et al. (1975), these basalts have an age range of approximately 8.2 to 7.9 Ma. This is coeval with those dated by McCurry (2002) in the Cassia Mountains, ID using $^{40}Ar/^{39}Ar$ dating as approximately 7.5-8.0 Ma. Chemically, they resemble the basaltic unit previously identified by McCurry and Rodgers (2009) that crops out to the north adjacent to the southwestern side of the Cassia Mountains (ID) (Brueseke et al., 2014). Quaternary alluvium (Qal) is the youngest unit in the study area. Coats (1987) mapped extensive Qal deposits and they are described as being coarsely sorted and unconsolidated gravel and sand, most likely fluvial deposits.

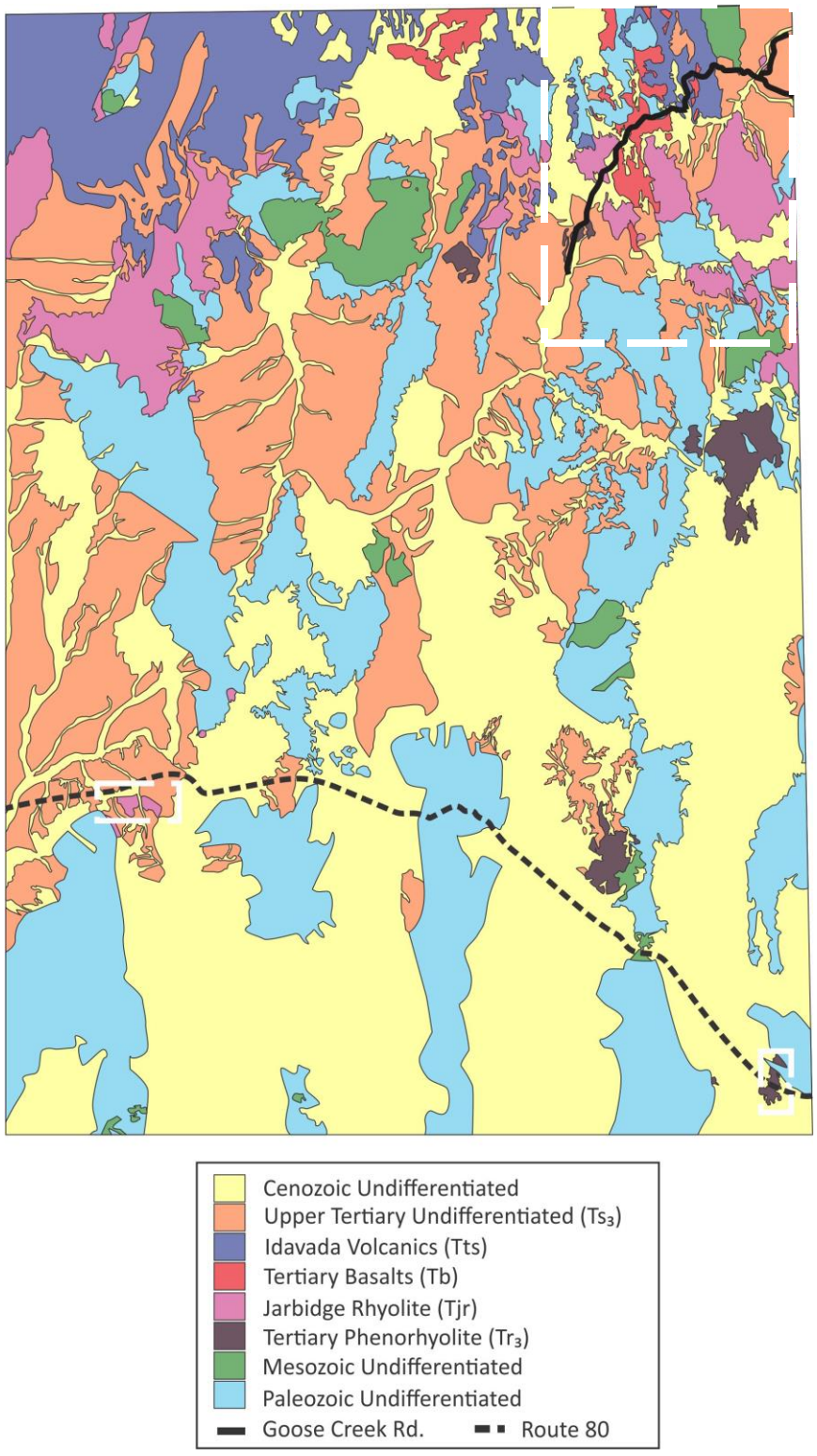

Figure 1.13: Map of northeastern Nevada; my study areas and presumed locally sourced Jarbidge Rhyolite is outlined in white. The access routes for my study were Goose Creek Rd. (solid black line) and Interstate 80 (black dashed line).

Chapter 2 - Methods of Investigation

2.1 Field Methods

Using the geologic map of Elko County, NV (Coats 1987, Figure 2.1), I identified probable bodies of interest including Jarbidge Rhyolite (Tjr), younger ash-flow tuffs(Tts), and Miocene basalts (Tb). I then spent two field seasons, each approximately one week, collecting samples I deemed of importance to the study. I focused on the collection of the main bodies of Jarbidge Rhyolite in the Little Goose Creek area as well as the outlying Jarbidge Rhyolite bodies in Wells and West Wendover, NV, as these samples are all important to the ongoing study of the temporal relationship between the Jarbidge Rhyolite and the mid-Miocene Basin and Range extension. Ash-flow tuffs were collected that showed stratigraphical relationships in order to constrain further the basin deposits associated with extension. Basalts were collected in the field to confirm whether young capping basalts occur in the area, similar to those studied by McCurry and Rodgers (2009) in Elko County, NV and mapped by Coats (1987). The samples were collected to maximize my time in the field, which was limited by poor weather and road conditions (e.g., monsoonal rains and impassable, poorly maintained roads in northeastern NV). Figure 2.2 depicts all sample locations on a map based off of Google Earth. The main study area was located in the Little Goose Creek Drainage area, NV and samples were taken off of Goose Creek Rd., which follows the route of the CA trail. These samples include the four Jarbidge Rhyolite (MB11-2;AI13-2,3,5), one Rock Springs Rhyolite (MB11-1), four ash-flow tuffs (AI12-2,3,4;AI13-1), and two basalts (MB11-3, AI12-1). Outside of the main study area an ash-flow tuff (AI12-5) was collected off Birch Creek Rd. in southern Idaho. Two Jarbidge Rhyolite samples were taken off of Interstate 80; the first was located outside of Wells, NV(JC-09-22) and the second was taken outside of West Wendover, NV (AI12-6). The main focus was the collection of targeted Jarbidge Rhyolite bodies in eastern Nevada (Figure 2.3). I also collected various unclassified ash-flow tuffs (Tts) to constrain the youngest, based on mapping, extensive silicic eruptive units in the study area. The basalts were collected to help further constrain the timing of basin formation in the Little Goose Creek region. Sample collection was done via foot traverses from a vehicle using standard tools (i.e. rock hammer and 10x hand-lens). Adjustments were made to the sampling because of the aforementioned stormy weather; some of the targeted Jarbidge Rhyolite and planned detailed geological mapping in the 1:24,000 Mustang Draw

quadrangle was impossible due to the weather. Thus, the focus of this thesis became the field reconnaissance and fundamental data collection for the area. Rock samples were collected based on their freshness, as well as a general change in physical volcanology-related textures (e.g., vitrophyre, change in crystallinity, etc.). All locations of the samples were recorded using a Gamin e-trex global positioning system hand held device set to Universal Transverse Mercator (UTM) coordinates and North American Datum (NAD) of 1927. The UTM coordinates of sampled locations, as well as field-descriptions of sampled material are in Appendix A.

2.2 Laboratory Methods

2.2.3 Thin-section Petrography

Thin-section analysis was performed using a Nikon petrographic microscope. Photomicrographs were taken using a Nikon camera and SCOPE software. Point counting occurred at KSU geology, using a 10x scope targeting 1000 counts per slide on a 1 x 1 mm grid. The average number of counts per slide was 777. The seven rhyolite slides were counted between 750 and 850 counts.

2.2.2 Sample Preparation for Bulk Rock Geochemistry

Samples were processed in the Department of Geology, Kansas State University. Approximately fist-sized samples collected in the field were split and crushed using a Rocklabs hydraulic splitter/crusher with tungsten carbide faces. The samples were first split using the "knife edge" arm of the rocklabs machine in order to remove maximum alteration as well as reduce the samples to a size of less than 2.5 x 2 x 2 cm. Any remaining weathering rinds, apparent alteration, and contaminants (e.g., calcite coatings, zeolites, etc.) were removed using a diamond tipped rock saw as well as silica carbide sandpaper mounted on a grinding wheel. Thin section blanks were cut using the same rock saw to fit a standard 24 x 44 mm thin section template. The samples were then scrubbed and washed in a deionized water bath in order to remove "mud" from the sawing/grinding or sandpaper grit. The thin section blanks were sent to Spectrum Petrographics Inc. for thin section creation. The samples were then crushed using the Rocklab crusher plates and reduced to a sample diameter of <5 mm. To make sure the sample was completely homogenous prior to final powdering, a cone and quarter method was used to obtain the 15-20 ml needed for the shatter box in order to produce the rock powder. The sample

was pulverized to a clay-size fraction by a Spex Industries aluminum oxide shatter box. Each sample was placed in a 30 ml glass bottle to be sent for analysis of major and trace element by X-ray fluorescence spectroscopy (XRF).

2.2.3 Geochemical Analysis Preparation

Rock powders were sent to Franklin and Marshall College for bulk rock major and trace element analyses via XRF following the methods outlined in Mertzman (2000). In addition to bulk major and trace element results, loss on ignition (LOI) was determined for all samples. LOI= $((mass_{initial}-mass_{final})/(mass_{initial}))*100$. The $mass_{initial}$ is the approximately one gram (actual weight calculated on site in a ceramic crucible) of processed sample powder before heating, while the $mass_{final}$ is the sample powder after it has been heated in a muffle furnace at 950°C for one hour, allowed to cool to ambient temperature, and reweighed.

Major and trace element chemistry was obtained using a Panalytical PW 2404 X-ray fluorescence spectrometer. There is a difference between the preparation for the major and the preparation of trace elements at Franklin and Marshall College. The major element preparation starts by transferring 0.4000 grams of the whole rock powder into a bottle with 3.6000 grams of $Li_2B_4O_7$ (Lithium tetraborate). The sample is mixed for 10 minutes in the Spex mixer-mill before it can be fused to make a glass disc. The homogeneous powder is transferred into a 25 cc 95% Pt-5% Au crucible, then three drops of a 2% solution of lithium iodide (Lil) is added to the powder to reduce the viscosity of the mixture as it is heated over a Meeker burner. The lid to the crucible acts as the mold in which the molten sample will be poured to form a disc shape. The heating period is normally 10 minutes, while the sample is vigorously swirled. Finally, the Pt-lid is removed from the crucible and heated over a second Bunsen burner until it is red-hot and any remaining contents from the crucible is poured over the lid. The sample will cool in 3 to 5 minutes. The major element oxides, SiO_2, Al_2O_3, Fe_2O_3, MnO, K_2O, Na_2O, TiO_2, P_2O_5, CaO, MgO, are determined using this technique together with trace elements Sr, Zr, Cr and V. The remaining trace elements (Rb, Sr, Y, Zr, Nb, Ni, Ga, Cu, Zn, U, Th, Co, Pb, Sc, Cr, V, La, Ce, and Ba) are determined using 7.0000 grams of whole rock powder combined with 1.4000 grams of copolywax into a clean sample bottle. The sample is then mixed for 10 minutes in the Spex Mixer-mill. From there the sample is pressed to make a briquette, this requires the sample to remain at 40,000 psi for a minimum of three minutes. Data collection was performed by Dr.

Stanley A. Mertzman. Precision and accuracy measurements were taken on June 2011 for the XRF analysis by Karen Mertzman. The precision and accuracy of the data collection is detailed in the Appendix. The analyses represent all the errors that could accrue from weighing, mixing, preparation of the fusion glass disk and trace element briquette, and the actual peak and background measurements made by the PW2404 Panalytical, Inc. XRF vacuum spectrometer (Mertzman, 2014).The raw data was then normalized to anhydrous for plotting purposes by myself. I used the following corrections in the normalization procedure:

Oxidation ratio: (OX)=FeO/(FeO+Fe_2O_3)= 0.93-0.0042 SiO_2-0.022 (Na_2O+K_2O)

Fe_2O_3=[0.899813(OX)(Fe_2O_3*)-0.899813(Fe_2O_3*)]/[-0.899813-0.100187 (OX)]

FeO=(Fe_2O_3*-Fe_2O_3)/1.111342

2.2.3 $^{40}Ar/^{39}Ar$ Geochronology

The three samples chosen for analysis were AI12-6, JC09-22, and MB11-1. AI12-6 was chosen as the eastern most body of Jarbidge Rhyolite in West Wendover, NV. JC09-22 was chosen because Wells, NV is a minor outcrop of Jarbidge Rhyolite and lies directly west of AI12-6. MB11-1 was chosen as the underlying rhyolite unit in the Rock Springs stratigraphy to constrain basin extension. Additional samples of Jarbidge Rhyolite and ash-fall tuffs have been sent for dating and are still being processed as of when this thesis was submitted. The three samples were dated at Auburn University's Auburn Noble Isotope Mass Analysis Laboratory (ANIMAL) using $^{40}Ar/^{39}Ar$ geochronology by Dr. Bill Hames. The three samples are listed in the appendix with the sample numbers and ages, as well as their locations. Locations and quantity of samples are as follows: one sample from Wells, NV, one sample from a West Wendover, NV outcrop, and one sample 38 km SE of Jackpot, NV.

Multiple (27-13) sanidine crystals were dated for each sample by a 50W Synrad CO_2 infrared laser. The high sensitivity and low blank of the instrument permits measurement of 10-14 mole samples to within 0.02% precision. An analysis is the result of eight cycles of measurement over a range of masses and half masses from m/e=40 to m/e=35.5. Data collection and reduction is facilitated by National Instruments hardware and a Labview program written by lab personnel specifically for ANIMAL. Initial data reduction is accomplished through an in-house Excel spreadsheet, with final reduction using Isoplot (Ludwig, 2012). All external tuff age data was standardized to Fish Canyon tuff (28.02 Ma).

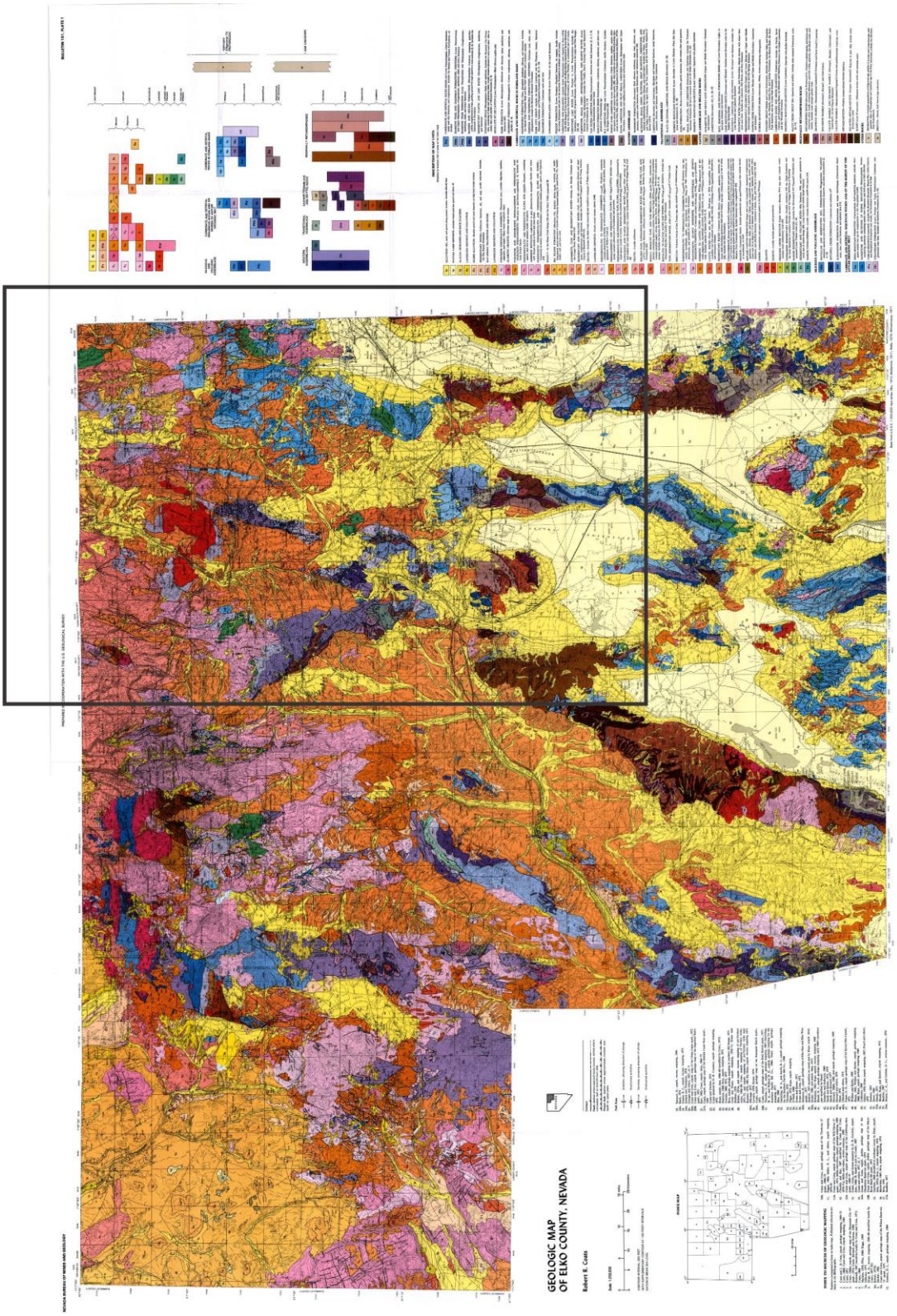

Figure 2.1: Original geological map of Elko County, NV as created by Coats (1987). The black box outlines my study area as shown in Figure 2.2.

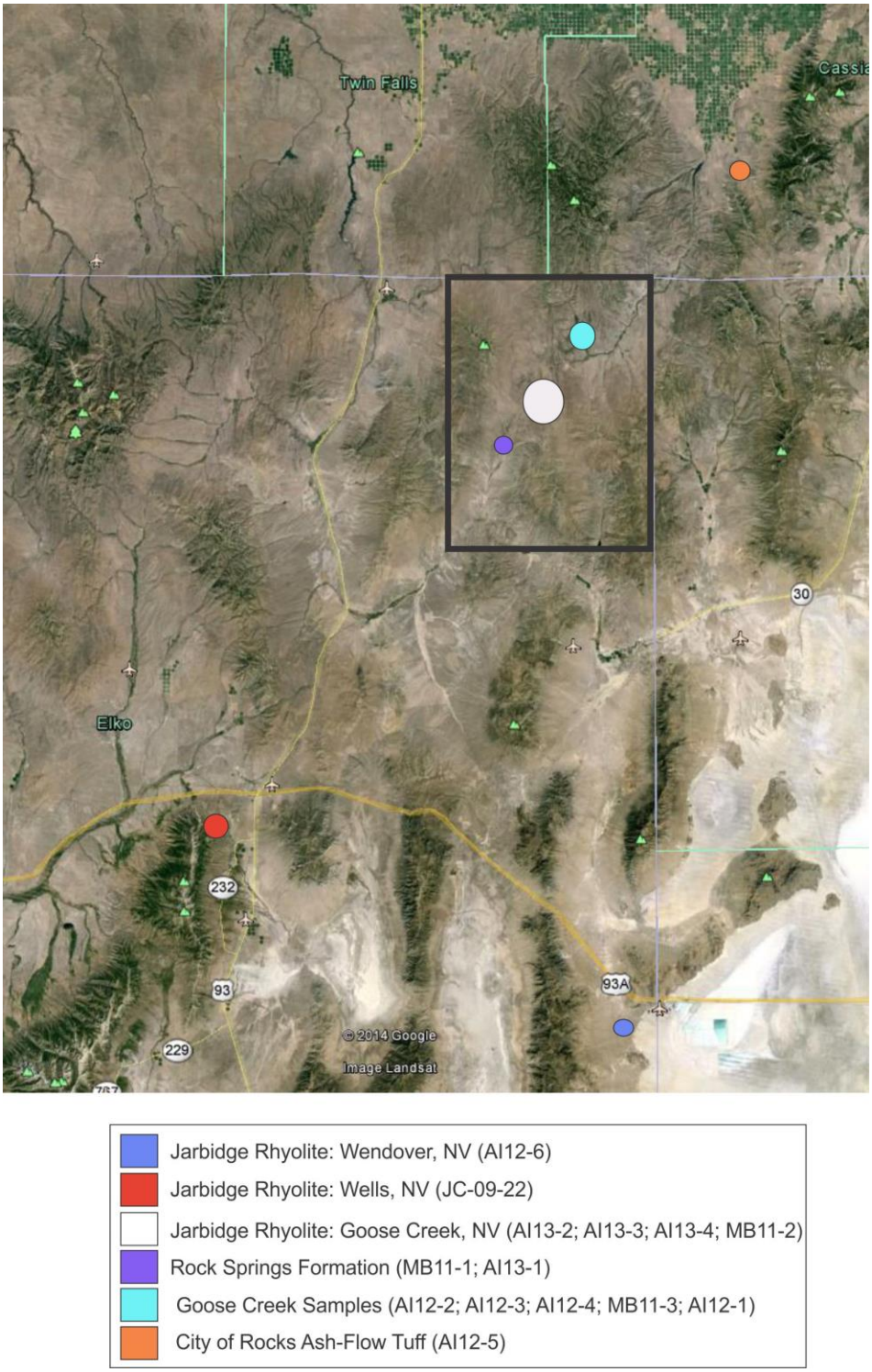

Figure 2.2: Google earth image of my entire study area. Colored circles represent my samples. The black rectangle denotes the Little Goose Creek area (NV), which is detailed in Figure 2.3. The green triangles directly north of the black rectangle represent peaks in the Cassia Mountains, ID.

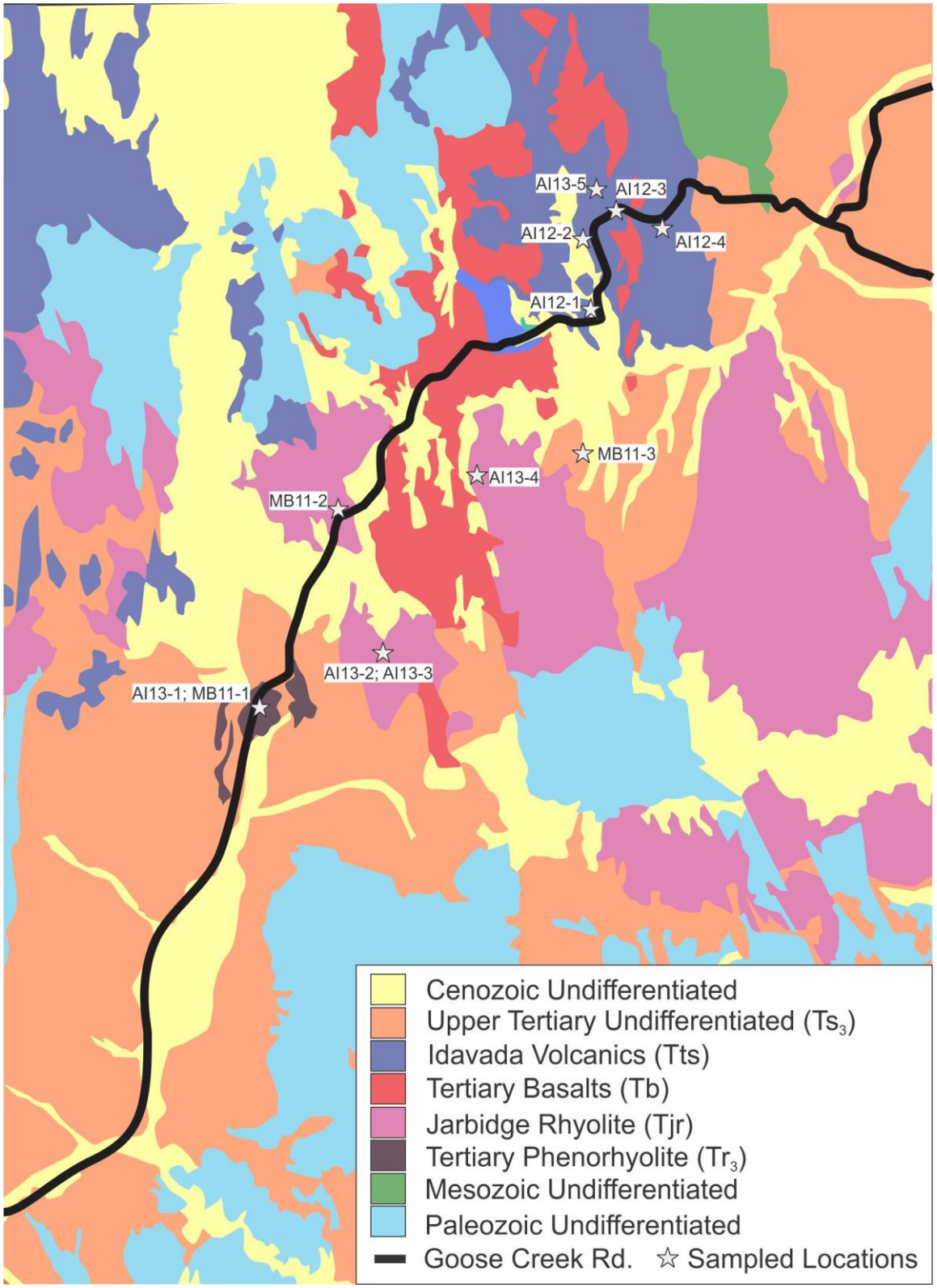

Figure 2.3: A simplified map of Coats (1987). This is the portion of my study area known as the little Goose Creek area. It is outlined in black on Figure 2.2.

Chapter 3 - Field Relations

The samples collected over a two year period were from within and around the Little Goose Creek drainage (Figure 2.3), West Wendover, NV, Wells, NV, and City of Rocks on Birch Creek Road. Four samples were collected previously by Dr. Matthew Brueseke from the Goose Creek drainage area (MB11-1, MB11-2, and MB11-3) and Wells, NV (JC-09-22).

3.1 Basalts

The two basalt samples collected from the field were AI12-6 and MB11-3 from the Goose Creek drainage area. The AI12-6 flow field contained two zones totaling five meters thick (Figure 3.1). These two zones include an upper oxidized and vesiculated zone (e.g., quenched lava margin) (Figure 3.2) and a lower, interior massive zone (sample AI12-6). The AI12-6 outcrop contained a layer of sinter above the lava. MB11-3 was collected east of Dry Gulch Canyon where three to four flows are present. Both of these lavas exhibit inflation features like pahoehoe lobes, which is consistent with a subaerial eruption for this unit. Abundant 3 to 5 mm plagioclase laths are present.

3.2 Ash-flow tuffs

AI12- 2, 3, 4 and AI13-5 are samples collected along Goose Creek Road. There is one ash fall (AI12-2) and three ash flows (AI12-3,4; AI13-5). The only samples used for geochemical analysis are the ash flows. You can see from the ash-fall (Figure 3.3) that the bedding is tilted (hammer is approximately horizontal) and contains very small particles, less than sand sized. The bedding thickness for this unit is approximately 1 to 3 cm. The little Goose Creek (GC) ash-flows have a very similar composition at the hand-sample level. There are phenocrysts (<3%) of plagioclase and sanidine crystals, and fragments of glass. The average size of phenocrysts is under 1 mm, with the rare 1 to 2 mm crystal. The groundmass has a light grey glassy texture. The groundmass is also very fine grained as well as poorly welded. There was minor hydrothermal alteration in some samples (AI12-3). Figure 3.4 shows two units of tilted bedding, a basal vitrophyre and an overlying devitrified welded tuff unit. The vitrified unit was sampled in 2013: AI13-5. The ridge where the sample was taken can be seen in Figure 3.4 as unit B in the middle of the photograph. The vitrophyre unit (10 to 15 m) is undergoing devitrification

and is “split” into a lower waxy portion, which was highly weathered into blades (Figure 3.5) and a blocky layer, where the sample (AI13-5) was collected.

Another ash-flow was sampled just outside the main study area in Idaho on Birch Creek Road (AI12-5). This was from a massive outcrop that is 70-m-thick (Figure 3.6). Texturally, it is highly welded, with a visible phenocryst range of 10 to 15%. The phenocryst assemblage, based on field analysis, appears to be sanidine, quartz, plagioclase, and pyroxenes. This is confirmed below in thin section analysis. The average phenocryst is around 1 mm, with the plagioclase and pyroxenes ranging from 1 to 3 mm. The larger feldspars were not stretched from flow welding, but in some cases the flow seems to wrap around the phenocrysts.

The first sample collected in year two was collected near Rock Springs, NV (Figure 2.2). The hill (Figure 3.8) from which AI13-1 was sampled is part of a series of fault-bounded hills (likely half-grabens) (Figure 3.7) that exposed volcanic and volcaniclastic strata interbedded with sedimentary basin fill (Figure 3.9; Figure 3.10). This sequence appears to directly overlie exposures of unit Tr_3, as mapped by Coats (1987). It is a fault-dissected lava (e.g., Rock Springs rhyolite) that was sampled previously by M. Brueseke (MB11-1) and will be discussed below. Capping the sequence is an ash-flow tuff unit approximately 2.5 meters in thickness (**Figure 3.11**). This ash-flow tuff has three distinct zones: 1.5 m of vitrophyric tuff with numerous 5 to 7.5 cm diameter spherulites (), which is overlain by 0.5 m of stretched lithophysae with the largest being 13 cm wide, that grades into 0.5 m of massive blocky-jointed tuff that is highly welded. The blocky-jointed tuff, where I sampled, had a phenocryst abundance by volume of ~10%. Visible phenocrysts include sanidine (1 to 2 mm), pyroxene (~1 mm), and plagioclase (0.5 mm to 1 mm). These sizes represent the phenocrysts assemblages at their largest, there were also much smaller versions of these crystals. There are fragments of quartz, although they are too small to measure accurately in the field. The groundmass has a brown glassy texture.

3.3 Rhyolite lavas

The rhyolites I studied were several distinct bodies of coalesced rhyolite lavas and domes from a number of different location, including the Little Goose Creek region. The only Jarbidge Rhyolite body sampled in year one was AI12-6, near West Wendover, NV. It is a rhyolite dome based on map patterns (e.g., radial outflow) with an approximate diameter of 245 meters (Figure 3.13). Spheroidal weathering is evident throughout as it is highly coarse-grained. Phenocryst

abundance by volume is upwards of 30 to 40 %. The main mineral phases are smoky quartz (1 to 3 mm; rare 1 cm crystals), sanidine (1 to 2 mm), plagioclase (1 to 2 mm), and pyroxene (<1 mm) (unable to determine through hand sample due to oxidation). The weathering caused the mafic phenocrysts to alter fully into oxides.

In 2013, two samples of Jarbidge Rhyolite were collected from a lava approximately six km north-northeast of Rock Springs: AI13-2,3 (Figure 2.3). This lava exhibits ramping in both the upper vitrophyre and lower lithoidal rhyolite portions (Figure 3.14). The lithoidal rhyolite layer shows signs of sheet jointing (Figure 3.14), due to coarse crystalline nature, this is a common feature of ramping. The lithoidal rhyolite is highly weathered and the pyroxenes (<1 mm) were oxidized. The upper vitrophyre (Figure 3.15) contains flow ramping above the lithoidal rhyolite and it is brecciated in places (carapace breccia). Carapace breccia is a typical characteristic of lavas (Manley, 1996; Manley, C.R., and McIntosh, 2002,). This brecciated vitrophyre, according to Bonnichsen and Kauffman (1987), is known as an autobreccia. This is a common feature in a silicic lava where the crust of a flow has been broken up and fragmented by movement of the flow interior. It is due to this stress that the crust fractures in a brittle manner, producing angular, smooth-faced blocks. Equant vitrophyric clasts in a fine-grained matrix are common for an autobreccia. Clasts in the breccia range up to boulder-sized (Figure 3.16). The vitrophyre has a waxy texture from devitrification. Phenocryst are abundant in the vitrophyre (40 to 45% by volume). The phenocryst assemblage includes quartz (1 to 4 mm), sanidine (2 to 4 mm; rare 1-2 cm), plagioclase (2 to 4 mm; rare 1 to 2 cm), as well as small pyroxene (Figure 3.17). The same crystal distribution in found in the lithoidal sample (AI12-2), except the phenocryst abundance is 35% by volume, which is lower than the vitrophyre sample (AI12-3).

The Dry Gulch Jarbidge Rhyolite is a massive lava approximately eight km northeast of the AI13-2,3 samples described above in the Dry Gulch valley (Figure 2.3). The eastern steep wall of the valley, which corresponds to a fault (Coats, 1987), is the Jarbidge Rhyolite lava. This lava comprised of multiple lobes approximately 35 to 50 m thick (Figure 3.18). These lobes are circular and resemble, on a much larger scale, the lobate form of basaltic pillow lavas, which indicates emplacement into water, most likely a Miocene lake. Bonnichsen (1982) describes subaerial lobes as part of the 13 to 7.5 Ma Bruneau-Jarbidge eruptive center and Branney et al. (2008) uses the presence of these lobes to help distinguishes Snake River-type lavas from ash-flow tuffs. There are also clear instances of ramping, as shown in Figure 3.18. The mineralogy of

the Dry Gulch Jarbidge Rhyolite is very similar to that of the other Jarbidge Rhyolite in the area. The phenocryst abundance is 30% by volume. The main crystal assemblage is quartz (1 to 2 mm), sanidine (1 to 3 mm), plagioclase (1 to 3 mm), oxides, and mafics (most likely pyroxenes). There were large sanidine crystals in the Dry Gulch Jarbidge Rhyolite, upwards of 6 mm in size.

MB11-1 was taken from Rock Springs, NV (Figure 2.3). It is the underlying rhyolite unit in the formation from Figure 3.8. The unit is different in physical appearance from the crystal-rich Jarbidge Rhyolite. The matrix is gray to pink and is much less weathered. It has a similar phenocryst assemblage as the Jarbidge Rhyolite, except these crystals are much smaller (1 to 2 mm) and less abundant (20% by volume). Some larger (3 to 4 mm) quartz and feldspar crystals are present, but they are rare. The main phenocryst phases visible in hand sample are quartz, sanidine, and plagioclase.

MB11-2 is a Jarbidge Rhyolite sampled off of Goose Creek Rd (Figure 2.3). The matrix is pink to purple, and is partially altered. Smoky quartz is abundant and ranges up to 0.6 cm in size. Plagioclase phenocrysts range up to 0.5 cm in length. Sanidine shows no alteration.

All examined Jarbidge Rhyolite display a porphyritic texture (20 to 40% phenocrysts by volume), and none have eutaxitic texture or fiamme, including the vitrophyre sample which would be the most likely candidate to preserve remnant glass shards and vitroclastic textures (Anderson and Branney, 2011). Overall, the rhyolites studied lack any indication of explosive eruptions. There are clear instances of ramping and lobes formed through rhyolite flows.

In summary, the Jarbidge Rhyolite I have sampled [1] show no macro- or microscopic pyroclastic textures, including in the vitrophyre (AI13-3); [2] have lobate morphologies (AI13-4); and [3] have autobreccias (AI12-2). Although the other textures (ramping, flow banding, breccias, sheet joints, etc.) are not clear indications of lava flows, as they can easily form from ash-flow tuffs, what I have seen is all mirrored and identical to those Jarbidge Rhyolite lavas studied by Brueseke et al. (2014). This is consistent and suggestive of lava origin.

Figure 3.1: AI12-1. A 5-m-thick basalt outcrop underlying sinter. The lava is characterized by an upper, vesiculated and oxidized zone (A) (e.g., quenched lava margin) and a lower, interior massive portion (B) that was sampled.

Figure 3.2: This basalt (AI12-1) sampled on Goose Creek Road (Figure 2.3) has a dark-gray fine matrix and is physically similar to SROT lavas that characterize the Snake River Plain.

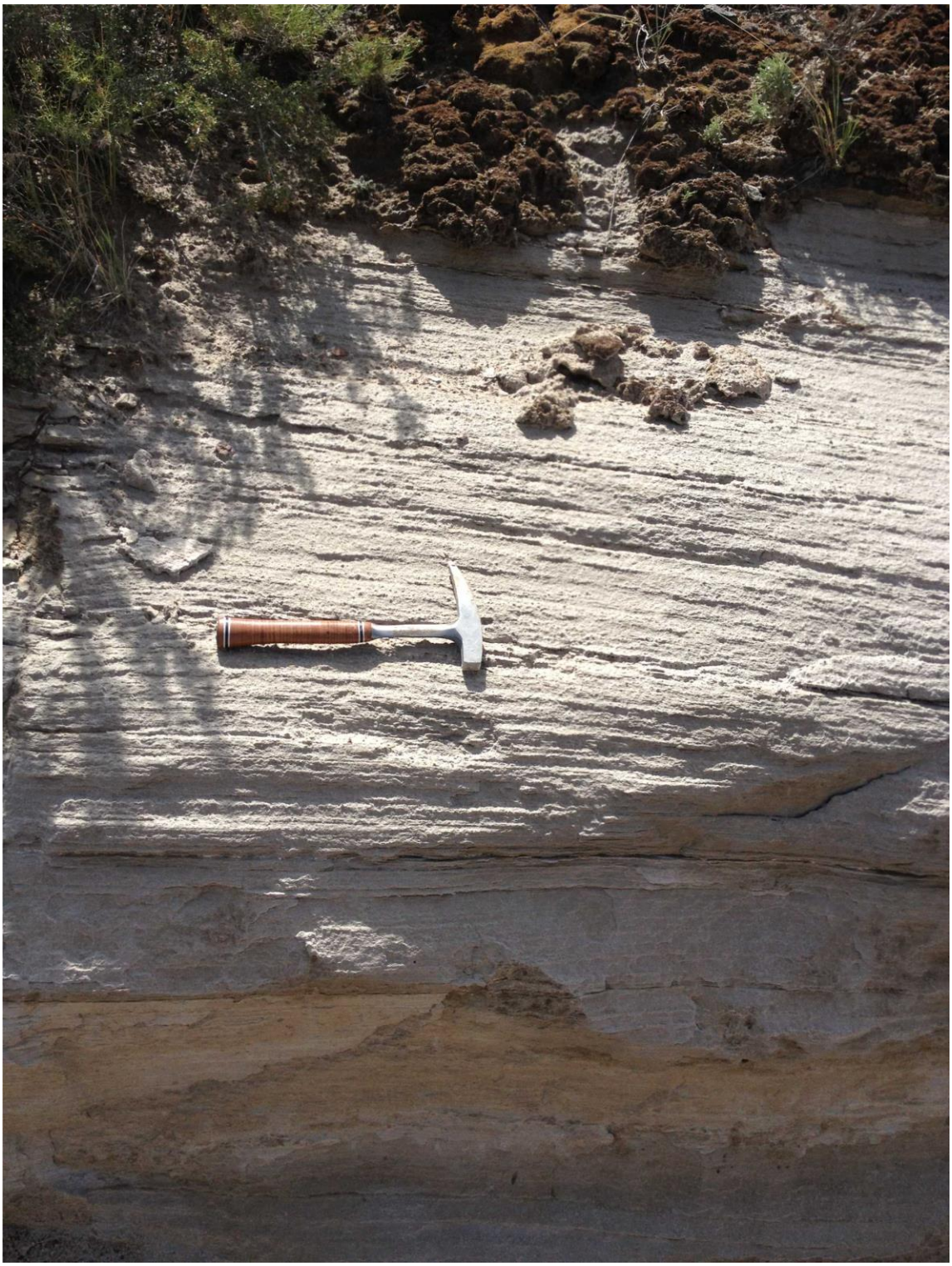

Figure 3.3: A bedded ash-fall deposit (AI12-2) on Goose Creek Road (Figure 2.3). The hammer is 30 cm long and is horizontal.

Figure 3.4: Here we sampled AI12-3 on Goose Creek Road (Figure 2.3), an ash-flow tuff. In the left side of the image two distinct units labeled with an 'A' and 'B' and a yellow line separating the two units. This is an ash-flow tuff that was poorly welded. The layers are from tilted beds, where unit 'B' is a basal vitrified layer sampled as AI13-5 and unit 'A' is the upper non-vitrophyric welded tuff, sample AI12-3, which was sampled near the right hand 'A'. It should be noted that the far A/B is likely an extension of these units, but were unsampled and cannot be confirmed aside from general morphology.

Figure 3.5: AI12-5. Vitrophyre in the process of devitrifying into "blades". The basal vitrophyre in Figure 5.4. The hand lens in the picture is 3 cm in length.

Figure 3.6: Ash-flow tuff sampled in ID along Birch Creek Road near City of Rocks (AI12-5). This outcrop is 70-m-thick.

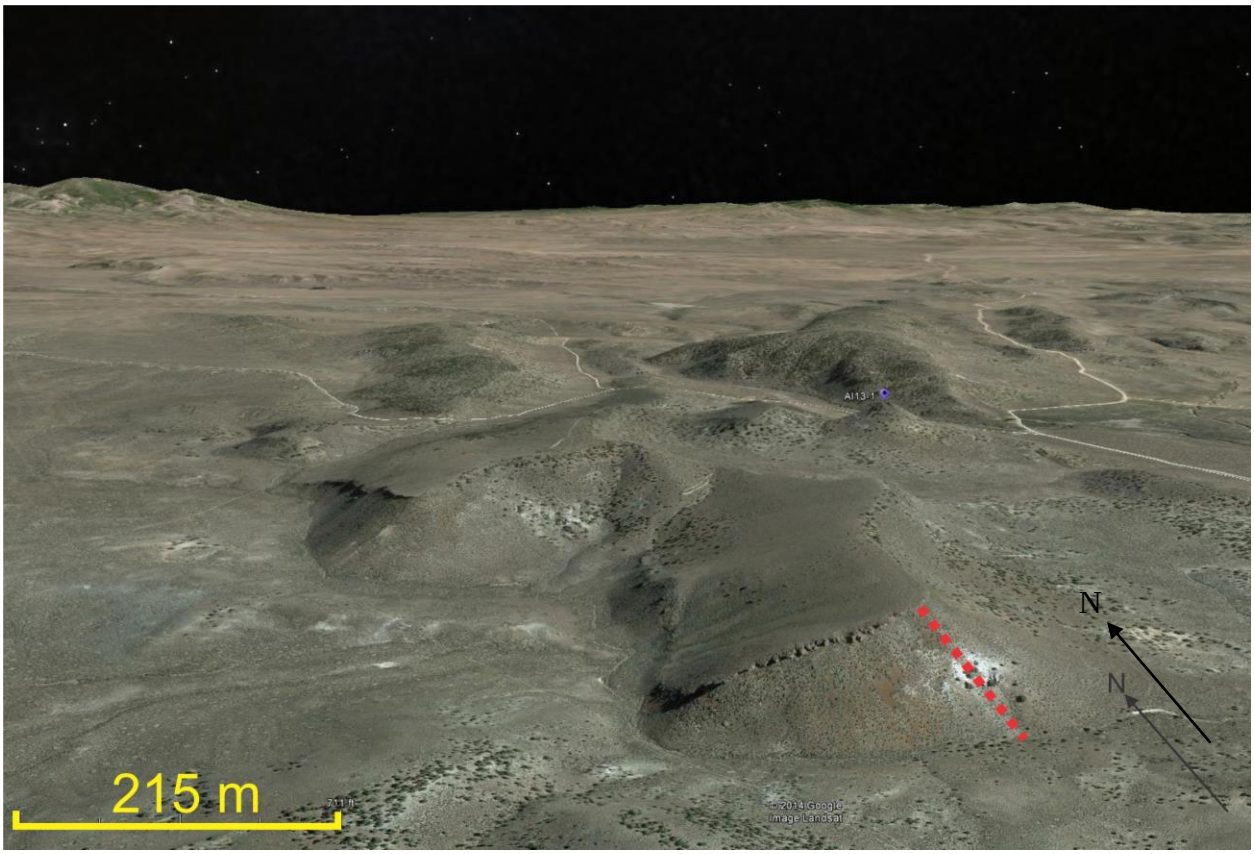

Figure 3.7: Image from Google Earth. The purple dot represents AI13-1 at Rock Springs (Figure 2.3). This image is oriented NE at the top, SW at the bottom of the image. These are fault-bounded hills (likely half-grabens, dipping to the west), where the normal fault trends NE-SW and is the front of the image in Figure 3.8. The red dashed line represents ~ approximate location of a generally east-dipping fault

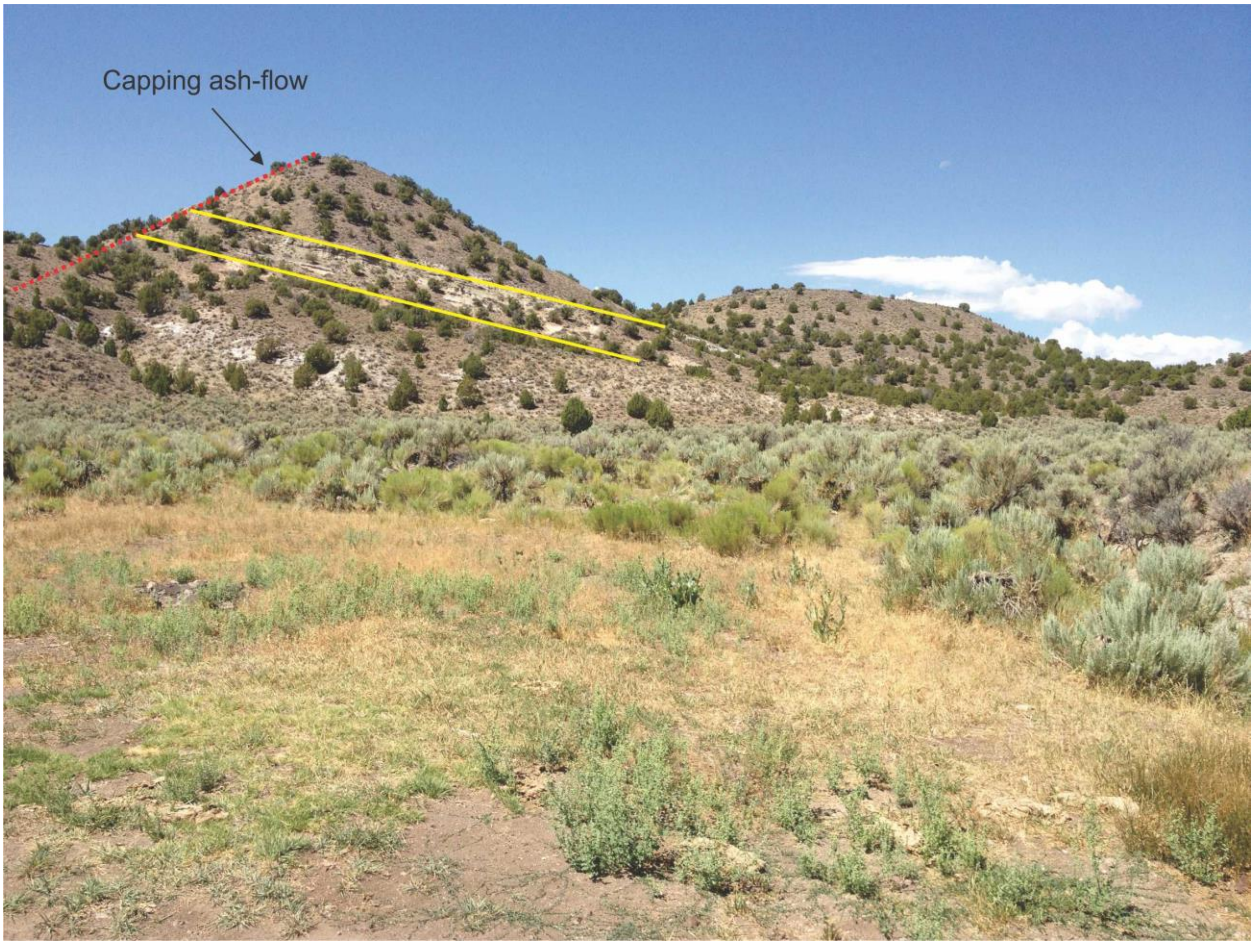

Figure 3.8: Photograph of sedimentary and volcanic strata of the Humboldt Formation, including a capping welded ash-flow tuff, exposed along a northeast (~5 m thick) trending normal fault (highlighted by a dashed red line) at Rock Springs. This forms a half-graben (Error! Reference source not found.**). The yellow lines outline an exposed air-fall tuff deposit, part of the Humboldt Formation. Sample AI13-1 was collected from the capping welded ash-flow tuff (highlighted with an arrow). Total thickness approximately 50 m.**

Figure 3.9: Close-up of exposed air-fall tuff unit at Rock Springs shown in Figure 3.8. The thickness of the unit here is ~1 m, but increases to 5 m on the eastern side. Bedding ranges in thickness from 1 to 5 cm.

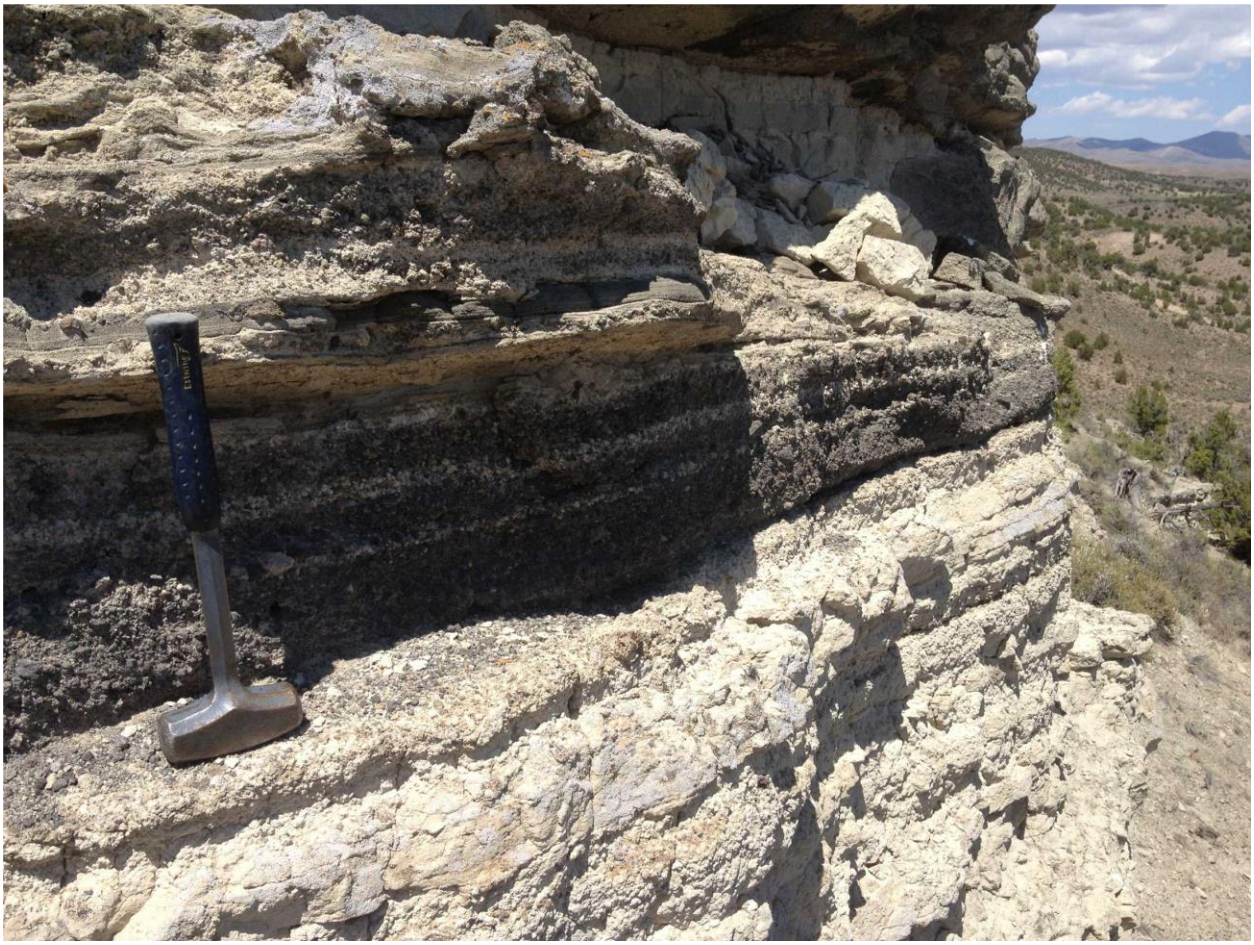

Figure 3.10: Close-up view of a basaltic lapilli tuff deposit in the Humboldt Formation strata exposed at Rock Springs, NV (Figure 2.3). Hammer is 40.6 cm long.

Figure 3.11: The capping welded tuff from Figure 3.8 (AI13-1) is divided into three distinct zones. Below the red line there is a basal vitrophyre characterized by abundant 5 to 7.5 cm spherulites (see Figure 3.12). Between the yellow and red lines the vitrophyre grades into non-vitrophyric welded tuff and is characterized by abundant, 10 to 13 cm long stretched lithophysae. The uppermost portion of the tuff (which was sampled) is highly welded and characterized by platy to blocky, sub-horizontal jointing. The outcrop is approximately 2.5 meters thick

Figure 3.12: Close up of spherulites in Figure 3.11. 40.6 cm long hammer for scale.

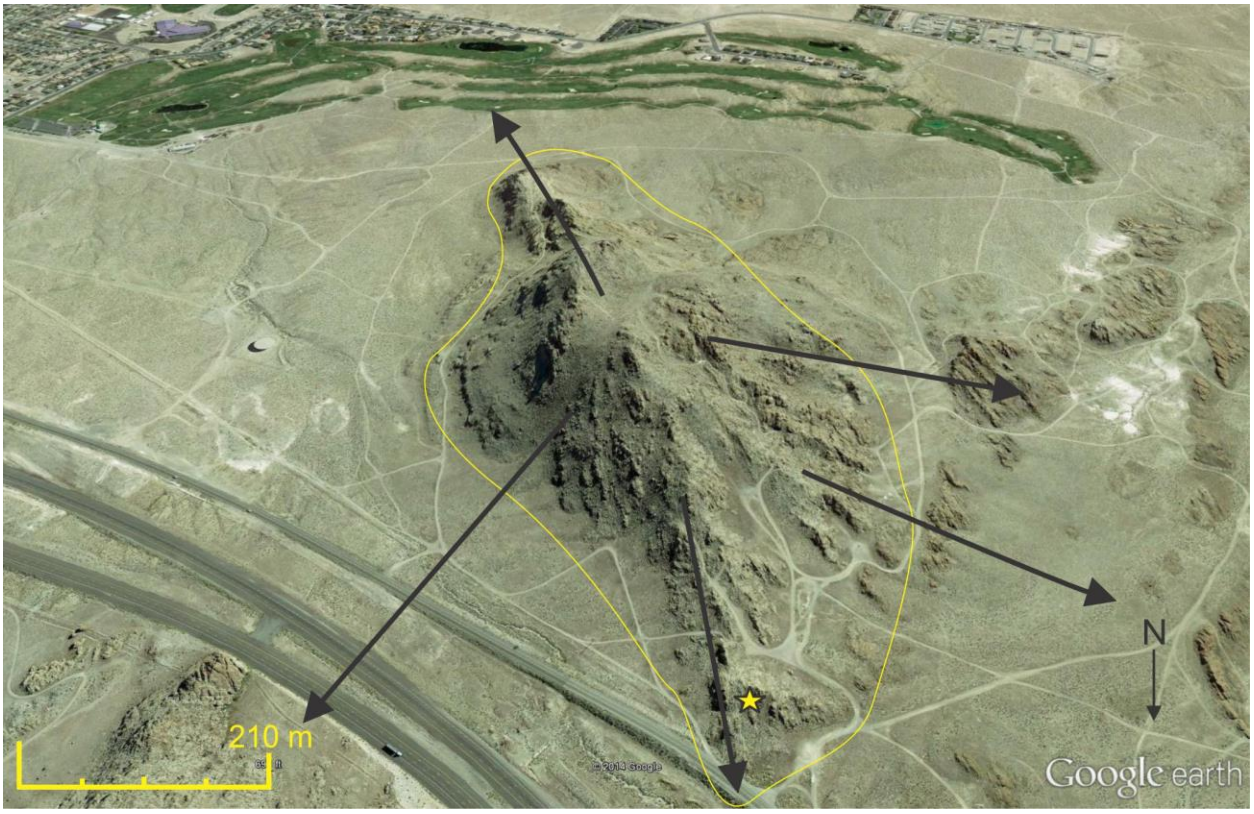

Figure 3.13: Google Earth image of inferred Jarbidge Rhyolite dome just west of West Wendover, NV along and under interstate I-80 (Figure 2.3). AI12-6 was collected from the starred location. Yellow outline is defined dome formation. Black arrows represent approximate outflow direction and correlated rhyolite lava on the right hand side as well as the bottom left hand corner of the photo.

Figure 3.14: Sample AI13-2 and -3. This is a photograph of Jarbidge Rhyolite off Goose Creek Rd., west of Dry Gulch, displaying ramping (Figure 2.3). The sub-horizontal lines are used to accentuate the sheet jointing that has occurred due to ramping. Carapace breccia lies within the yellow lines, lithoidal rhyolite lies below the bottom line. This is an upper vitrophyre breccia in contact with lithoidal rhyolite.

Figure 3.15: A13-3. Upper vitrophyric breccia (carapace breccia) of Jarbidge Rhyolite lava; vitrophyre blocks (autobreccia) are in an oxidized, fine-grained matrix and are up to 0.5 m long. Hammer is 40.6 cm in length.

Figure 3.16: AI13-3. Boulder of vitrophyre from Jarbidge Rhyolite upper breccia. Notice typical crystal-rich nature of the Jarbidge Rhyolite (crystals up to 2 to 3 cm). GPS unit on boulder is ~13 cm long.

Figure 3.17: AI13-3. Close-up of boulder in Figure 3.16. Quartz, plagioclase, and sanidine phenocrysts range from 2 to 4 mm. Plagioclase and sanidine crystals have a maximum size of 1-2 cm seen in the center plagioclase crystal (2 cm). 40 to 45% crystallinity.

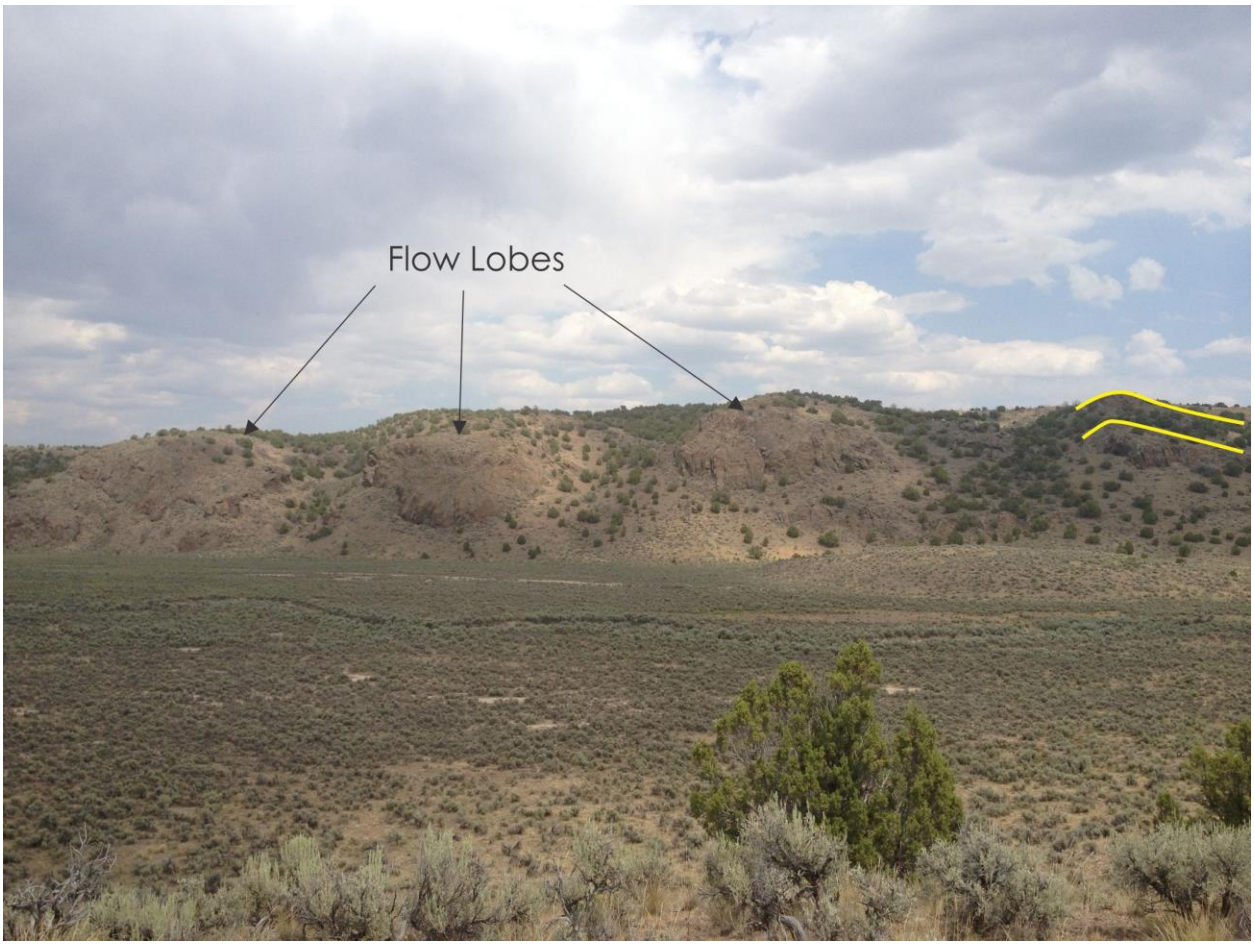

Figure 3.18: Sample AI13-4. Dry Gulch Jarbidge Rhyolite (Figure 2.3). Cross-sectional view of th lava exposed along normal fault shows at least three well-defined lobes, as well as potential ramping (right side of image). The lobes are circular and the joint-pattern, especially in the center lobe, resembles joint patterns in mafic pillow lavas. This outcrop is 35 to 50 m tall and is exposed for approximately 8 to 9 km in the Dry Gulch Canyon.

Chapter 4 - Petrography

Appendix A includes UTM coordinates and field notes of sample locations, petrographic description of samples, and point-counted modes for all Jarbidge Rhyolite and Rock Springs Rhyolite. Point counting occurred at KSU geology, using a 10x scope targeting 1000 counts per slide on a 1 x 1 mm grid. The average counts = 777 per slide.

4.1 Basalts

4.1.1 Hand Samples

Two basalt samples were collected: AI12-1 and MB11-3. In hand sample, the basalts have a dark-gray fine matrix with a vesicular texture and a phenocryst abundance of 30%. They are olivine-phyric and have plagioclase crystals up to 5 mm.

4.1.2 Thin Section

All samples collected are holocrystalline in thin section. The groundmass is composed mainly of plagioclase crystals laths that are subhedral to anhedral; it also contains olivines, pyroxenes, and oxides.

The two basalt samples contain a high percent of phenocrysts: MB11-3, 30%; AI12-1, 45% (Figure 4.1). Phenocryst phases in the basalts are plagioclase, orthopyroxene, clinopyroxene, olivine, sanidine, oxides. Plagioclase, olivine, orthopyroxene, and clinopyroxene are the primary mineral phases of the basalts. The few textures that appear throughout the basalts, including zoning feldspars and dual-sized plagioclase. All the mineral phases exhibit zoned rims, embayed crystals, and fracturing. Crystal modes are similar for the two samples. However, MB11-3 has much finer plagioclase crystals in the matrix than AI12-1.

Plagioclase is the most abundant mineral phase, occurring as both groundmass and phenocryst. It ranges from euhedral to subhedral, and is found to be anywhere from microcrystalline to 5 mm in length. Crystals show evidence of compositional zoning. Most of the plagioclase occurs in glomeroporphyritic clusters of plagioclase and olivine (Figure 4.1).

Olivine occurs in both the groundmass and as a phenocryst. It ranges from euhedral to anhedral and was 5 mm in length at its maximum. Textures include altered rims, embayments, and fracturing.

Clinopyroxene and orthopyroxene range from subhedral to anhedral and were also found in the groundmass and as phenocrysts. At its maximum, pyroxenes are 1 mm in length. Individual pyroxene crystal textures include intergrowths and fracturing.

Oxides occur in both the AI12-1 and MB11-3 samples and are thought to be magnetite.

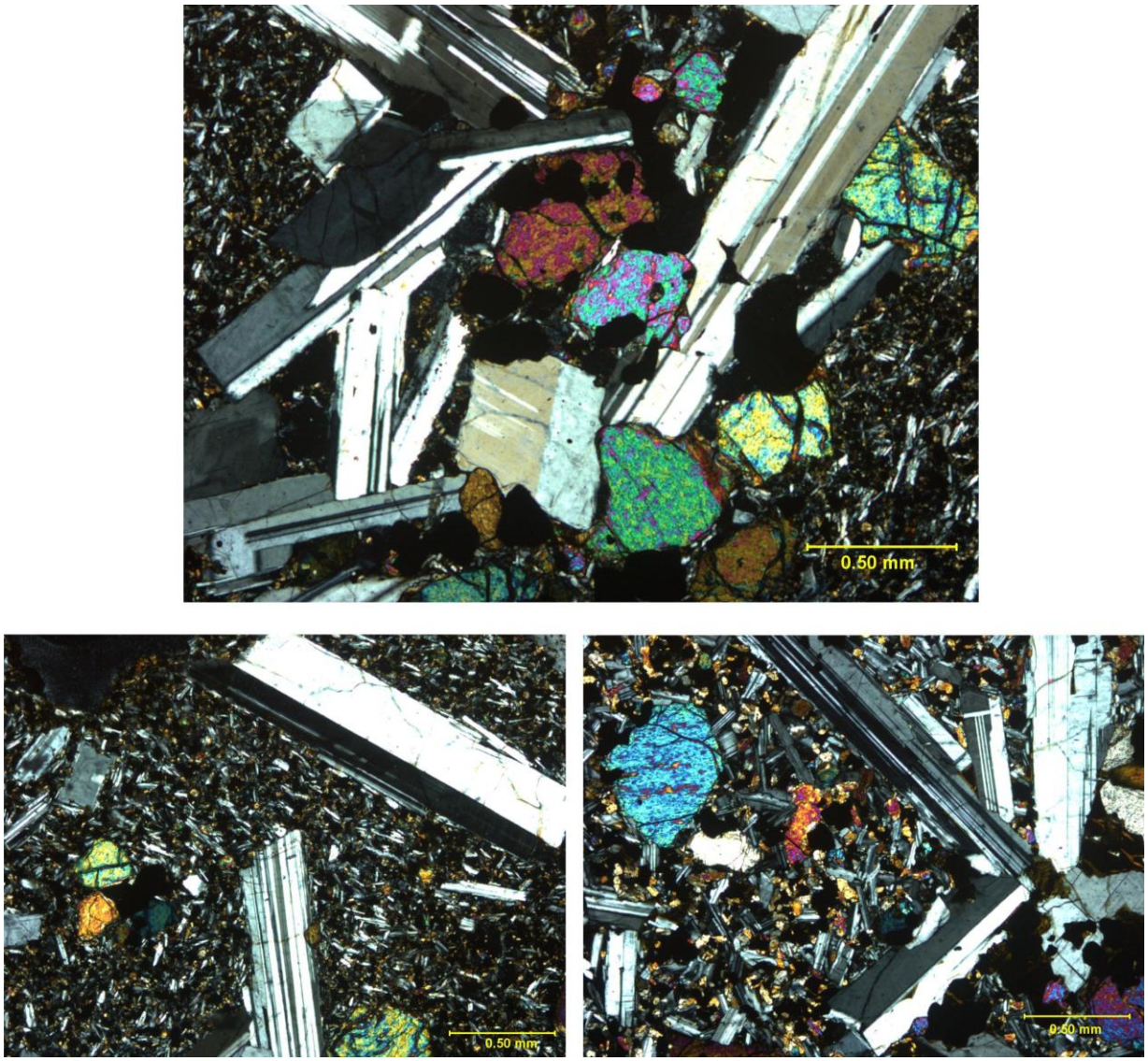

Figure 4.1: All images in XPL. The top image an example of glomeroporphyritic clusters of plagioclase and olivine. The left image is sample MB11-3 and shows the smaller groundmass crystals and fewer phenocrysts compared to the right image, AI12-6.

4.2 Ash-flow tuffs

4.2.1 Hand Samples

Five pyroclastic deposits were sampled. Three welded ash-flow tuffs (including a vitrophyric portion) were sampled in a similar location: Goose Creek (GC), one was taken from a massive outcrop near City of Rocks (CoR) along Birch Creek Rd., and the final was from Rock Springs (RS). The samples were either weakly or highly welded, with Rocks Springs and City of Rocks samples being more intensely welded. Both the Rock Springs and City of Rocks samples were massive blocky-joined tuffs. They also had a much higher phenocryst content (~10%), while the other three Goose Creek samples contained ~1 to 2% phenocrysts. The Rock Springs/City of Rocks phenocrysts included plagioclase (1 to 2 mm), sanidine (<=1 mm), pyroxene (1 mm), and quartz (<1 mm). The Goose Creek phenocrysts included plagioclase (1 mm), sanidine (1 mm), and some quartz fragments (<0.25 mm).

4.2.2 Thin Section

All samples collected are hypocrystalline in thin section. In the Goose Creek samples, the glassy groundmass is 98 to 99% of the sample. AI12-4 is the most poorly welded of the samples. AI12-3 and AI13-5 both have weakly welded groundmasses (Figure 4.2). The City of Rocks and Rock Springs samples, AI12-5 and AI13-1, have 10% and 15% phenocrysts respectively. The groundmass in both of these samples is very highly welded (Figure 4.2), showing mineral orientation in the direction of the flow.

Although the percentage of phenocrysts differs in the samples, the type, size, and overall textures remain similar. Phenocryst phases in the ash-flow tuff samples are quartz, sanidine, plagioclase, ± Fe-Ti oxides, ± clinopyroxene, ± orthopyroxene, ± hornblende, ± biotite, ± zircon, ± monazite. Quartz, plagioclase and sanidine are the primary phenocryst phases. Open system textures are very minimal compared to the Jarbidge Rhyolite, but include embayment, skeleton, zonation, and inclusion textures. Both the RS/CoR contained a higher quantity (3% versus <1%) and size of pyroxenes (Figure 4.2), specifically they contained orthopyroxene, which the GC samples did not. As well, the RS/CoR samples had a few oxidized hornblende crystals (<1 mm), which again the GC samples did not.

In thin section, quartz crystals are subhedral to anhedral, varying in size from microcrystalline to 2 mm. Quartz textures include embayments and parallel fracturing. Of the primary minerals, it is least abundant (<1% by volume in GC; 3% in RS/CoR).

Sanidine crystals are more common, ranging from subhedral to anhedral. Their size varies from microcrystalline to 2 mm. Sanidine rarely shows simple twinning in the samples. Textures for sanidine in the Tertiary ash-flow tuffs include zoning, embayments, skeletal, and plagioclase inclusions in a few instances.

Plagioclase crystals were equally as common as sanidine crystals in most samples. Like sanidine, they were subhedral to anhedral. Their size varies from microcrystalline to 2 mm. Plagioclase often shows albite twinning and common textures include skeletal, embayment, zonation, and sieve crystals.

Clinopyroxene and orthopyroxene are subhedral to anhedral where they appear (orthopyroxene only appears in the RS and CoR samples). In all instances they are under 1 mm in length and most crystals show alteration rims. Oxide phases (e.g., magnetite and ilmenite) occur in all samples, more so in the RS/CoR samples due to the higher phenocryst abundance by volume.

Accessory phases include zircon and monazite. Zircon occurs as independent crystals, within plagioclase clots, in groundmass, and as inclusions in clots and feldspars. It is euhedral to subhedral, while monazite is subhedral. Monazite was found only in the Rock Springs ash-flow tuff.

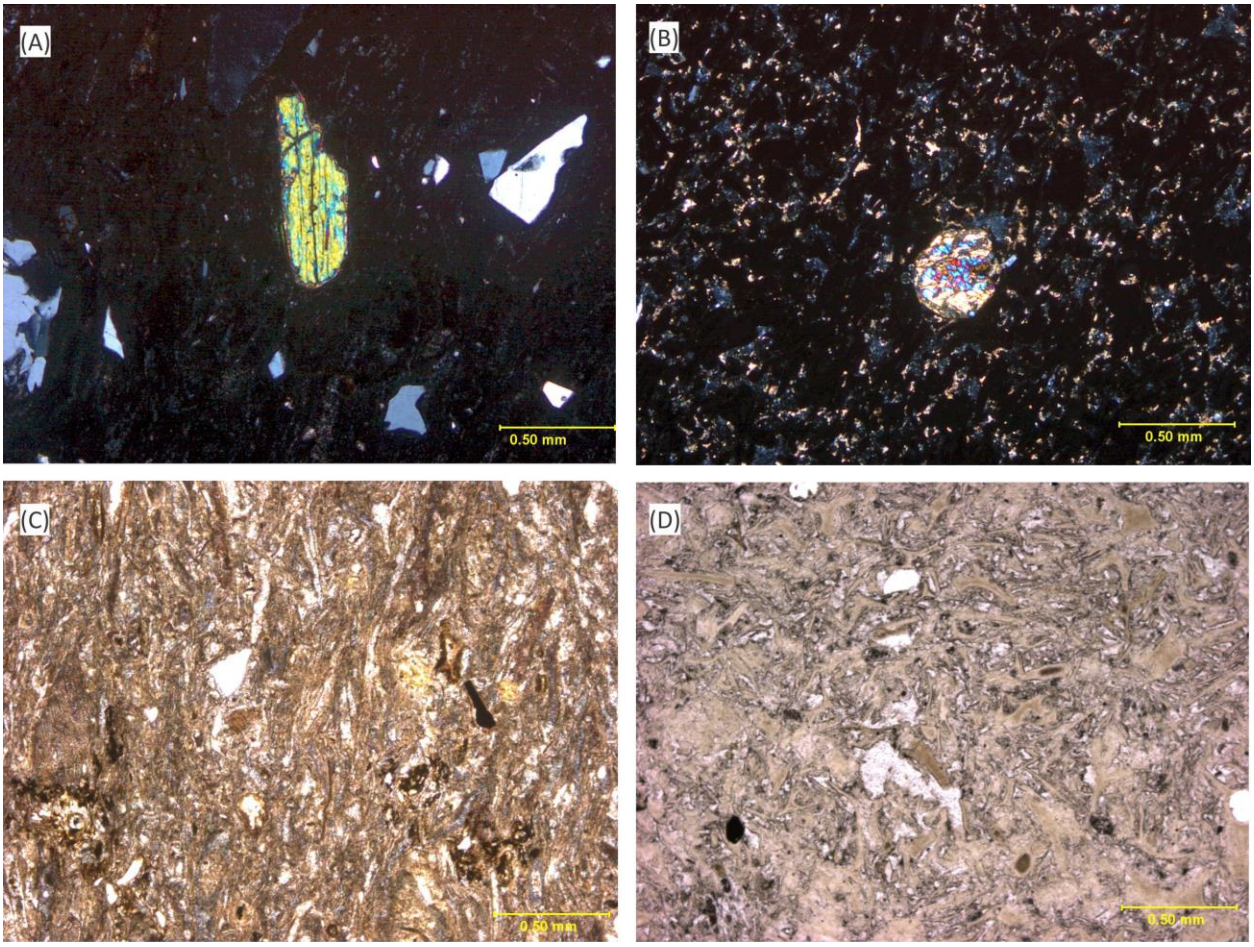

Figure 4.2: Both (A) and (B) images in XPL. Both (C) and (D) are in PPL. (A) is a clinopyroxene and shows the typical size of a pyroxene in the RS/CoR samples, while (B) shows the maximum size of the clinopyroxene in the Goose Creek samples and is one of the only pyroxenes found. C) shows the high degree of welding from AI13-1, as well as the brown matrix color. (D) shows the lower degree of welding (AI12-3), as well as the tan to grayer matrix color.

4.3 Jarbidge Rhyolite and Rock Springs Rhyolite

4.3.1 Hand Samples

Six Jarbidge Rhyolite samples were collected from the field as well as one Rock Springs Rhyolite sample. The Jarbidge Rhyolite units I studied have a phenocryst abundance of 30 to 40 modal %, while the Rock Springs Rhyolite has a phenocryst abundance of 20%. They are all considered to be smoky quartz-phyric. The smoky quartz is typically 2 to 4 mm in size in the Jarbidge Rhyolite (1-3 mm in Rock Springs Rhyolite), but can be found upwards of 2 cm (West Wendover, NV) and the majority of the quartz is fractured and subhedral. Both plagioclase and sanidine are also phenocrysts in the Jarbidge and Rock Springs Rhyolite. In hand samples, the plagioclase is an average of 1 to 4 mm and has reaction rims and is typically subhedral. Sanidine is indistinguishable from plagioclase in most samples, but is 1 to 4 mm in length. Finally, altered mafics, in most cases pyroxenes (however some are too altered to tell in hand sample), can be found in the hand samples of a select number of rhyolites (AI12-6, AI13-2). In the case of West Wendover, NV Jarbidge Rhyolite (AI12-6), they are ~0.5 to 1 mm in size and are altered almost completely into an oxide (possibly magnetite or hematite, but again indistinguishable in hand sample).

4.3.2 Thin Section

Six samples of Jarbidge Rhyolite and one sample of rhyolite from Rock Springs were described petrographically and also point-counted. The seven rhyolite samples are holocrystalline to hypocrystalline. The single vitrophyre sample collected (AI13-3) has a glassy groundmass. The lithoidal rhyolite samples are devitrified and contain microcrystalline feldspar, quartz, and oxides as well as accessory minerals in their matrix. Common accessory minerals in the Jarbidge Rhyolite samples are zircon and apatite; in the Rock Springs rhyolite (MB11-1), monazite is present in the groundmass. Pilotaxtic groundmass is found in some of the rhyolites. Many of the samples' groundmass contains needle-like radial sanidine clusters due to devitrification and one sample (AI13-4) shows banding (Figure 4.3).

Phenocryst phases in the Jarbidge Rhyolite are quartz, sanidine, plagioclase, Fe-Ti oxides, ± clinopyroxene, ± orthopyroxene, ± garnet, ± zircon, and ± apatite. Quartz, plagioclase and sanidine are the primary mineral phases and average modal proportions are as follows: quartz (20.5%), plagioclase (5.25%), and sanidine (7.15%), while the ranges are as follows:

quartz (18-24 %), plagioclase (2-8%), and sanidine (3-10%). The modal proportions of the Rock Springs rhyolite are as follows: quartz (15%), plagioclase (3%), and sanidine (4%). Open system textures are common and vary between samples. Open system textures include: oscillatory zoning, patchy zoning, spongy (sieve) and boxy cellular texture and reactions rims. These were found mostly in the plagioclase and sanidine. However, quartz exhibited dissolution rims. The Rock Springs rhyolite had the only case of myrmekitic texture of plagioclase and quartz intergrowth (Figure 4.3).

Quartz crystals range from euhedral to anhedral and vary in size from microcrystalline to 4 mm in length. Quartz has the highest modal percentage of the primary minerals, ranging from 18 to 24 % by volume. Textures that are common within the rhyolites include fracturing (parallel) and embayments (Figure 4.4). Independent crystals may be linked by crystallographic orientations, indicating that these now separate crystals are structurally connected. Plagioclase was found as inclusions within the quartz crystals (Figure 4.4).

Sanidine crystals rarely had simple twinning and had to be separated from quartz crystals via analysis of their optic sign or cleavage. Sanidine occurs as euhedral to anhedral crystals, with a size range from microcrystalline to 4 mm; however a small subset of crystals (AI13-2; AI12-6; AI13-3) were 6 to 7 mm in length. Sanidine has the second highest modal percentage of the primary minerals, ranging from 3 to 10% by volume. Textures include parallel fracturing, clots, plagioclase inclusions, zoning, sieving, embayment, spongy, and skeletal. Several samples contain plagioclase inclusions within sanidine phenocrysts. Groundmass sanidine exhibits pilotaxtic texture (AI13-2).

In thin section, plagioclase is subhedral to anhedral. The size of a single crystal ranges from microcrystalline to 3 mm, but has been found to exceed 6 to 7 mm in some cases (MB11-2; MB11-1). Textures include sieve, clots, skeletal, patchy, spongy (Figure 4.4), and boxy. Plagioclase clots are common and typically include zircon, apatite, Fe-Ti oxides, pyroxenes and altered mafic phases (Figure 4.4).

The Jarbidge Rhyolite contain both orthopyroxene and clinopyroxene, which range from anhedral to subhedral. The Rock Springs Rhyolite does not contain pyroxenes. In all cases both ortho- and clinopyroxenes are highly altered septo-altermorphs. The secondary mineral in this alteration is magnetite. The pyroxenes are all less than 1 mm and mostly range from 0.1 mm to 0.5 mm. The only textures they exhibit are fracturing and heavy rimming alteration. The Fe-Ti

oxides phases include both magnetite and ilmenite, based on higher pleoclorism. Sizes vary from groundmass to several mm. No other mafic minerals were observed.

Accessory minerals include zircon and apatite in the Jarbidge Rhyolite and Rock Springs Rhyolite and monazite in only the Rock Springs Rhyolite. Zircon is ubiquitous in the samples and occurs as single crystals, in inclusions, and within the groundmass. It ranges from euhedral to subhedral. Euhedral apatite is found mostly in groundmass and inclusions. They were 0.25 to 0.5 mm in length, although some were much smaller.

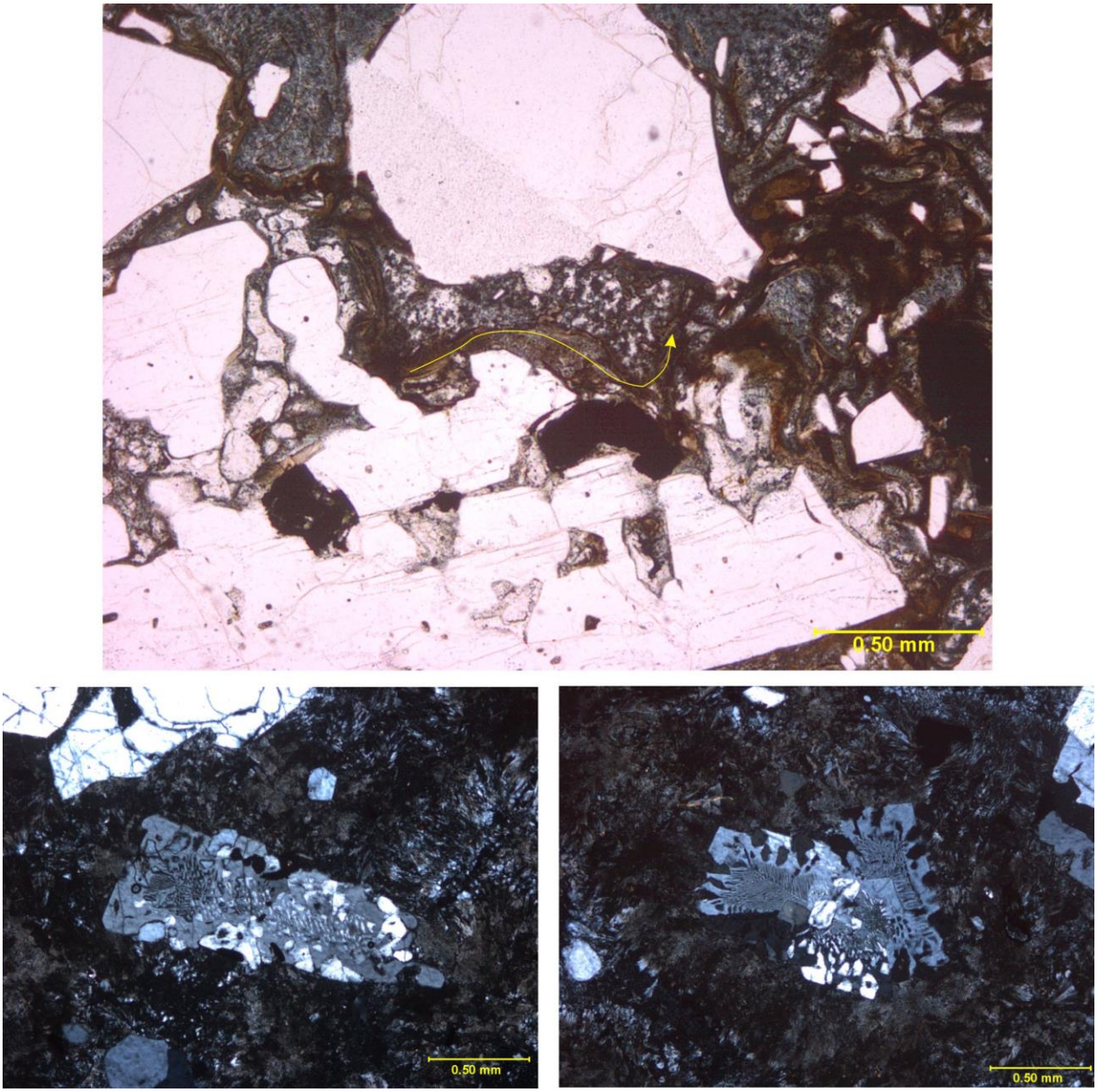

Figure 4.3: Top image shows flow banding around crystals in sample AI13-4. Bottom two images are of sample MB11-1, the Rock Springs Rhyolite is the only example of the myrmekite texture.

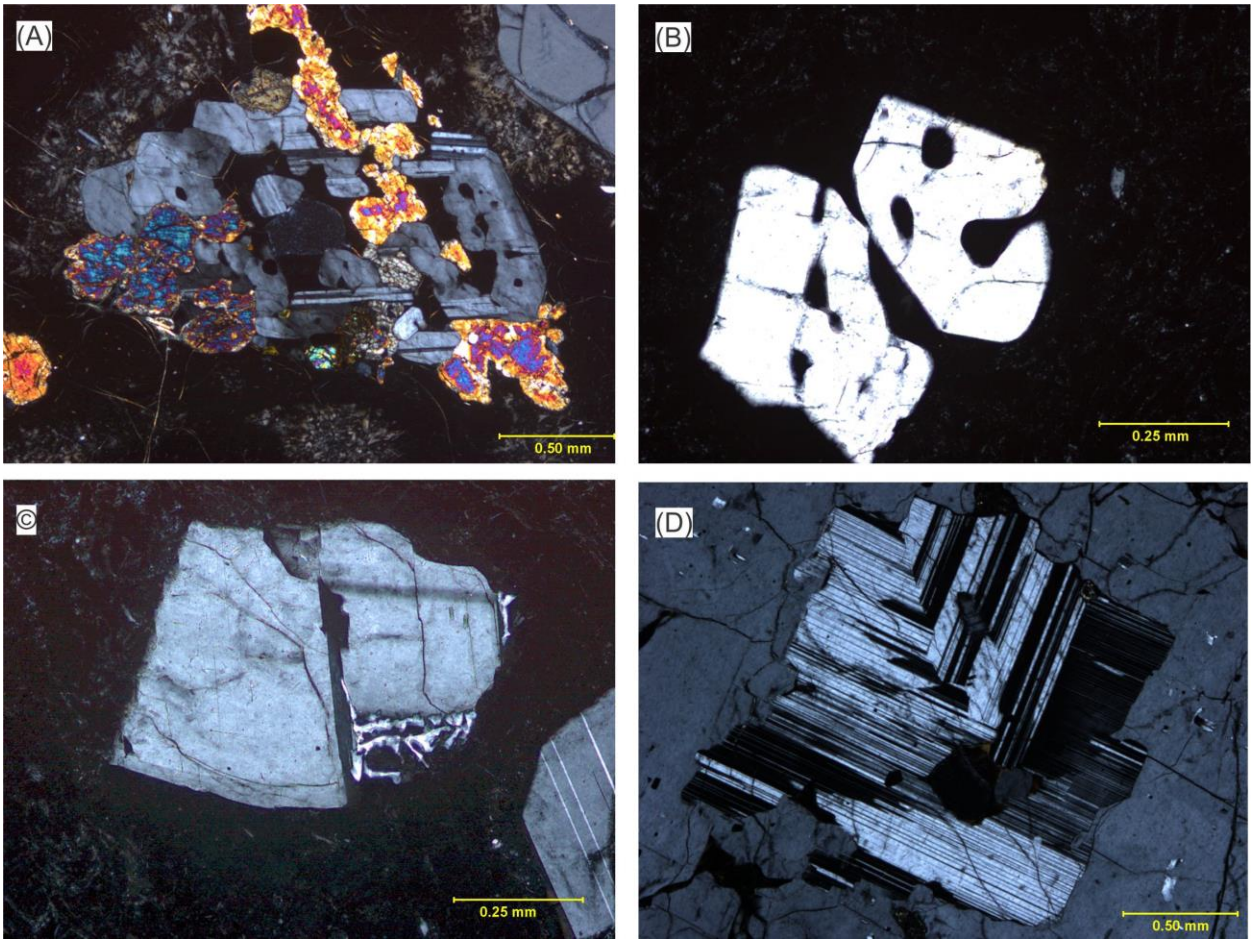

Figure 4.4: A) Represents clotting/cumulate texture in the Jarbidge Rhyolite (plagioclase, pyroxene, and quartz). B) Quartz embayments in vitrophyre. C) Spongy texture in the bottom right of the plagioclase crystal. D) Plagioclase inclusion in a large (5 mm) quartz crystal.

Chapter 5 - Geochemistry

Major and trace element data were obtained on 14 samples (seven rhyolite lavas, five ash-flow tuffs, and two basalts). Major elements are reported in weight percent (wt. %) oxide and trace and rare earth elements are reported in parts per million (ppm). In this discussion and in all geochemical diagrams, major element data are reported 100% anhydrous. Raw chemical data (major, trace, LOI, and totals) can be found in Appendix B.

5.1 Classification and Major Element Geochemistry

On the total alkali silica diagram of Lebas et al. (1986), the six Jarbidge Rhyolite, Rock Springs rhyolite, and the ash-flow tuffs plot as rhyolites (Figure 5.1). All of these samples plot within the A-type felsic magma field of Whalen et al. (1987) (Figure 5.2). According to Patino Douce (1997) as well as Whalen et al. (1987), A-type rhyolites are characterized as having a high FeO/MgO and $(Na_2O+K_2O)/Al_2O_3$ ratio as well as low Al and Ca contents compared to calc-alkaline silicic magmas. All of these samples also plot as meta- to slightly peraluminous on the Shand's Index by Maniar-Piccoli (1989), though the ash-flow tuffs are dominantly peraluminous (Figure 5.3).

5.1.1 Basalts

The two samples of basalt, MB11-3 and AI12-1, plot on the total alkali silica diagram (TAS) by Lebas et al. (1986) in the tephrite-basanite field (Figure 5.1); since they are olivine and plagioclase-phyric, they are considered basalts. On an AFM diagram, the two samples plot in the tholeiitic field (Figure 5.4) and when their normative mineralogy is considered via CIPW calculations and the basalt tetrahedron, they fall in the olivine tholeiite field (e.g., lack normative nepheline)(Figure 5.4).

The basalt samples in this study are low in silica ranging from 41.5 to 43.6 wt. %, with an average of 42.5 wt. % silica. The samples have higher CaO (9.21 to 9.36 wt. %), MgO (5.06 to 5.56 wt. %), and TiO_2 (4.23 to 4.38 wt. %) compared to the rhyolites, while K_2O (0.44 to 0.63 wt. %) is lower. The samples also have high values of FeO*(18.7 to 20.05 wt. %) and Al_2O_3 (12.59 to 13.25 wt. %) (Figure 5.6).

5.1.2 Ash-flow Tuffs

The sampled ash-flow tuffs are meta- to slightly peraluminous. This means that ASI plots with a range of 0.98 to 1.08 and a mean ASI of 1.02. The ash-flow tuffs have a FeO# range of ~ 0.89 to 0.94, with a mean Fe# of 0.92 (Table 1). According to Frost et al. (2001), this range classifies these samples as ferroan. Plotting these ash-flow tuffs on the MALI diagram, shows they are alkali-calcic (Figure 5.3).

Table 1: FeO# for tertiary ash-flow tuffs.

Sample	SiO_2	FeO*	MgO	FeO#
AI12-3	71.92	2.02	0.24	0.89
AI12-4	72.25	2.11	0.24	0.90
AI12-5	74.21	2.76	0.19	0.94
AI13-1	75.11	2.24	0.17	0.93
AI13-5	71.71	2.44	0.16	0.94

The silica range of the sampled tuffs is between 71.7 to 75.1 wt. % and the average silica concentration is 73.0 wt. %. There are two groupings of samples according to silica: three samples (Goose Creek Tuffs) that range from 71.7 to 72.3 wt. % and two samples that range from 74.2 to 75.1 wt. % (RoC and RS tuffs). There is a separation of the major element oxides between these two groupings. The higher silica group has lower CaO, MgO, and K_2O. They also have distinctly higher FeO*and Na_2O, as well as showing no change in Al_2O_3, TiO_2, and P_2O_5 (Figure 5.5). When compared to the rhyolite lavas a distinguishable difference can be noted. The ash-flow tuffs, specifically the GC tuffs, have a higher K_2O value (>5 wt. %). Although they have an inverse CaO trend with respect to increasing silica just like the rhyolite lavas, for the same wt. % of silica the values for CaO are much lower.

5.1.3 Jarbidge Rhyolite and Rock Springs Rhyolite

The Jarbidge Rhyolite samples have an Aluminum Saturation Index (ASI) range of 0.93 to 1.04 with an average of 1.00. According to Frost et al. (2001), Jarbidge Rhyolite samples are defined as ferroan, having an Fe#= ~0.75 to 0.98 (all but one sample are above 0.90) with a mean Fe# of 0.93 ($FeO\# = FeO_{tot}/(FeO_{tot}+MgO)$ (Table 2). This, according to Frost et al. (2001), confirms that Jarbidge Rhyolite is indeed an A-type rhyolite, rather than a Cordilleran granite/rhyolite. When plotted on the Modified Alkali Lime Index (MALI), the Jarbidge Rhyolite

samples plot as mostly calc-alkalic, though a few lie in the alkali-calcic field (Figure 5.3). The Rock Springs Rhyolite has a Fe# of 0.97, this defines it as ferroan according to Frost et al. (2001). The Rock Springs Rhyolite also has an ASI of 1.04, which categorizes it according to Frost et al. (2001) as an A-type rhyolite. The wt. % silica of the Rock Springs Rhyolite is too high to be accurately plotted on a MALI diagram. This is likely due to post-emplacement silicification, which can be seen in the amorphous quartz alteration in the groundmass of MB11-1.

Table 2: FeO# data inferring ferroan or magnesian for the lithoidal rhyolites. ***Frost et al. (2001)***

Sample	SiO_2	FeO*	MgO	*FeO#*
AI12-6	76.98	1.36	0.15	*0.90*
AI13-2	75.84	1.03	0.34	*0.75*
AI13-3	73.74	2.81	0.09	*0.97*
AI13-4	75.52	3.00	0.05	*0.98*
MB11-2	78.42	2.55	0.04	*0.98*
MB11-1	76.41	1.34	0.05	*0.97*
JC-09-22	77.39	1.29	0.05	0.96

The sampled Jarbidge Rhyolite are all high in silica, which ranges from 73.7 to 78.2 wt. % with an average silica value of 76.3 wt. %. It is difficult to distinguish a relationship between the major oxides and an increase in silica. However, CaO has an inverse relationship, while Na_2O and K_2O are unchanged with respect to an increase silica (Figure 5.5).

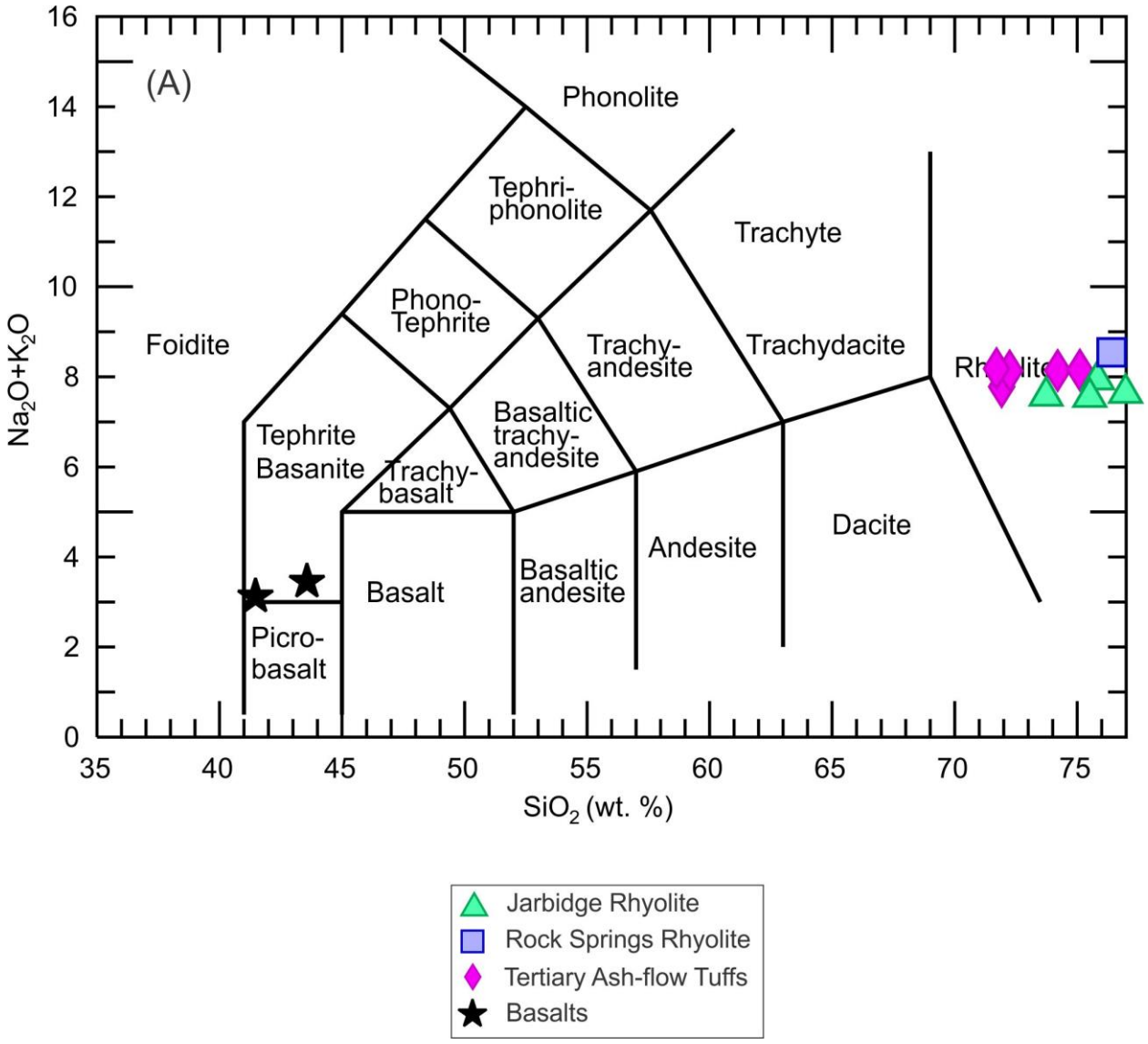

Figure 5.1: Figure (A) is a TAS diagram of Lebas et al. (1986). The samples plot as rhyolite for the Jarbidge and Rock Springs Rhyolites as well as the ash-flow tuffs. The basalt samples plot as Tephrite Basanite.

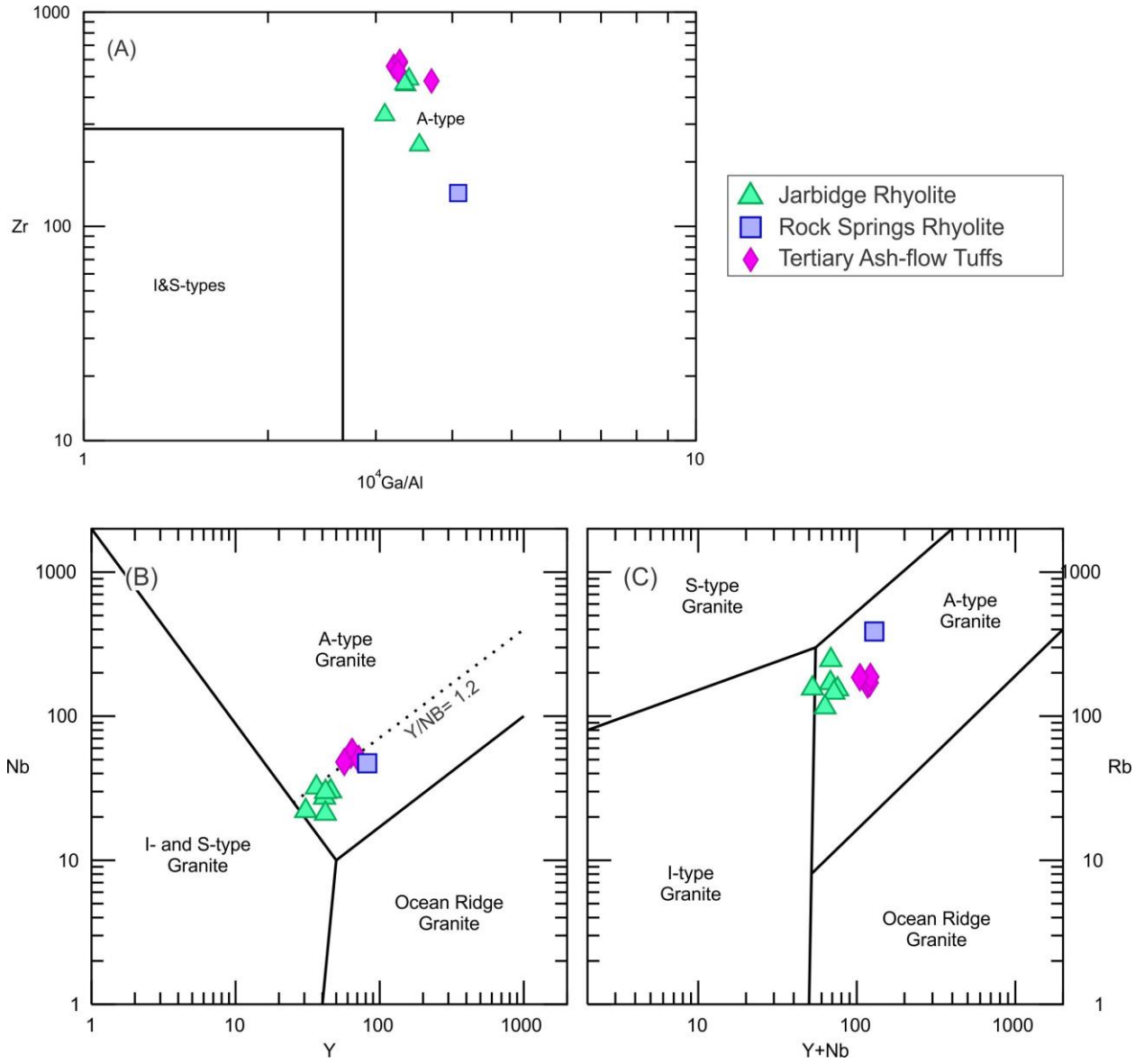

Figure 5.2: Diagrams that show different methods of granite type classification. In (A), (B), and (C) the rhyolites all plot as A-type granite. (A)Whalen et al. (1987); (B) Pearce et al. (1984); (C) Pearce et al. (1984)

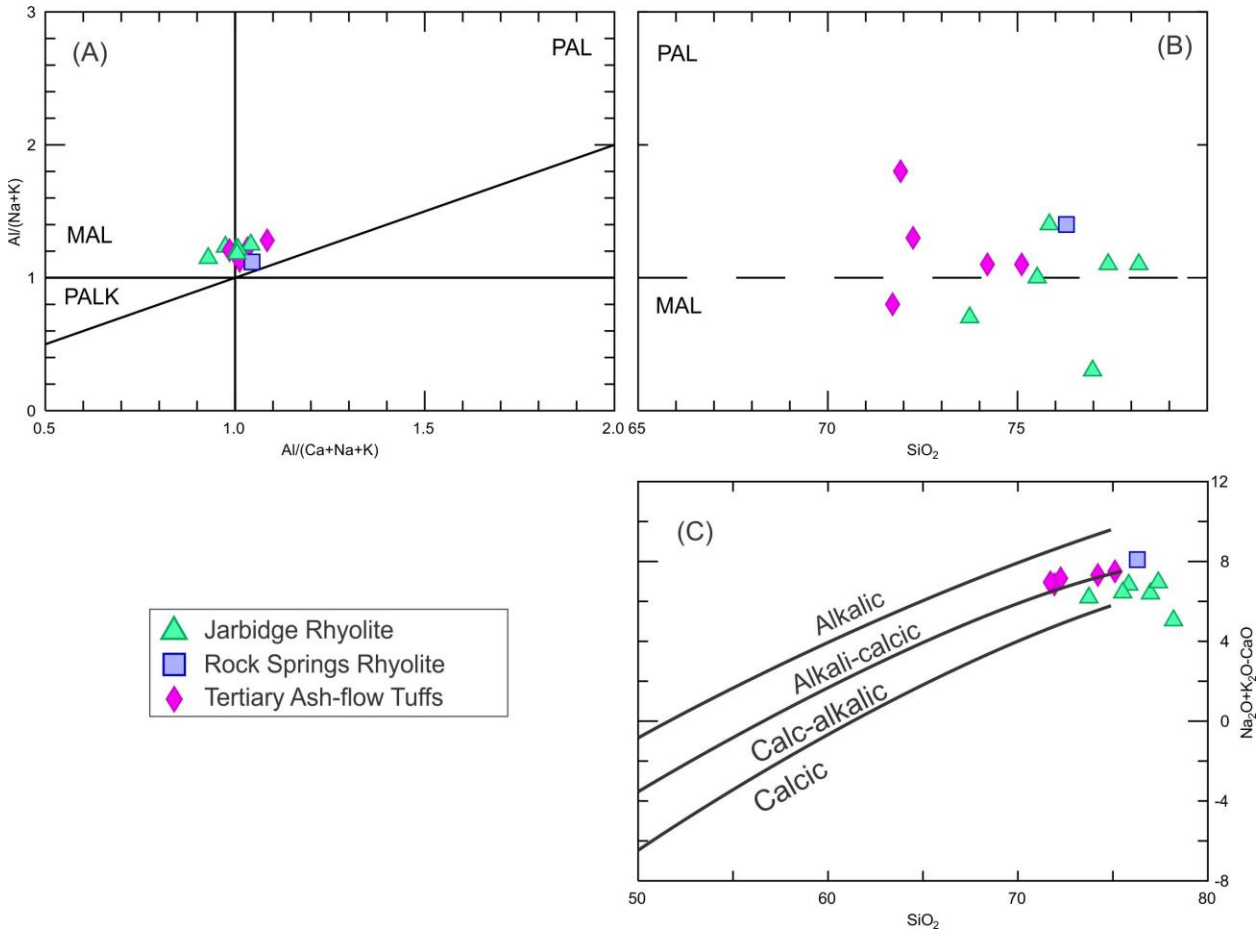

Figure 5.3: (A) Aluminum Saturation Index (ASI) plot (Maniar and Piccoli, 1989). Abbreviations are MAL= metaluminous field, PAL=peraluminous, PALK=peralkaline field. (B) Diagram that shows metaluminous vs. peraluminous compositions. The dashed line represents the separation between the two fields. (C) Modified Alkali Lime Index (MALI) plot (Frost et al., 2001). Jarbidge Rhyolite samples are dominantly calc-alkalic, while the ash-flow tuffs plot mainly as alkali-calcic. The Rock Springs rhyolite is outside the MALI plot range according to Frost et al. (2001) due to a high silica wt. %.

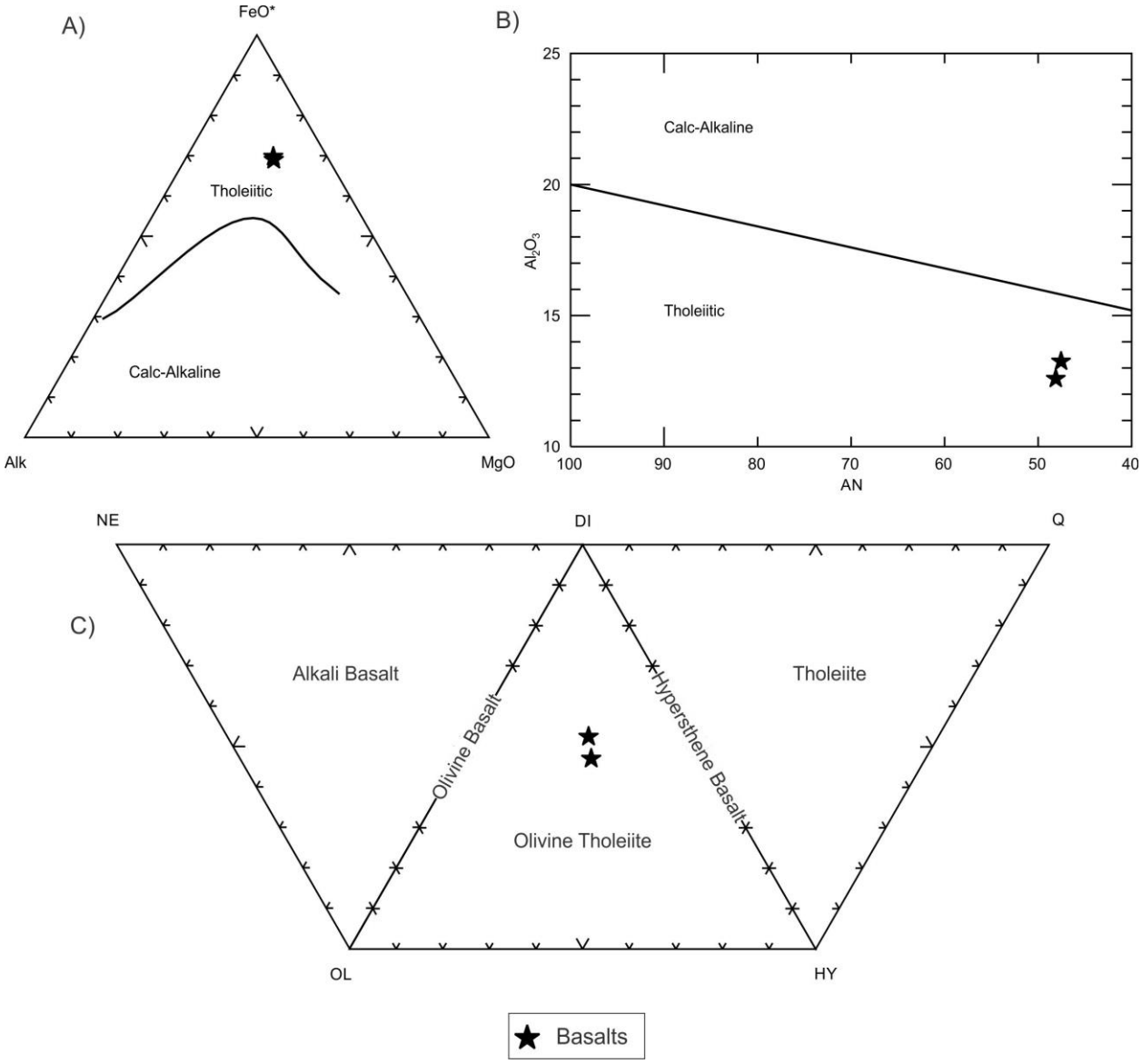

Figure 5.4: Classification diagrams for basalts. Diagrams 'A' and 'B' indicate tholeiite origin. Diagram 'C' further constrains the basalt samples using a fundamental basalt tetrahedron (Yoder and Tilley, 1962). The tetrahedron has been expanded and flattened to fit the page.

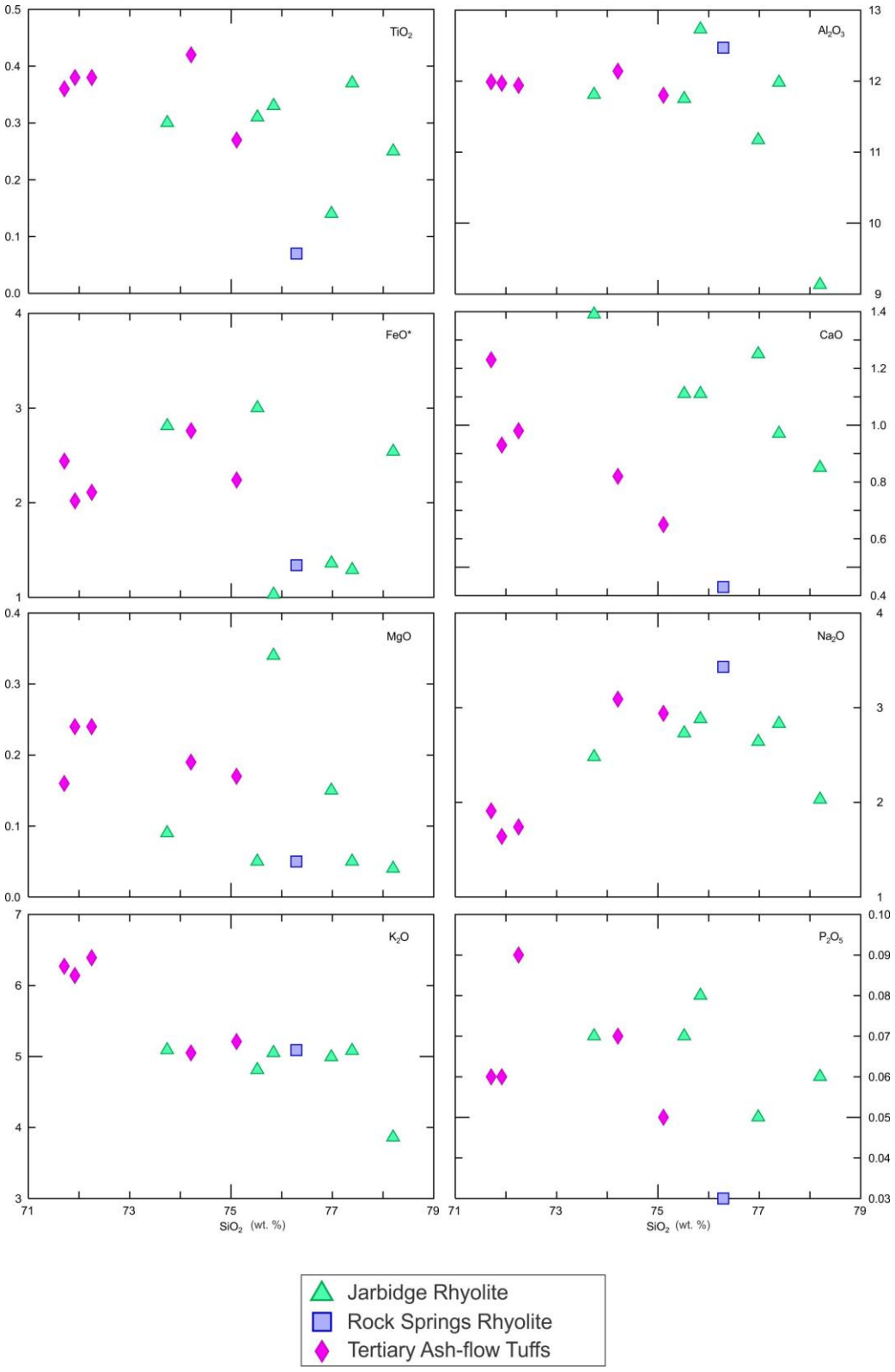

Figure 5.5: Harker diagrams of the felsic rocks with major element oxides identified in the upper right corner of the diagrams. All major elements are plotted as wt. %.

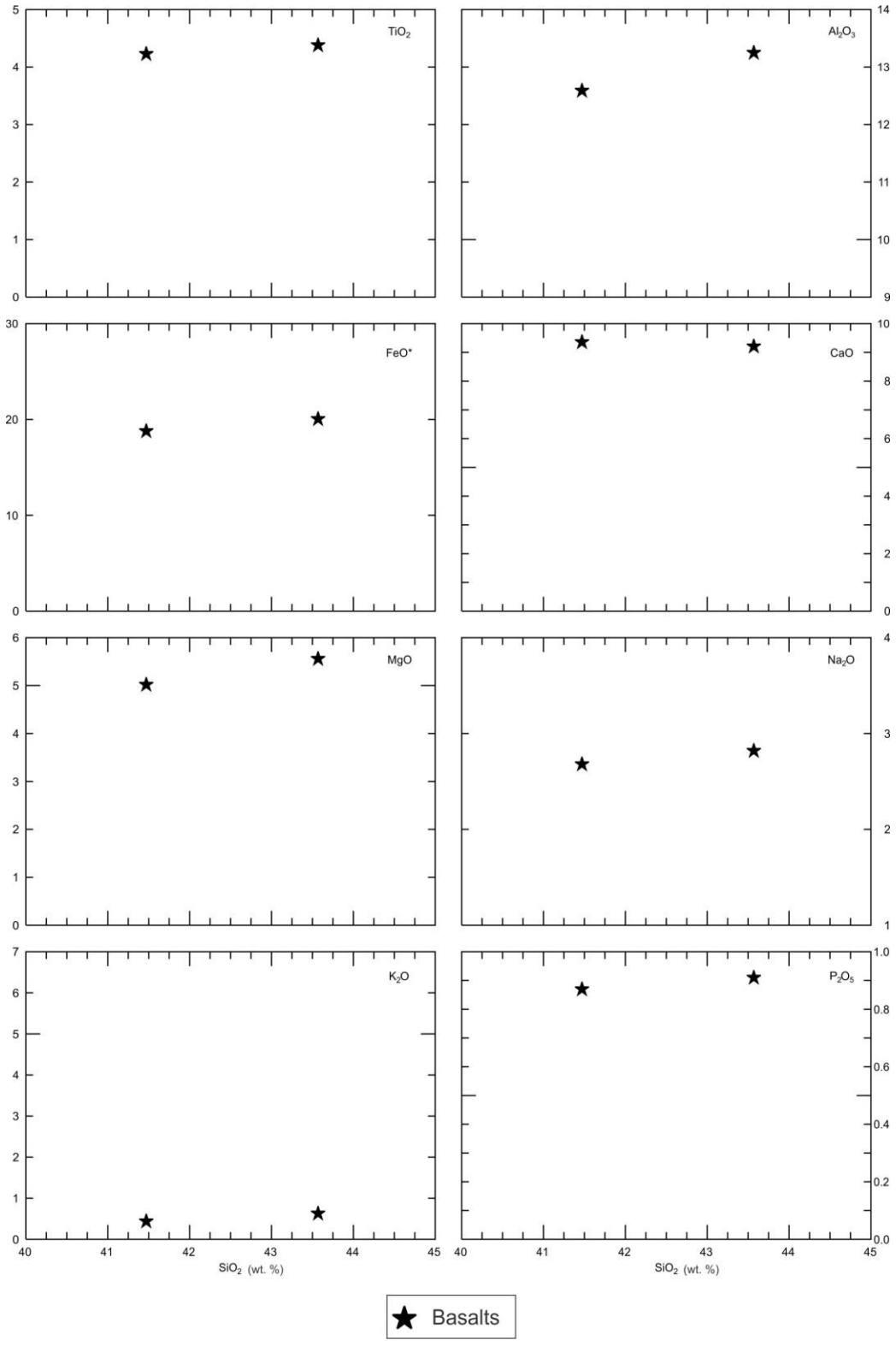

Figure 5.6: Harker diagrams of this study's basalt samples with major element oxide identified in the upper right corner of the diagram. All major oxides are represented in wt. %.

5.2 Trace Element Geochemistry

5.2.1 Basalts

Th, Rb, and Ba increase with increasing silica, whereas Sr and Cr/Ni decrease. There is no change in Zr with an increase in silica. MB11-1 has a greater concentration of Th (50 ppm) than AI12-6 (~8 ppm). The trace elements will be used to further constrain these basalts within the two groups of SROT (I or II) as described by Leeman (1982) later in the discussion section. The basalt samples in this study have high Ba (>400) and Zr (>250) concentrations for "typical" basalts, while having low Rb (<10) and Cr/Ni (<4.5) value for basalts (Figure 5.9) (Leeman, 1982).

5.2.2 Ash-flow Tuffs

The Tertiary ash-flow tuffs show an inverse relationship between Ba and SiO2 and a positive relationship with Zn. Other trace elements (Sr, Zr, Rb, and Nb) show no variation with increasing SiO2 wt. % (Figure 5.7). The ash-flow tuffs are distinct from the Jarbidge Rhyolite in having much higher Nb concentrations (Figure 5.7).

5.2.3 Rhyolite Lavas

The trace elements in Jarbidge Rhyolite that show an inverse relationship with wt. % silica are Ba, Sr, Zn, Zr, Cr, and Cu, while Rb is the only trace element that displays a positive relationship (Figure 5.7). The remaining trace elements, Nb (Figure 5.7), V, Co, Ni, and Y show no change with respect to wt. % silica. The plot of Ba vs. silica shows that two groups of Jarbidge Rhyolite are present: a high (1143-1798 ppm) and a low (477 ppm) group. These two groups are evident when barium is plotted versus other elements and trace element ratios (Figure 5.8). This feature of the Jarbidge Rhyolite (Ba groups) was noted by Brueseke et al. (2014). See the "Discussion" section for a comparison of studies. The Rock Springs Rhyolite does not plot with the Jarbidge Rhyolite in terms of the trace elements. It has lower Ba (48 ppm), Sr (13 ppm), Zn (45 ppm), and Zr (143 ppm) concentrations. However, the Rock Springs Rhyolite plots along a linear extension of the trend shown by Jarbidge Rhyolite samples in all the graphs.

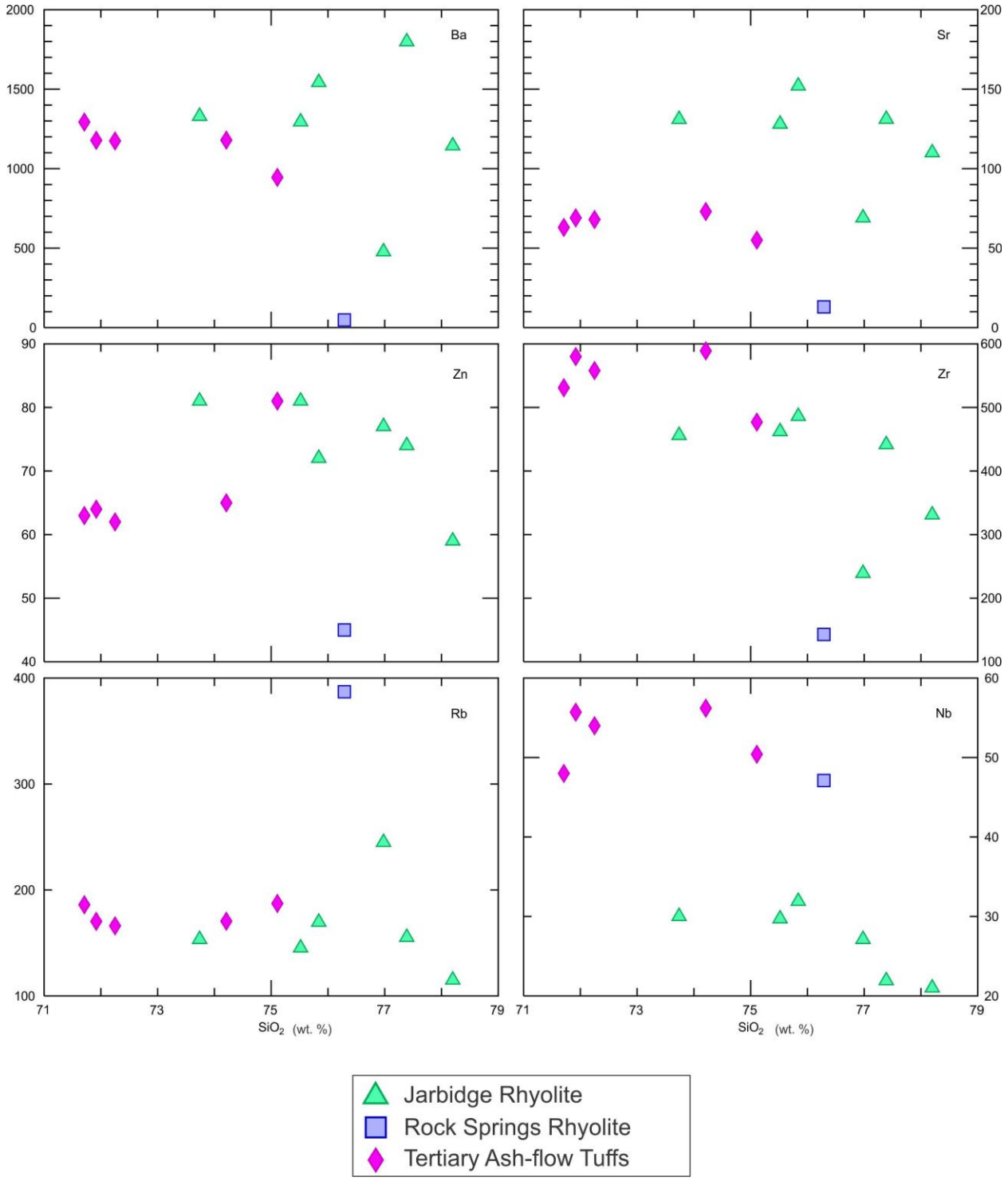

Figure 5.7: Harker diagrams with trace elements identified in the upper right corner of the diagram. Silica is represented in wt. %. All trace elements are plotted in ppm.

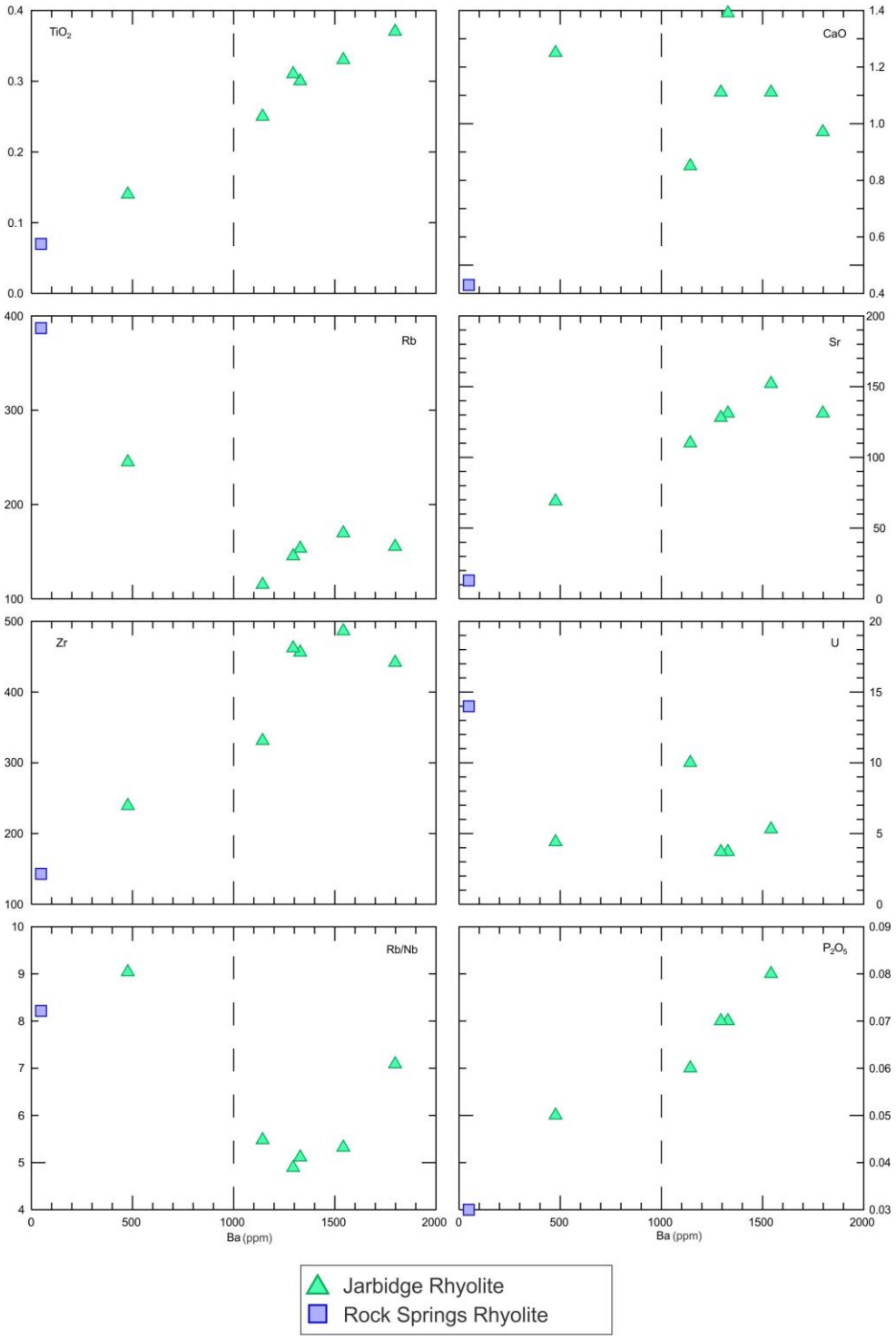

Figure 5.8: Barium vs. select major and trace elements and Rb/Nb. The element or ratio is identified in the upper right or left corner of the diagram. The dashed line represents the arbitrary distinction between the low and high barium groups (1000 ppm). Trace elements represented as ppm. Major oxides are shown in wt. %

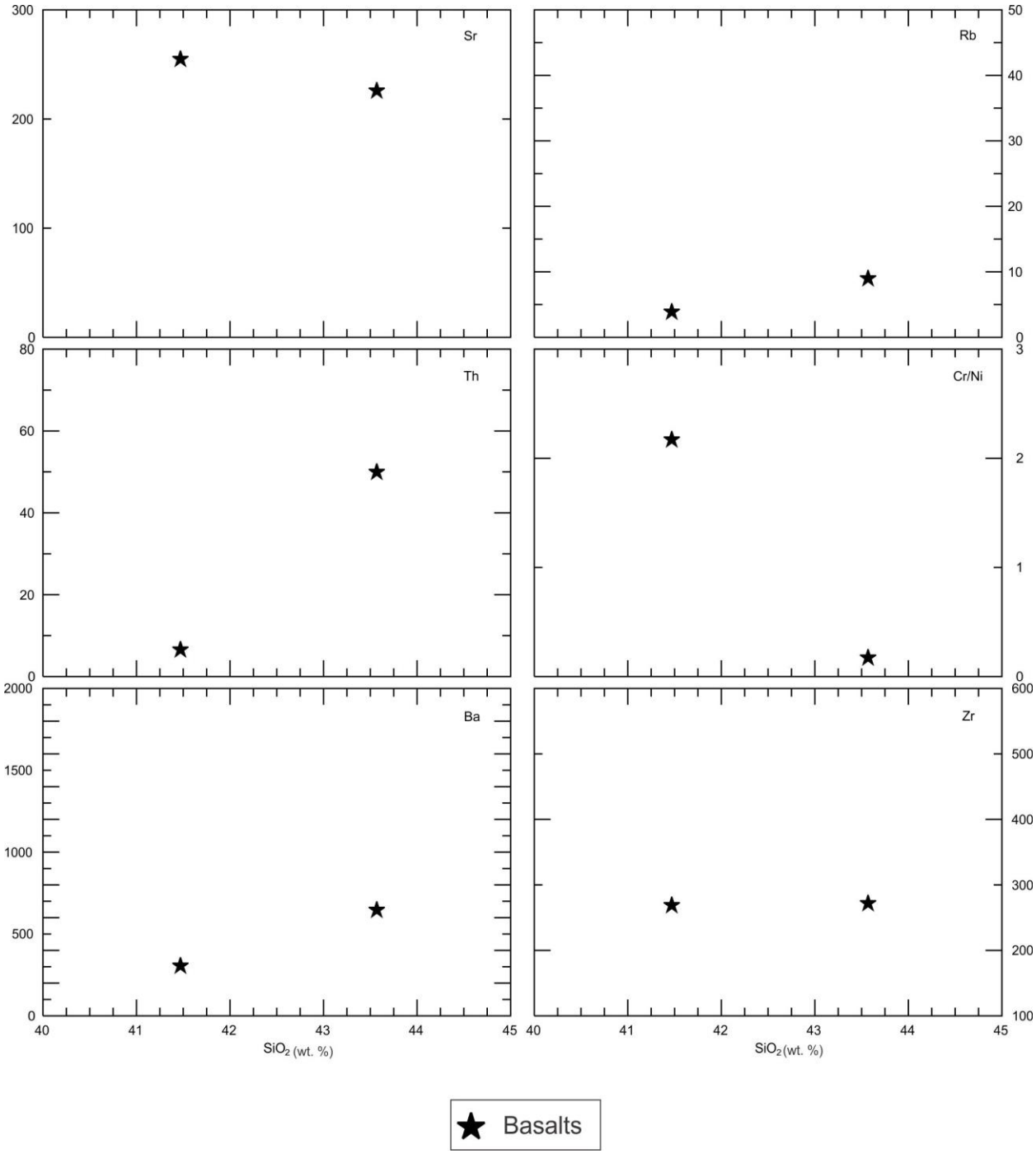

Figure 5.9: Trace element diagrams with the trace element or ratio identified in the upper right corner of the diagram. Trace elements are shown as ppm. Silica is plotted as wt. %.

Chapter 6 - Geochronology

Four samples were chosen for $^{40}Ar/^{39}Ar$ geochronology based on their distance from each other as well as from the previously studied area of north central to northeastern Nevada where voluminous Jarbidge Rhyolite packages crop out (e.g., Brueseke et al., 2014). JC-09-22 (Wells, NV), AI12-6 (West Wendover, NV), MB11-1 (Rock Springs, NV), MB11-2 (off Goose Creek Rd.) were chosen originally as part of an ongoing study to correlate the Jarbidge Rhyolite to "17-0 Ma" Basin and Range extension, while the Rock Springs Rhyolite was chosen to compare the age of its eruption to the age of Jarbidge Rhyolite. However, it is also being used to constrain local basin extension. Sample locations and respective ages are plotted on a base map(Figure 6.1) and UTM coordinates are in Appendix A. Samples have reported ages from sanidine single crystal laser fusion analysis (Table 3).

Table 3 : Table summarizes sanidine single crystal analysis. Abbreviations are MSWD for mean standard weighted deviate and "N" = the number of crystals analyzed per sample.

Sample	Location	MSWD	N	Age (Ma)	±2σ
JC-09-22	Wells, NV	3.8	27	15.249	0.080
AI12-6	West Wendover, NV	2.0	13	13.686	0.068
MB11-1	38 km SE of Jackpot, NV	1.4	27	13.561	0.062
MB11-2	35.5 km SE of Jackpot, NV	1.06	20	13.827	0.021

Sample JC-09-22 near Wells, NV produced an age of 15.249±0.040 Ma. An ideogram displays a narrow base and peak (Figure 6.2). The recorded age for AI12-6 produced through single crystal analysis is 13.686±0.034 Ma. The age for AI12-6 near West Wendover, NV, has a narrow peak, but also contains a smaller trailing peak which could reflect inherited (e.g., xenocrystic) crystals or crystals entrained in the magma body (Brueseke et al., 2014) (Figure 6.3). At Rock Springs, NV, MB11-1 produced an age of 13.561±0.031 Ma. MB11-1 has a tight peak and base displayed on this ideogram (Figure 6.4). Given the low MSWDs and the fairly tight age distributions, these ages are interpreted as eruption ages of these lavas. Sample MB11-2, northeast of Rock Springs produced an age of 13.827±0.021 Ma. An ideogram displays a narrow base and peak (Figure 6.5).

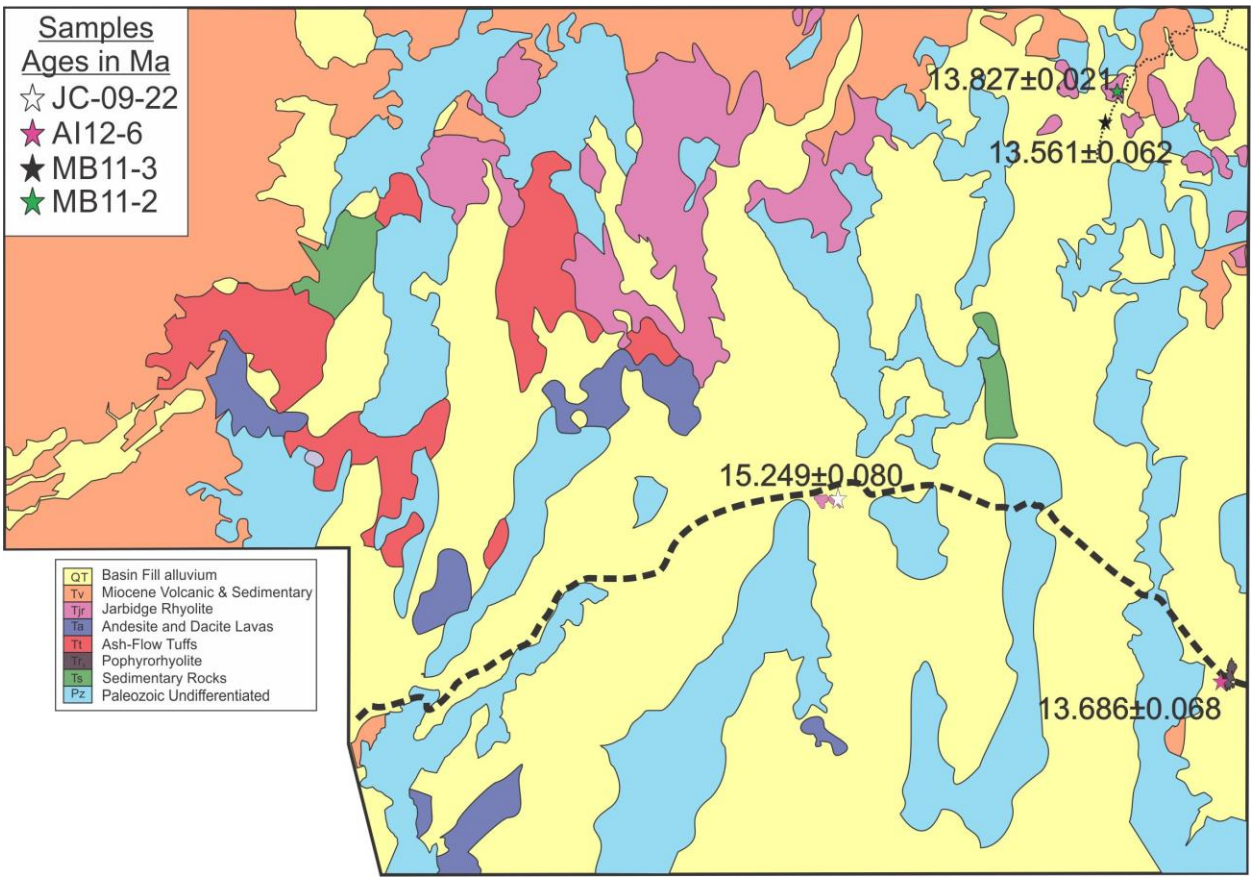

Figure 6.1: Simplified Geological map adapted from Coats (1987) map of Elko County, Nevada. Depicts the location of dated samples, and ages in millions of years ago. Standard deviation is 2 sigma. Thick dashed black line represents Interstate 80. Think dashed black line represents Goose Creek Rd.

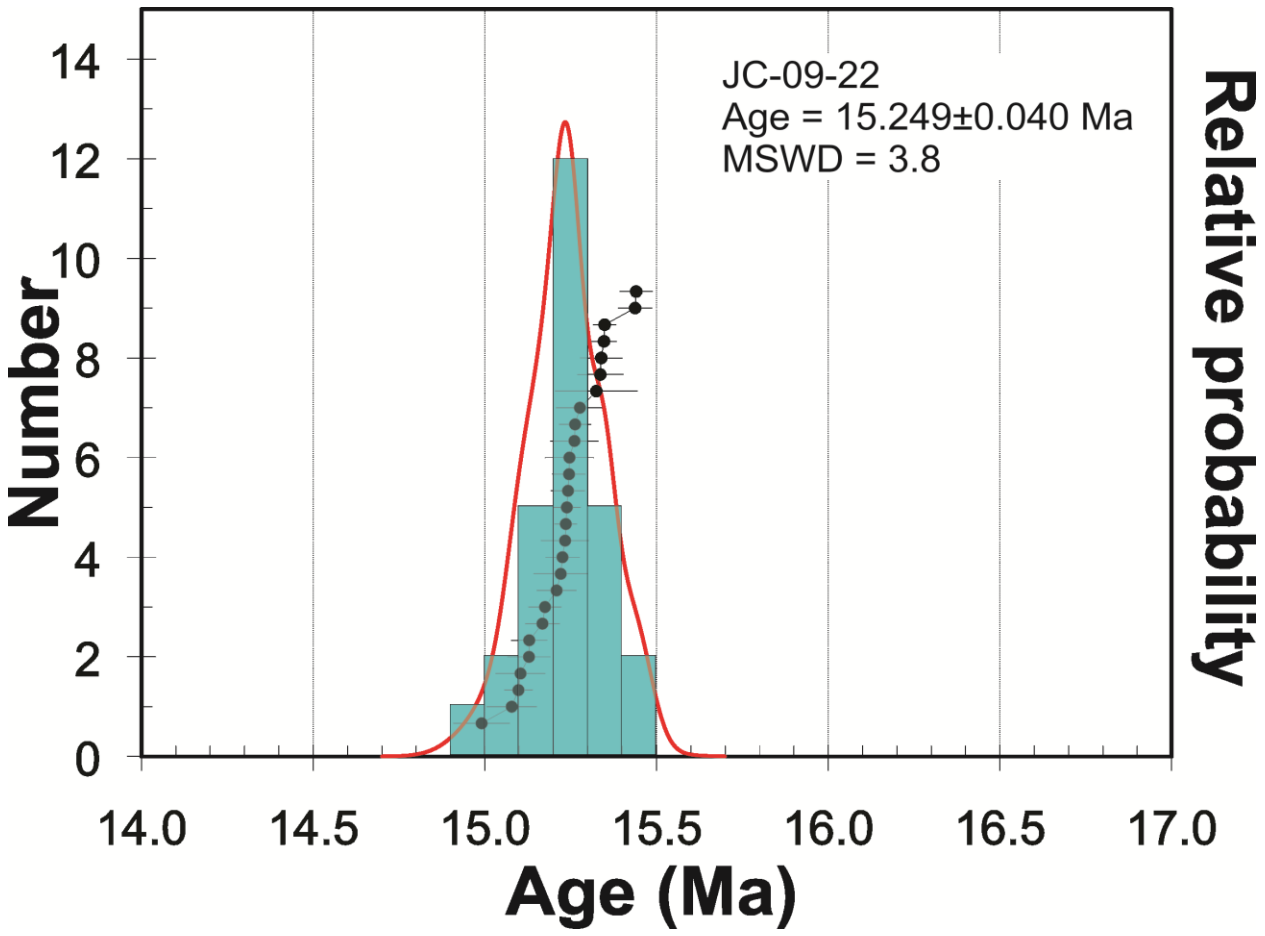

Figure 6.2: Ideogram of sample JC-09-22. Reported standard deviation is one sigma.

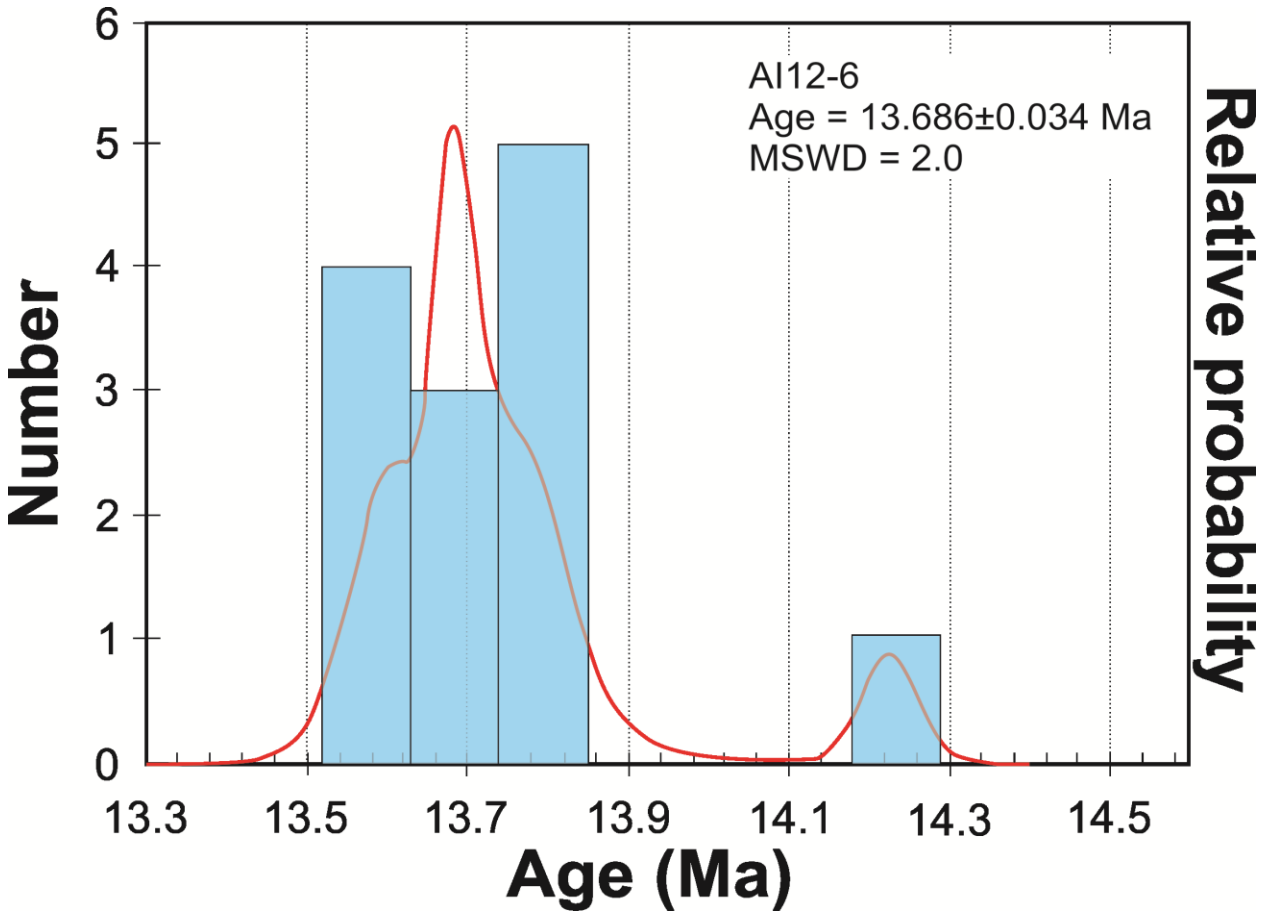

Figure 6.3: Ideogram of sample AI12-6. Reported standard deviation is one sigma.

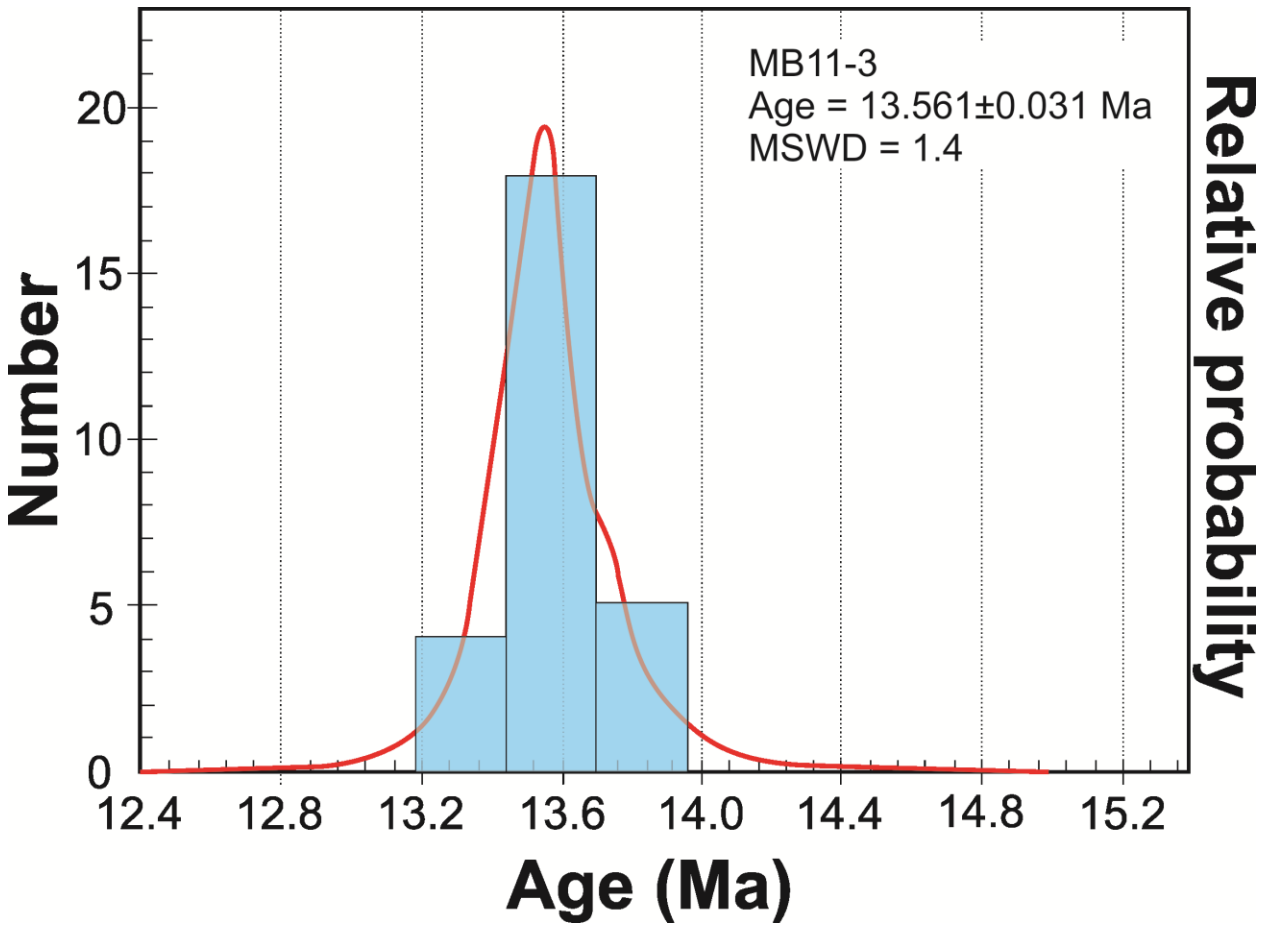

Figure 6.4: Ideogram of sample MB11-1. Reported standard deviation is one sigma.

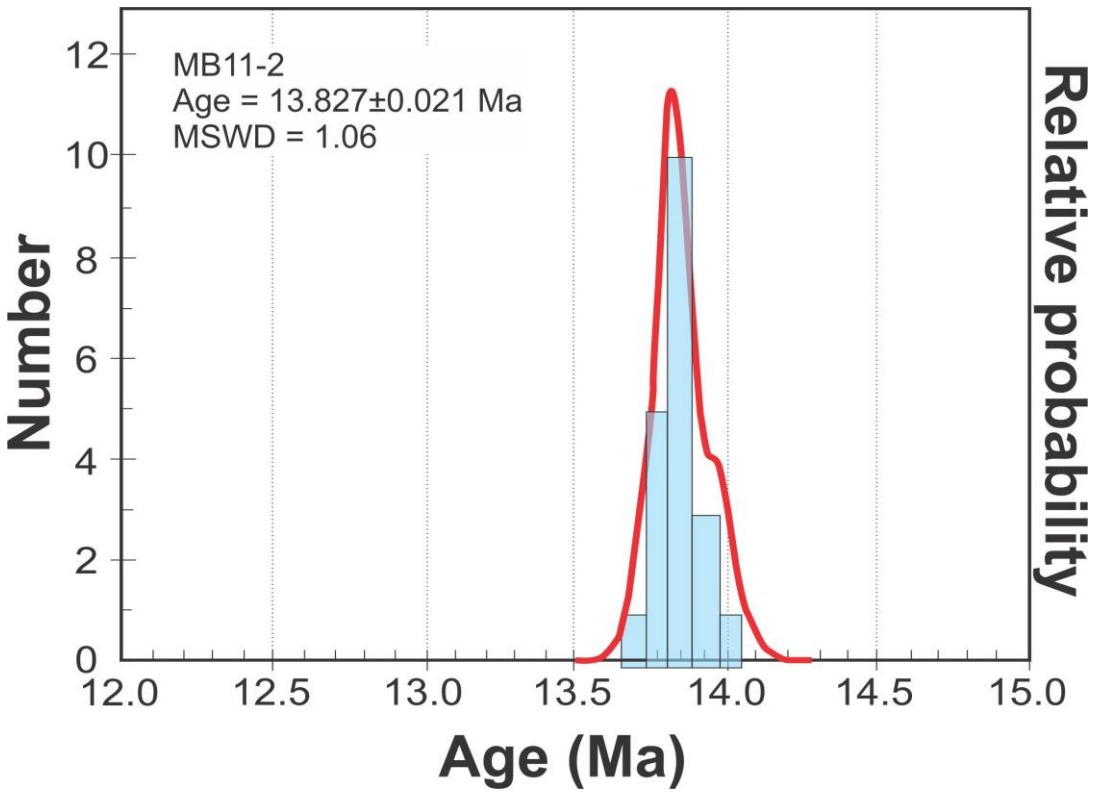

Figure 6.5: Ideogram of sample MB11-2. Reported standard deviation is one sigma.

Chapter 7 - Discussion

In this section I will compare my samples with the potentially correlative regional volcanism. I will use the data outlined earlier to provide interpretations about the spatiotemporal relationships of my samples to those studied by McCurry (unpub.), Hughes (unpub.), in the Snake River plain basalt database provided by E. Christiansen (pers. comm.), Leeman et al. (1977, 1982), Bonnichsen (2008), Wright (1998), Ellis et al. (2010), and Brueseke et al. (2014) (Figure 2.2). From there, I will use these comparisons to [1] decipher whether the sampled Jarbidge Rhyolite should actually be considered Jarbidge Rhyolite (e.g., based on prior work of Callicoat, 2010 and Brueseke et al., 2014), [2] discern possible correlations with my sampled ash-flow tuffs and basalts with regionally exposed units, and [3] discuss whether the younging eastward "trend" of the Jarbidge Rhyolite, as highlighted by Brueseke et al. (2014), does actually extend through my study area.

7.1 Studied Basalt Samples vs. Snake River Olivine Tholeiites

The petrography of the Snake River olivine tholeiites (SROT) is very similar to that of the samples collected in the northeastern portion of Nevada for this thesis. Although olivine tholeiites, specifically the McKinney basalt (50 Ka) and those described by McCurry and Hughes (unpub.) in the Cassia Mountains (~7.5 Ma), all have a variable texture, there are many characteristics that are similar throughout the SROT. Using the basic constraints discussed earlier in Chapter 4.1.2 Thin Section, I can compare the SROT of McCurry and Hughes (unpub.) and determine how closely related my samples are to them as well as other younger and similarly-aged olivine tholeiites of the Snake River Plain (SRP). Plotting these basalt samples from this study and hundreds of other SROT in the Christiansen dataset including samples from McCurry and Hughes (unpub.), via TAS and Harker diagrams (Figure 7.1), we can clearly see that the majority of Hughes and McCurry (unpub.) dataset plot within the basalt field, while most of the Leeman (1976) data plot within the trachybasalt. Only one of the McKinney basalts (Leeman, 1977;1982) and one of the McCurry (unpub.) samples (Deadline Ridge) plot within the same tephrite basanite field as this study's samples. On an AFM diagram (Figure 7.2), the samples from this study plot within the tholeiitic field, along with the other SROT. However, the basalt samples from this study have a higher FeO* than most of the tholeiites, except the

Deadline Ridge sample from McCurry (unpub.).Bonnichsen et al. (2002) identifies specific chemical constraints to identify SRP olivine tholeiites as late Miocene. In order to utilize these constraints, my samples must first be inferred through geochemistry as late Miocene (~7 to 9 Ma) basalts rather than the much younger (50 Ka) McKinney basalts studied by Leeman (1976). Figure 7.3 and Figure 7.4 show significant compositional differences in Rb, Zr, La, Ce/Ni for a given SiO_2 between the late Miocene and the Pleistocene olivine tholeiites. The late Miocene (McCurry, unpub.; Hughes, unpub.) basalts have low Rb (<25 ppm), Zr (<400ppm), La (<60 ppm), and Ce/Ni ratio (<5), whereas the Pleistocene McKinney basalts (Leeman, 1976), have much higher Rb (>25 ppm), Zr (>800ppm), La (>80 ppm), and Ce/Ni ratio (>15). When comparing the trace elements Cr, Ce, and Ni to SiO_2 wt. %, (Figure 7.4), the McKinney basalt have a much lower Ni (<10 ppm) and higher Ce (>250 ppm) concentrations for a given SiO_2 than the basalt samples in this study and the late Miocene basalts from McCurry and Hughes. Cr of the basalt samples from this study (8, 76 ppm) as well as Deadline Ridge are very low (17 ppm).Based on these geochemical data, the basalt samples in this study appear to be more closely related to the late Miocene Deadline Ridge sample from McCurry (unpub.) than to the Pleistocene McKinney basalts. Using a multi-element diagram normalized to primitive mantle (Figure 7.5), I show a clear compositional similarity of my samples towards the Deadline Ridge McCurry (unpub.) (7.26±0.06 Ma; William et al., 1999) sample. The negative cerium anomaly in AI12-1 is most likely due to hydrothermal alteration, since Ce^{3+} is soluble and thus fluid mobile at low temperatures (Neal and Taylor, 1988) (see Appendix C for the high L.O.I. content of AI12-1 for potential indication of hydrothermal interaction; Neal and Taylor, 1988). At sample site AI12-1, there was sinter capping the basalt unit, which is physical evidence of a hydrothermal interaction.There is also a positive Th and P anomaly with both samples (Th: MB11-3[50 ppm] greater than AI12-1[6.6 ppm]).This chemical similarity of the Deadline ridge (McCurry, unpub.), McCurry (unpub.) samples, Hughes (unpub.) samples, and the basalt samples from this study is consistent with a late Miocene origin of my basalts and allows me to use the criteria from Bonnichsen et al. (2002) for classifying late Miocene SRP basalts as olivine tholeiites.

Bonnichsen et al. (2002) has differentiated late Miocene SRP basalts by their Al_2O_3 content as well as their Fe_2O_3 concentrations. The basalts studied by McCurry (unpub.) and Hughes (unpub.) are labeled as SROT and therefore according to Bonnichsen et al. (2002), they

should have an Al_2O_3 of less than 15.99 wt. % and Fe_2O_3 of less than 14.99 wt. %. This study's basalt samples have an Fe_2O_3 range of 6.12 to 6.79 wt.% , classifying them as olivine tholeiites. McCurry (unpub.) basalts range from Fe_2O_3 3.26 to 6.85 wt. %, with the Deadline Ridge basalt measuring 6.85 wt. %. Hughes (unpub.) samples range from 3.56 to 6.52. The Al_2O_3 content range of the McCurry basalts were 16.59 to 12.92, with the majority being under 15.99 wt. %. Hughes's dataset ranges from 16.45 to 11.47 wt. %, again with the majority being under 15.99 wt. %. The basalt samples from this study have a range of 12.59 to 13.25 wt. % Al_2O_3 and are similar to those lavas studied by Bonnichsen et al. (2002). An interesting note to make is that although these basalts are plotting as olivine basalts, according to Hughes et al., (2002), the silica content of olivine basalts in the SRP ranges from ~45 to 51 wt. % silica, which is 3 wt. % higher on average than my samples. However, there are two samples which plot below 44 wt. %, including the Deadline Ridge sample from McCurry (unpub.). This, along with the normative CIPW (Figure 5.4) confirms the origin of the basalt samples from this study as late Miocene (~7 to 9 Ma) Snake River olivine tholeiites (SROT).

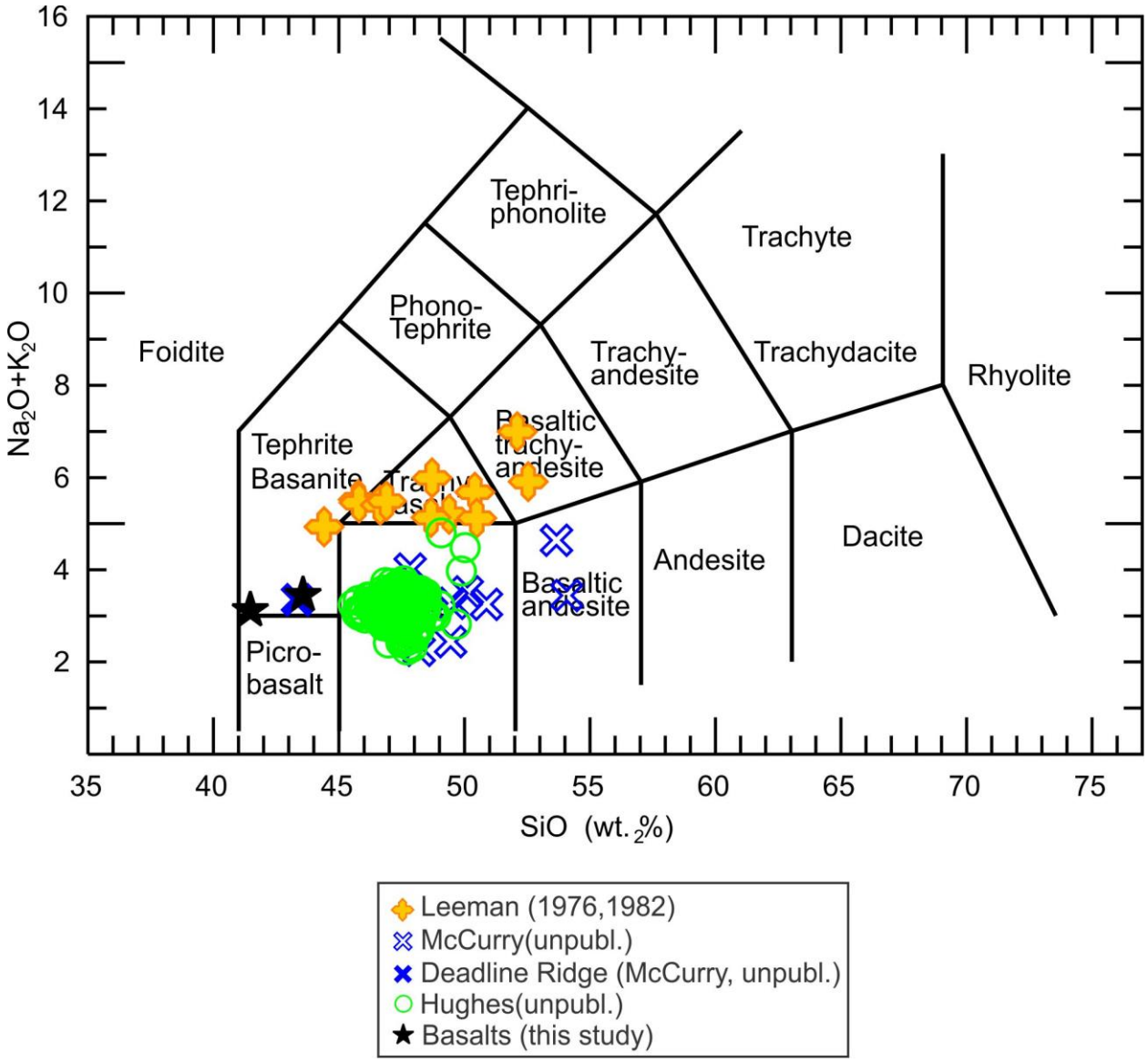

Figure 7.1: TAS diagram of Lebas et al., (1986). Leeman (1976, 1982) samples plot mainly in the trachybasalt field, Hughes and McCurry samples plot mainly in the basalt field. Basalt samples from this study plot within the tephrite basanite field.

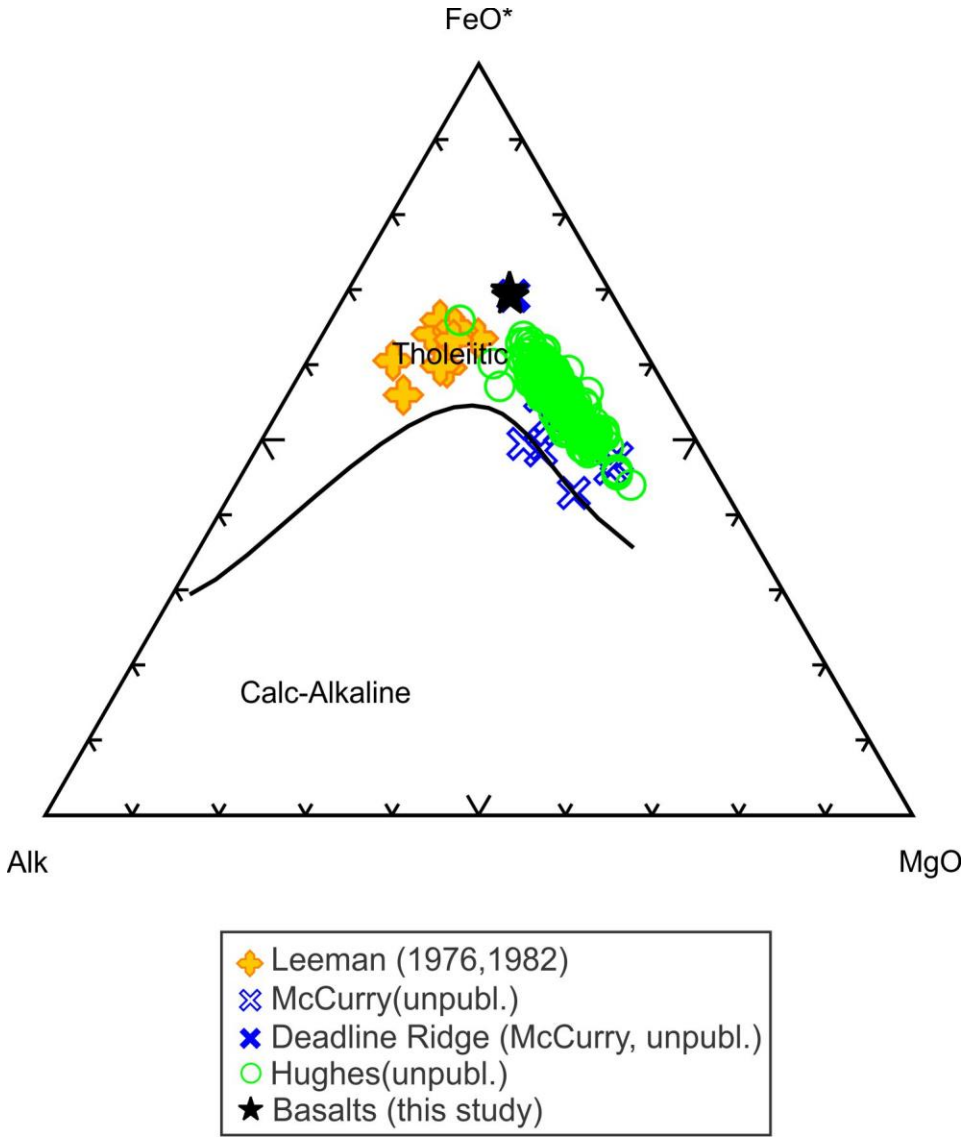

Figure 7.2: AFM diagram that compares this study's basalt samples (black stars) with the Snake River olivine tholeiites studied by Hughes et al., (unpub.), McCurry (unpub.), and Leeman (1976).

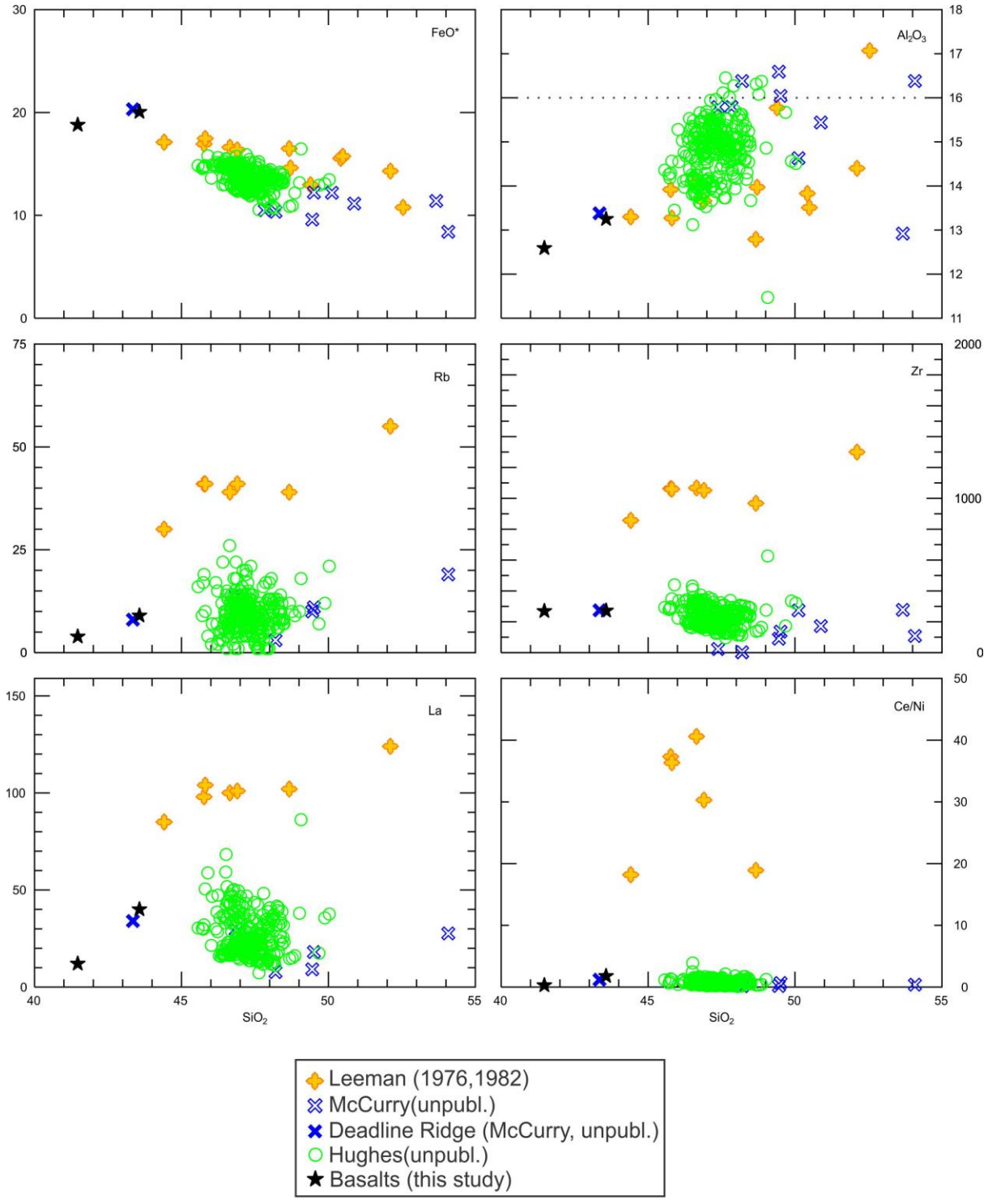

Figure 7.3: Harker diagrams comparing this study's basalts samples to the olivine tholeiites found within the Snake River Plain. Silica and other major elements (FeO*& Al_2O_3) are presented in wt. %. Trace elements (Rb, La, and Zr) are presented in ppm. Ce/Ni has no units.

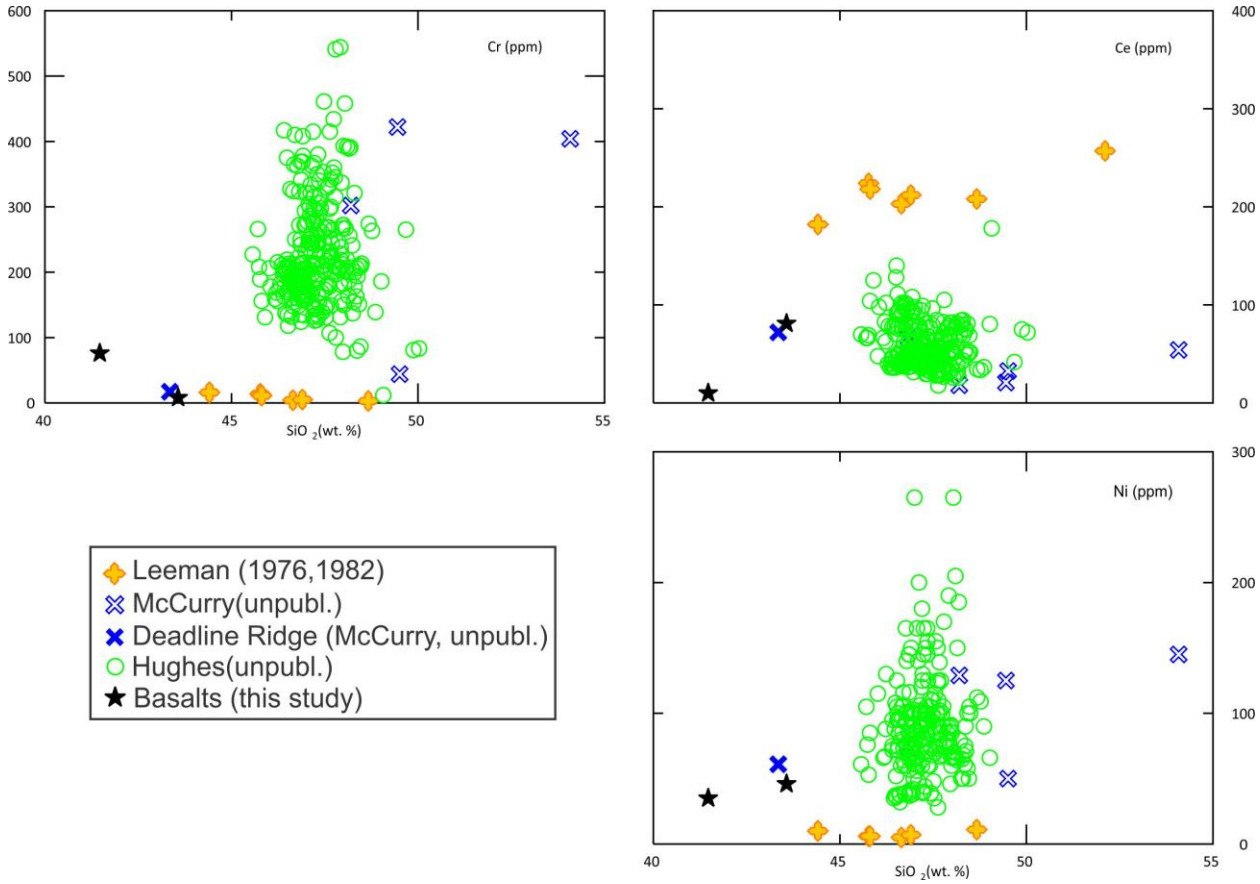

Figure 7.4: Harker diagrams comparing this study's basalt samples to the olivine tholeiites found within the Snake River Plain.

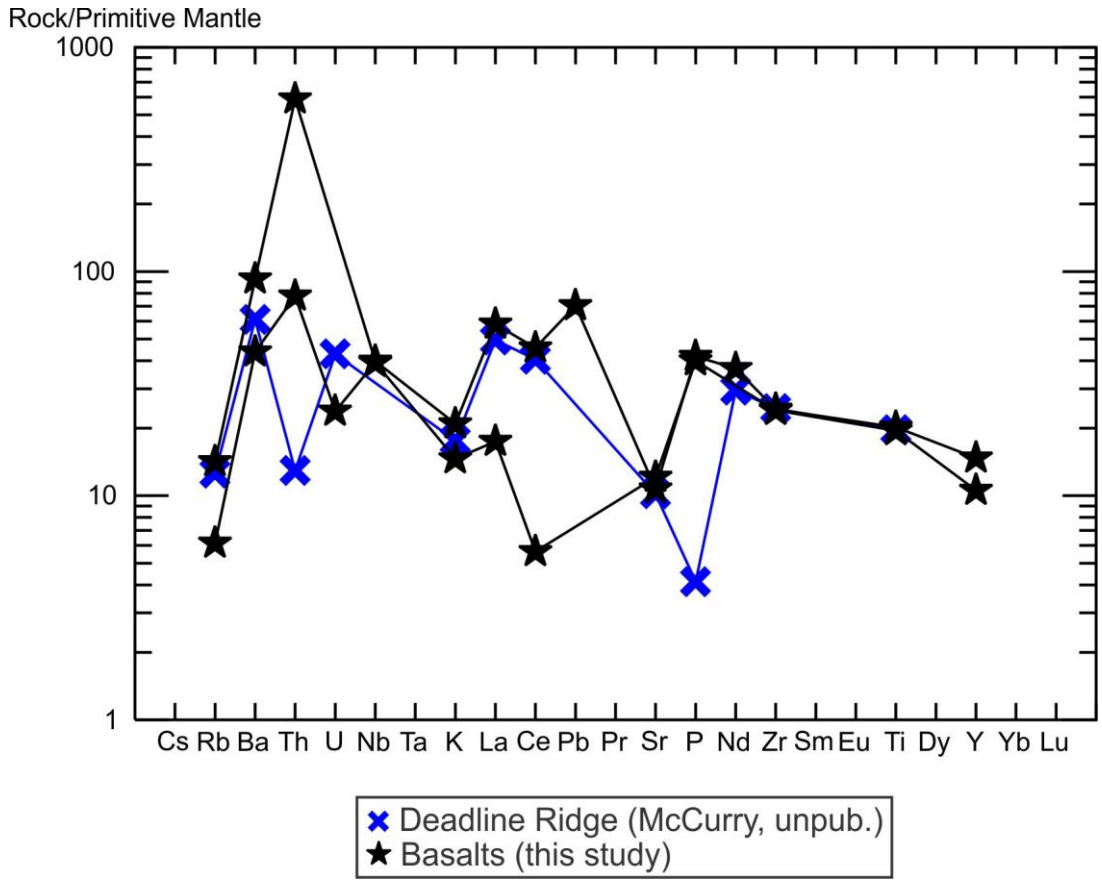

Figure 7.5: Multi-element diagrams from Sun and McDonnough (1989) normalized to primitive mantle comparing basanites to the Deadline ridge from McCurry (unpub.).

7.1.1 Regional Comparison

Using common basaltic magma cotectics with respect to their location on the basalt tetrahedron (Thompson, 1983), I can begin to interpret a possible depth (pressure) at which these basalts last equilibrated prior to eruption. It is here that the Hughes and McCurry samples diverge. The McCurry samples follow the low-pressure cotectic, while the Hughes samples seem to congregate at the end of the "deep crust" cotectic. The McCurry samples were sampled from the Cassia Mountains, Central Snake River Plain. This contrasts to the Hughes samples, which were sampled from the Eastern Snake River Plain. As shown above, there is a high degree of chemical similarity between the Deadline Ridge samples as well as the other McCurry (unpub.)

samples and the basalt samples from this study. This chemical affinity can be used in the interpretation of Figure 7.6. The basalt samples from this study plot between the 1 atm and 9 ± 1.5 kbar cotectics, however, because all McCurry's samples plot directly on the 1 atm cotectic, the data infer that this study's samples last equilibrated at low pressures and shallow depths in the crust, similar to the McCurry Snake River olivine tholeiites in the Cassia Mountains.

McCurry and Rodgers (2009) illustrate a conceptual model that indicates upper crust, rather than lower crust, acted as the primary density filter for the ascending basaltic magmas during the Yellowstone Snake River Plain volcanism. Partial melts of sub-crustal mantle in response to the thermal anomaly of the Yellowstone plume were able to bypass the Moho due to the high density Archean lower crust (~3.0 g/cm^3), which directly overlaid the mantle. The density of the likely primary melts (Mg olivine tholeiites) is ~2.8 g/cm^3 according to the McCurry and Rodgers (2009) model. These melts ascended until they stalled out in the lower-density Archean upper crust (~2.67 g/cm^3) where they created mafic interplating.

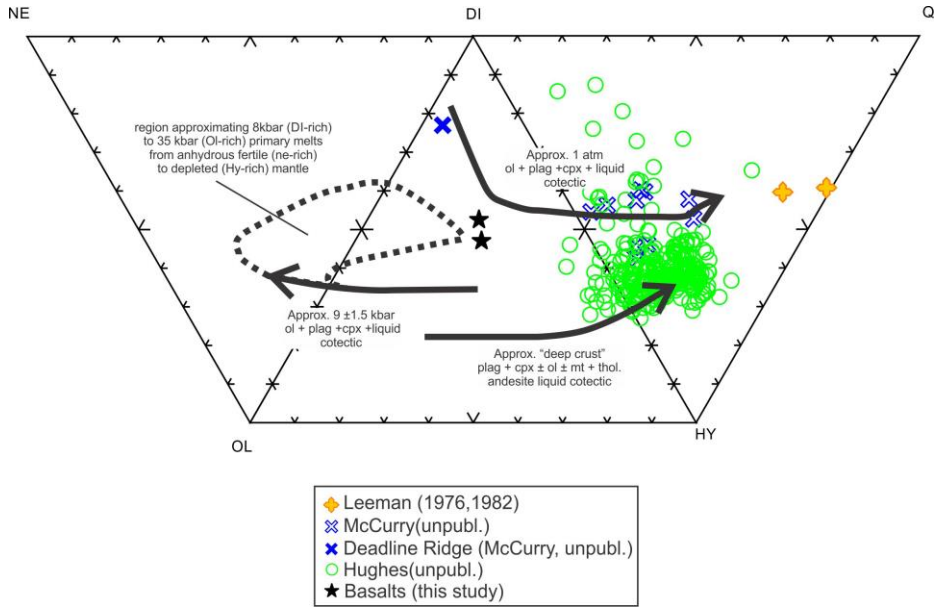

Figure 7.6: ***Adapted from Brueseke and Hart, 2009*****. This is an expanded basalt tetrahedron with experimentally derived primary mantle melt composition and differentiation paths (Thompson, 1983). The cotectics represent pressure/depth paths. SROT units are plotted via normative CIPW values. Abbreviations: NE, Nepheline; DI, Diopside; Q, Quartz; HY, Hypersthene; OL, Olivine.**

7.2 Tertiary Ash-flow Tuffs vs. Regional Explosive Silicic Volcanism

My samples were mapped by Coats (1987) as "Tertiary Ignimbrites" (unit Tts). All material in this unit was suggested by Coats (1987) to be correlative to the Cougar Point Tuff, which was derived from the ~13 to 7.5 Ma Bruneau-Jarbidge eruptive center located on the Snake River Plain, northwest of the study area (Figure 1.2). However, using physical and geochemical data, this study places the timing of some of these ash-flow tuffs (AFT) closer to the Twin Falls eruptive center (11 to 5.5 Ma).

Physical volcanology shows that the samples labeled as "Tertiary Ignimbrites" by Coats (1987) are indeed ash-flow tuffs. Although these eruptive centers show distinct differences in their physical and geochemical attributes, the central Snake River (SR)-type ash-flow tuffs have common traits that link them together. Ellis et al. (2010) states that SR-type ash-flow tuffs can be defined by a bimodality of welding: [1] an intensely welded, highly rheomorphic, lava-like ash-flow dominating, and [2] non-welded ash-flows subordinate. There are no moderately welded units found within the SR-type ash-flow tuffs. The ash-flows lack any pumice lapilli or fiamme, as well as any lithic fragments (Ellis et al., 2010; Branney et al, 2008). The mineralogy of the SR-type ash-flow tuffs are similar in phases and abundances according to Ellis et al. (2012). Phenocrysts assemblages include plagioclase + augite + zircon + apatite ± pigeonite ± orthopyroxene ± fayalite ± Fe-Ti oxides and in very minor cases sanidine and quartz. Biotite and hornblende are noticeably absent from all Central Snake River Plain (CSRP) rhyolites (Ellis et al., 2012). Crystal aggregates/clots are common features in Central Snake River Plain rhyolites, notably as multiple grains touching at point contacts. These descriptions are consistent with the physical characteristics found in the five samples from my study. The rhyolites of the Central Snake River Plain are typically Fe-rich with a silica concentrations ranging from 69 to 77 wt. %. These Tertiary ash-flow tuffs, as mapped by Coats (1987) and sampled by myself, can be confirmed as Central SR-type ash-flows from these characteristic physical and chemical traits, as outlined by Ellis et al. (2010, 2012) and Branney et al. (2008).

These five ash-flow tuff samples can be divided into two groups based on their phenocryst abundances, degree of welding, and mineralogy. The two groups are the Goose Creek (GC) tuffs (lower silica [71.7 to 72.3 wt. %]) and the Rock Springs/City of Rocks (RS/CoR) tuffs (higher silica [74.2 to 75.1]). The GC tuffs typically have a very fine matrix and contain roughly <5% phenocrysts, while the RS/CoR tuffs had a much higher phenocryst range of approximately

10-15%. By comparison, eruptive units of the ~12.75 to 10.82 Ma Cougar Point Tuff from the Bruneau-Jarbidge eruptive center have a phenocryst range of 2 to 10 modal % (Bonnichsen, 1982; Coats, 1987), while the tuffs from the Twin Falls volcanic field have a range of 3 to 15% by volume (Bonnichsen, 1982; Ellis, 2010).

The relative welding of the GC tuffs versus the RS/CoR tuffs also indicates a separation between the two groups. The GC tuffs are poorly welded, while the RS and CoR tuffs are highly-welded and the units are typically thicker and blockier than the GC units. Both of these groups contain very fine-grained, well sorted particles, less than sand-sized, which indicates that source was very distal. The groundmass that made up the RS/CoR tuffs was mainly a brown glass, while the GC was typically more grey. The brown glass is a common feature in Cougar Point Tuff (Bonnichsen, 1982). The last and most important difference between these two groups of ash-flow tuffs is their mineralogy. First and foremost, all CSRP rhyolites contain plagioclase, augite, zircon, and apatite, which is evident in these samples. The Cougar Point Tuff contains a higher amount of pyroxenes, both augite and pigeonite (Bonnichsen 1982). The pyroxenes within the RS/CoR tuffs are both larger in size (1-2 mm versus <0.1 mm) and higher in modal abundance.

Based on the mineralogy and physical characteristics, we can confirm that these ash-fall tuffs are of Snake River Plain origin. However, since the mineralogy and physical characteristics of all SR-type ash-flows are so homogenous, it is difficult to propose any definitive correlation between the two sets of samples (GC samples and the CoR/RS samples) and the respective volcanic fields (BJEC and TFEC). That stated, the stark differences in phenocryst abundance, degree of welding, and mineralogy gives a definite set of two ash-fall groups: [1] the Goose Creek (GC) samples and [2] the CoR/RS samples. Using these two initial groupings for the ash-flow tuffs, geochemical data were used to further constrain the samples in respect to the CSRP volcanic fields (Bruneau-Jarbidge and Twin Falls).

I use geochemical data provided by Bonnichsen (2008) for the Bruneau-Jarbidge (BJ) eruptive center for the Cougar Point Tuff (CPT) and data from Wright (1998) and Ellis et al (2010) for the Twin Falls (TF) eruptive center, specifically the McMullen Creek ash-flow tuff as well as the other Cassia Mountain ash-flow tuffs, to compare the geochemistry of the sampled ash-flow tuffs. My sampled ash-flow tuffs have two distinct silica wt. % groupings: (71.7 to

72.3), (74.2 to 75.1). This compares to the BJ silica range of (72.3 to 79.5 wt. %), while the TF silica range is (70.3 to 76.4 wt. %).

Figure 7.7 is a plot of A/CNK vs. wt. % SiO_2. In this diagram, samples from the TF eruptive center, as well as the ash flow tuffs from this study, plot around an A/CNK value of 1, while the BJ eruptive center deposits has a wide range of A/CNK from 1 to 2, consistent with peraluminous samples.

The Rb/Nb ratios of all the ash-flow tuffs are between 2 to 5.5. Such values are intermediated between average compositions of lower and upper crust (Rudnick and Gao, 2003), which is consistent with the source of the ash-flow tuffs in hybridized (e.g., both felsic crustal and mafic underplate contributions) Snake River plain crust (McCurry and Christiansan, 2008) (Figure 7.8**)**.

In a plot of modified alkali-lime index vs. SiO2, the Cassia Mountain ignimbrites range from calc-alkalic to slightly alkali-calcic. The GC tuffs are lower in silica than the majority of the Cougar Point tuff, and follow the Cassia Mountain trend of being slightly alkali-calcic. The Cougar Point Tuff, however, straddles the calc-alkalic/alkali-calcic border at a higher wt. % silica. The CoR and RS ash-flow tuffs follow the trend of these the Cougar Point Tuff more so than the TF eruptive center (Figure 7.8).

Using the major and trace elements of each unit (Figure 7.9), a clearer picture can be formed regarding the separation of the TF eruptive center from that of the BJ eruptive center and where my two tertiary ash-flow tuff groups fall. As seen in these Harker diagrams, the higher silica group has lower Zr and Ba, while they have a higher Rb/Sr ratio and La concentration. This follows with the Cougar Point Tuff sample set and shows an affinity towards the BJ eruptive center. Zr plot shows a strong downward trend with an increase of silica. The samples show elevated Th levels in relation to their increased silica, meaning CPT and RS/CoR samples all have higher Th concentrations than the TF AFT and GC samples. The readings for the CPT and TF AFT mirror exactly that of the low silica (GC) group having higher Zr concentrations, while the high silica (RS/CoR) samples have a much lower Zr ppm

In summary, the physical characteristics and the mineralogy show a clear difference between the two sample groups. The Goose Creek group has lower phenocrysts % by volume, less welding, and generally fewer and smaller pyroxene phenocrysts. Geochemical data, as represented in Harker, ASI and MALI diagrams, show that the Goose Creek group has a high

affinity towards the Twin Falls eruptive center outflow geochemistry, while the City of Rocks and Rock Springs samples showed a slight similarity towards the Cougar Point Tuff units from the slightly older Bruneau-Jarbidge eruptive center. More work is needed to confirm that both the City of Rocks and Rock Springs samples are indeed sourced from the Cougar Point Tuff. More work is also needed to confirm that none of the sampled ash-flow tuffs are correlative to named ash-flow tuffs found in the Rogerson graben region, near Jackpot NV (e.g., ~ 38 km northwest of the study area; Andrews et al., 2008).

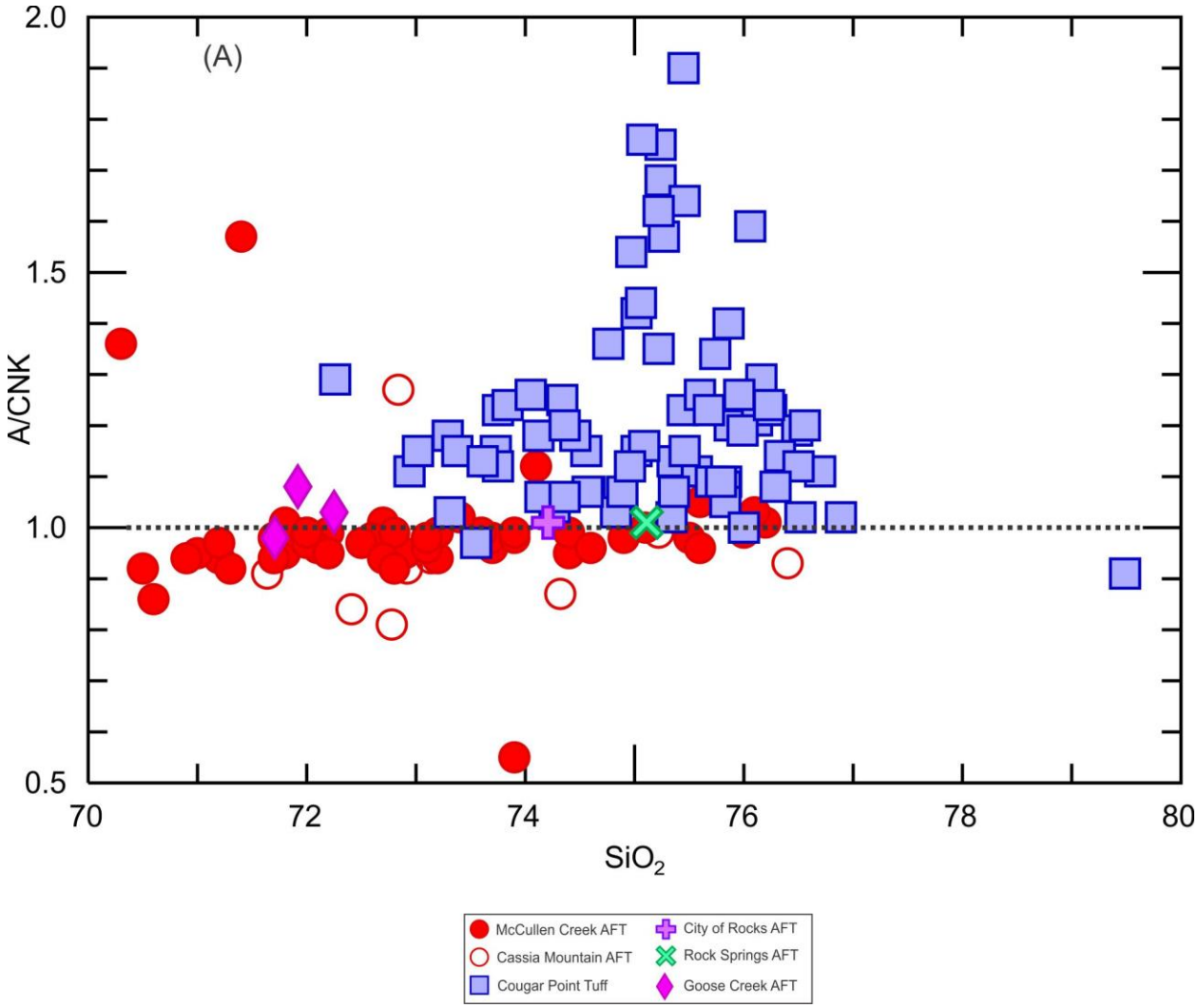

Figure 7.7: ASI diagram that shows the tertiary ash-flow tuffs lie around the A/CNK=1.0, which is the defining separation between metaluminous (A/CNK<1) and peraluminous (A/CNK>1).

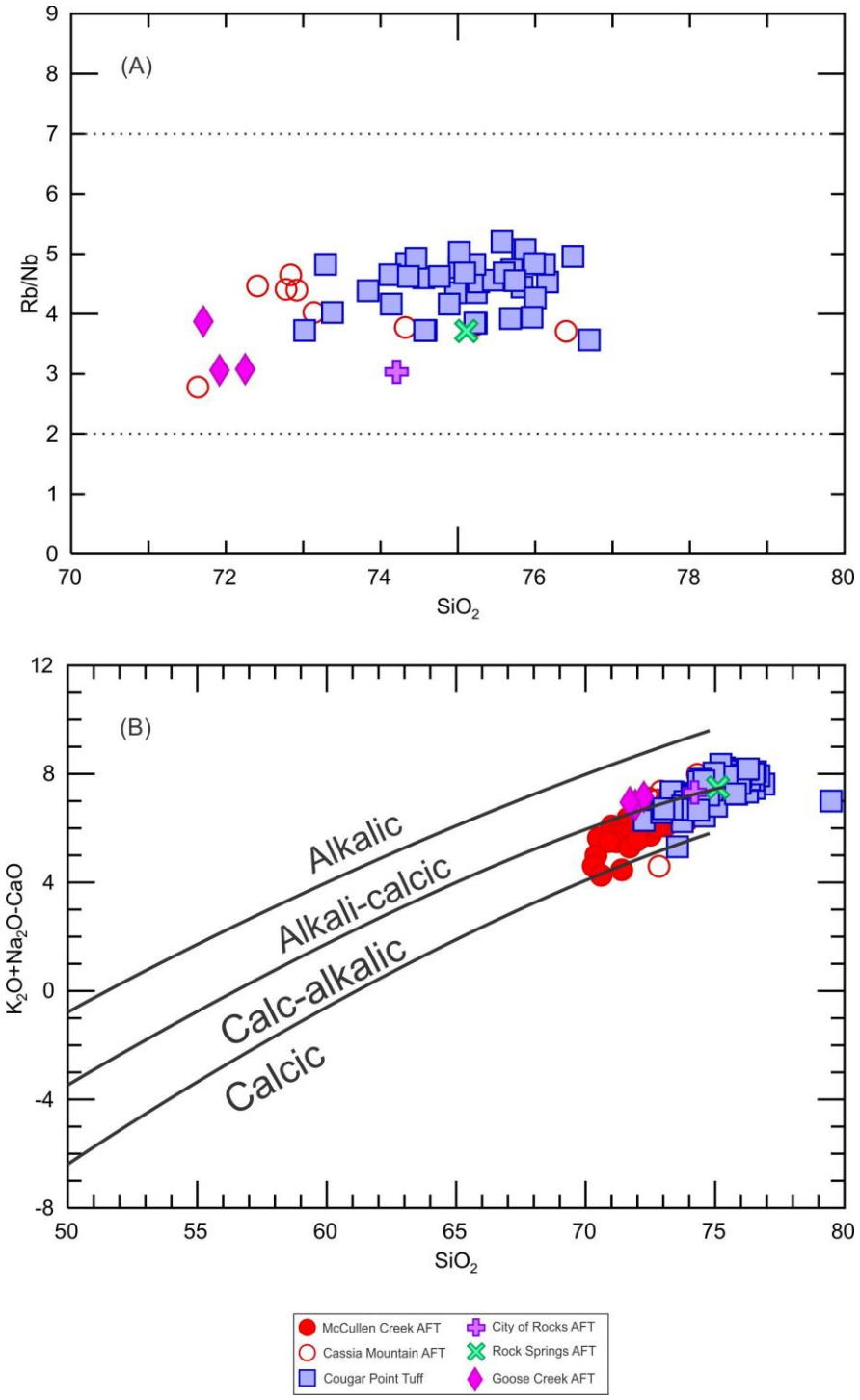

Figure 7.8: (A) Rb/Nb vs. wt.% silica showing the overall range of the pyroclastic deposits. The dashed lines represent standard values for upper crust (Rb/Nb=7) and lower crust (Rb/Nb=2) (Rudnick and Gao, 2003) (B) MALI diagram that shows the TF deposits are mostly calc-alkalic, while the BJ deposits hover between calc-alkalic and alkali-calcic

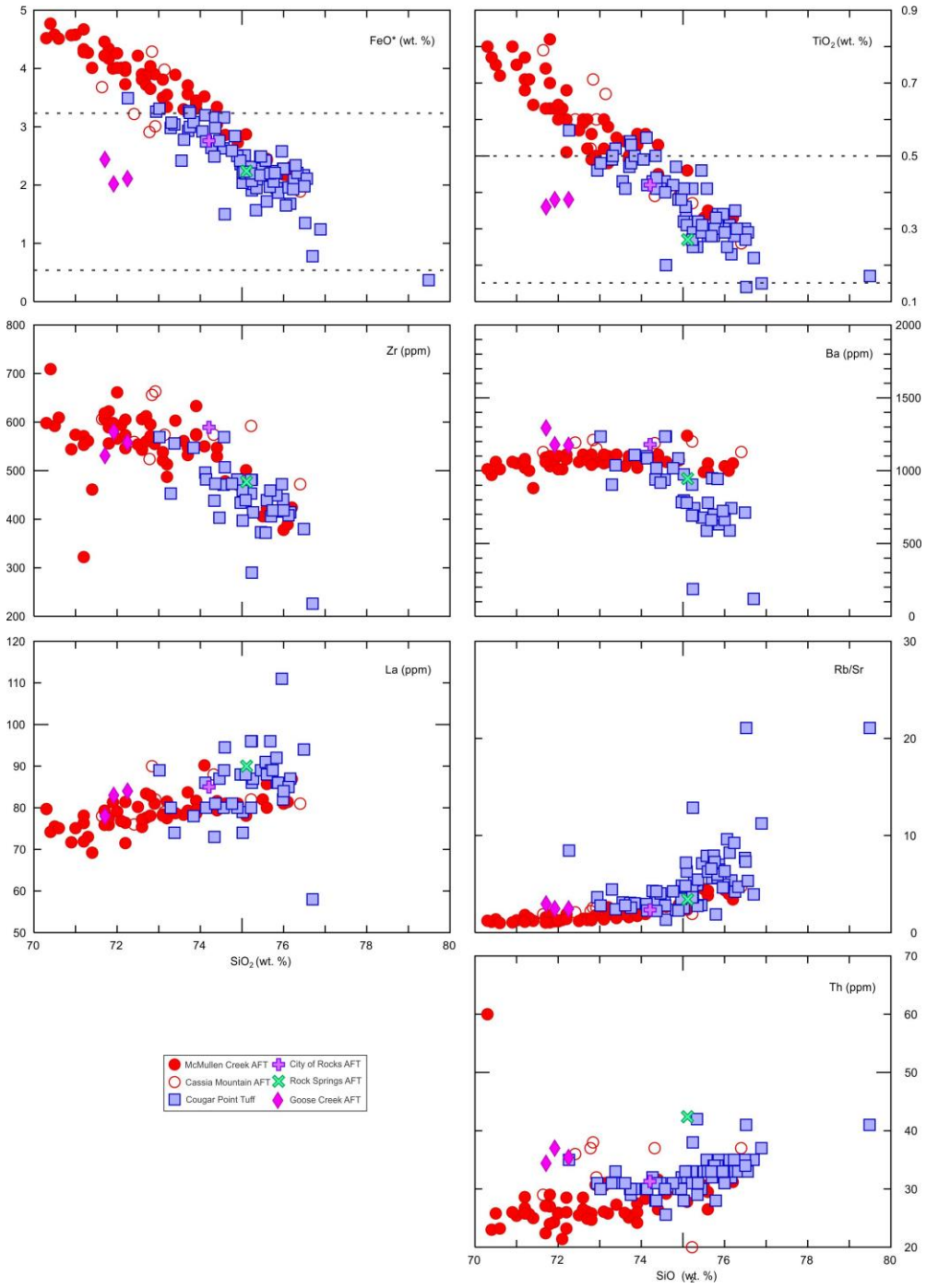

Figure 7.9: Major and trace element Harker diagrams portraying pyroclastic deposits from the two distinct eruptive centers: TF and BJ. The sampled Goose Creek ash-flow tuffs are represented as diamonds show an affinity on all diagrams to the TF ash-flow tuffs, while the Rock Springs and City of Rocks samples show an affinity towards BJ sourced ash-flow tuffs.

7.2.1 Implications of pyroclastic deposit correlations

These interpretations of the Elko County ash-flow tuffs provide me with new regional implications for both the extent of the Twin Falls eruptive center outflow as well as the Bruneau-Jarbidge eruptive center outflow. These interpretations also allowed me to provide a constraint on local basin extension in the Rock Springs area.

If the Goose Creek ash-flow tuffs did indeed erupt from the Twin Falls volcanic field, then we can reevaluate the previously documented maximum extent of the pyroclastic flows from the Twin Falls volcanic field. Figure 7.10 shows the prior distribution of Twin Falls outflow, as well as the new distribution inferred based on the Goose Creek samples from this study. The map (Figure 7.10) by Shervais et al. (2013) is a conservative representation of the outflow of the Twin Falls eruptive center and the outflow range is likely much greater than what is inferred.

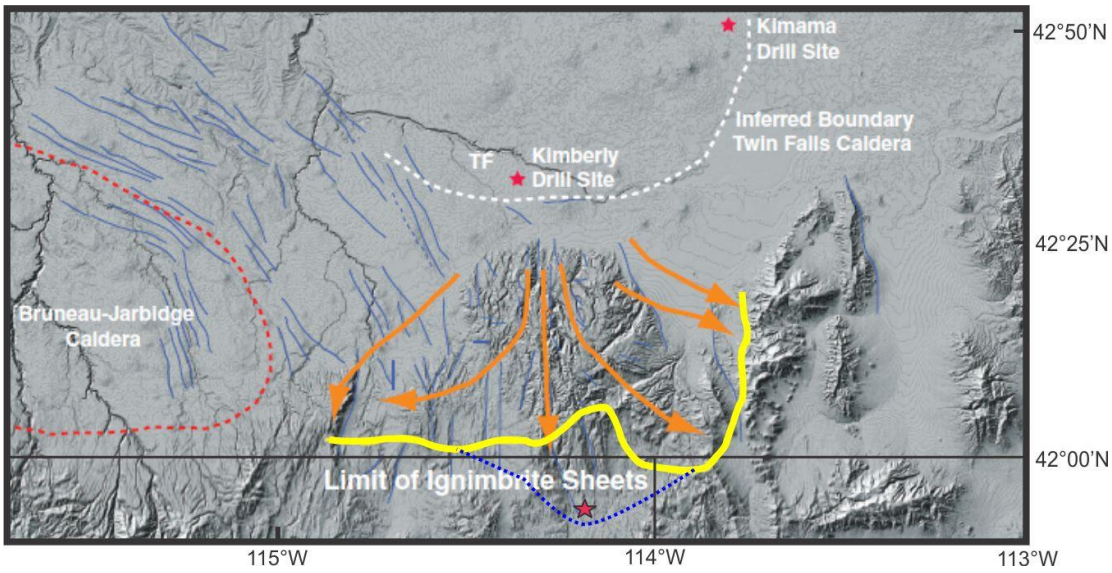

Figure 7.10: ***Adapted from Shervais et al. (2013).*** **The orange arrows show the flow direction of the ash-flow tuffs in the Cassia Mountains that were sourced in the 11-5.5 Ma Twin Falls volcanic field, as mapped by McCurry et al. (1996). The yellow line represents the southern most extent of the sheets. My Goose Creek samples are represented by the red star to the south of the Nevada border. The revised distribution is highlighted by the blue dashed line and is based on the addition of these new Twin Falls samples. The red dotted line is the Bruneau Jarbidge volcanic field, while the white dotted line is the Shervais et al. (2013) interpretation of the Twin Falls volcanic field (caldera) boundary. The red stars within the border are drill sites from the Shervais et al. (2013) study.**

If we assume that the CoR/RS ash-flow tuffs are indeed related to the Cougar Point Tuff, this extends the distribution of the outflow well past the Cassia Mountains, consistent with prior work. Although there are no current maps depicting possible extent of the outflow, there are studies that depict the extent of the CPT flow, which is mainly limited to south of the Bruneau-Jarbidge Caldera (Bonnichsen, 1982; Ellis et. al., 2013). My new sample data suggest that this outflow could extend much further to the south into Nevada and further to the east of Idaho (Figure 7.11).

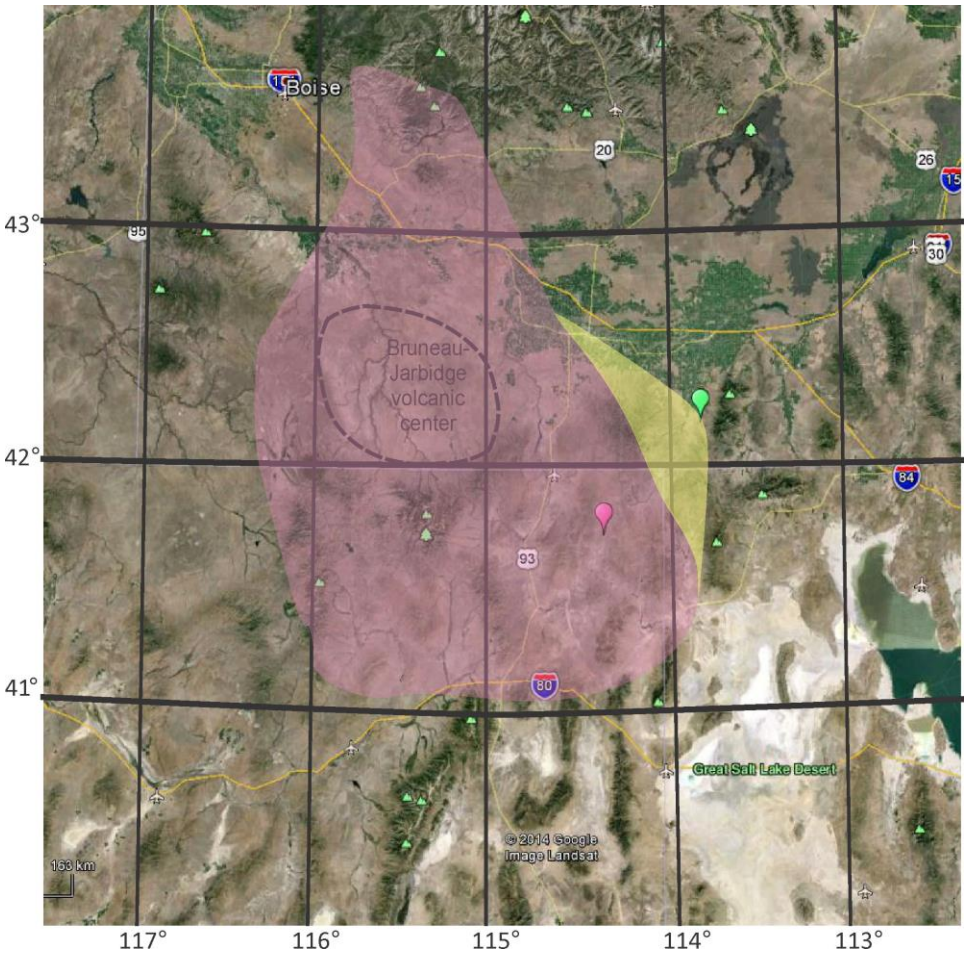

Figure 7.11: ***Adapted from Google Earth.*** **The shaded pink region is adapted from the Bonnichsen (2008) distribution of CSRP rhyolites from 13.0-10.4 Ma. The pink dot represents my Rock Springs ash-flow tuff and the green dot represents my City of Rocks ash-flow tuff. The yellow region is my interpreted extension of the BJ eruptive center extent.**

Using our previous geochronology data from the Rock Springs Rhyolite (13.561±0.031 Ma) as well as the $^{40}Ar/^{39}Ar$ geochronology data for the Cougar Point Tuff (Table 4) studied by Bonnichsen et al. (2008), we can provide initial constraints on the timing of the sedimentary basin strata in the Rock Springs area and the timing and duration of localized basin extension.

My discussion of the ash-flow tuffs above concludes that the RS ash-flow tuff is closely related to the Cougar Point Tuff, although it is difficult to distinguish which CPT unit the RS/CoR samples mirror, and therefore I will use that constraint to put an initial age range on the tuff (12.75 to 10.82 Ma) (Bonnichsen, 2008). The relative position of the units in this study is as follows (Figure 7.12): The Rock Springs Rhyolite is deposited, following that deposition basin sedimentation began as a result of localized extension of the area, finally the RS ash-flow tuff was deposited. This positioning of the units allows us to constrain the timing of sediment deposition and by inference, localized extensional basin formation, using the $^{40}Ar/^{39}Ar$ geochronology from the bracketing volcanic units. It must have occurred slightly after the RS rhyolite (13.561±0.062 Ma), but slightly before the RS ash-flow tuff (12.75 to 10.82 Ma), making the overall range on the duration of local basin formation ~0.8 to 2.8 m.y.

Table 4: Ar/Ar geochronology of Bonnichsen et al. (2008). Standardized to 28.02 Fish Creek Tuff.

				Std to 28.02	
Cougar Point Tuff Units	Initial Age	±1s	±2s	Age	±2s
CPT III	12.67	0.04	0.08	12.75	0.08
CPTIII	12.64	0.03	0.06	12.72	0.06
CPT IX	11.56	0.04	0.07	11.63	0.07
CPT XI	11.22	0.04	0.07	11.29	0.07
CPT XIII	10.82	0.03	0.06	10.89	0.06
CPT XIII	10.80	0.03	0.06	10.87	0.06
CPT XIII	10.75	0.04	0.07	10.82	0.07

Other studies have been produced that indicate similar dates with respect to local sedimentary deposition (and by inference, localized extension) in the region based on studies of the Humboldt Formation and equivalents (e.g., Salt Lake Formation in Utah and other units). For example, Perkins et al. (1995) study of Trapper Creek in south-eastern Idaho, just north of my main study area, dated a stratigraphic section that was previously studied by Armstrong (1975). Using the lowest unit in the Beaverdam Formation (two fallout tuffs), and the uppermost

datable tuff in the capping sequence (welded ash-flow tuff), Perkins et al. (1995) were able to put constraints via correlative dating of the tuffs using $^{40}Ar/^{39}Ar$ geochronology of the basin deposition caused by "modern" Basin and Range extension. The range in age for basin deposition of Trapper Creek as studied by Perkins et al. (1995), therefore, is 13.74±0.04 Ma to 10.02 ±0.03 Ma, giving us a duration of extension of ~3.6 m.y. Rodgers et al. (2002), conducted a study in Arbon Valley, south-eastern Idaho as well and showed that a stratigraphic column of basin fill from Trail Creek within Arbon Valley as a multitude of intercalated limestones and reworked tuffs (Rodgers et al., 2002). These lacustrine limestones are confined below by a 15.65 Ma tuff and capped by both a 12.67 basalt and rhyolite ash-fall tuff. This partially constrains the basin extension to 15.65 to 12.67 Ma in the Arbon Valley. However, above this large unit of lacustrine limestone and air-fall tuff, there is another unit of clast-supported conglomerate. Finally, above that sedimentary strata there is an upper ash-flow tuff (Arbon Valley tuff) dated by Kellog et al. (1994) through $^{40}Ar/^{39}Ar$ dating as 10.2 Ma. There is little to no basin fill preserved above the Arbon Valley tuff, indicating that the end of deposition is ~10.2 Ma (Rodgers et al., 2002). These local extensional constraints help to confirm the timing of "modern" Basin and Range extension in the northeast of Nevada into the northwest of Utah.

These studies of local extension, as well as my own, are integral in not only producing a time transgressive mapping of the extent of Basin and Range extension inception but also allow us to correlate this extension with effusive rhyolite volcanism in the region (e.g., Jarbidge Rhyolite and other, likely related units).

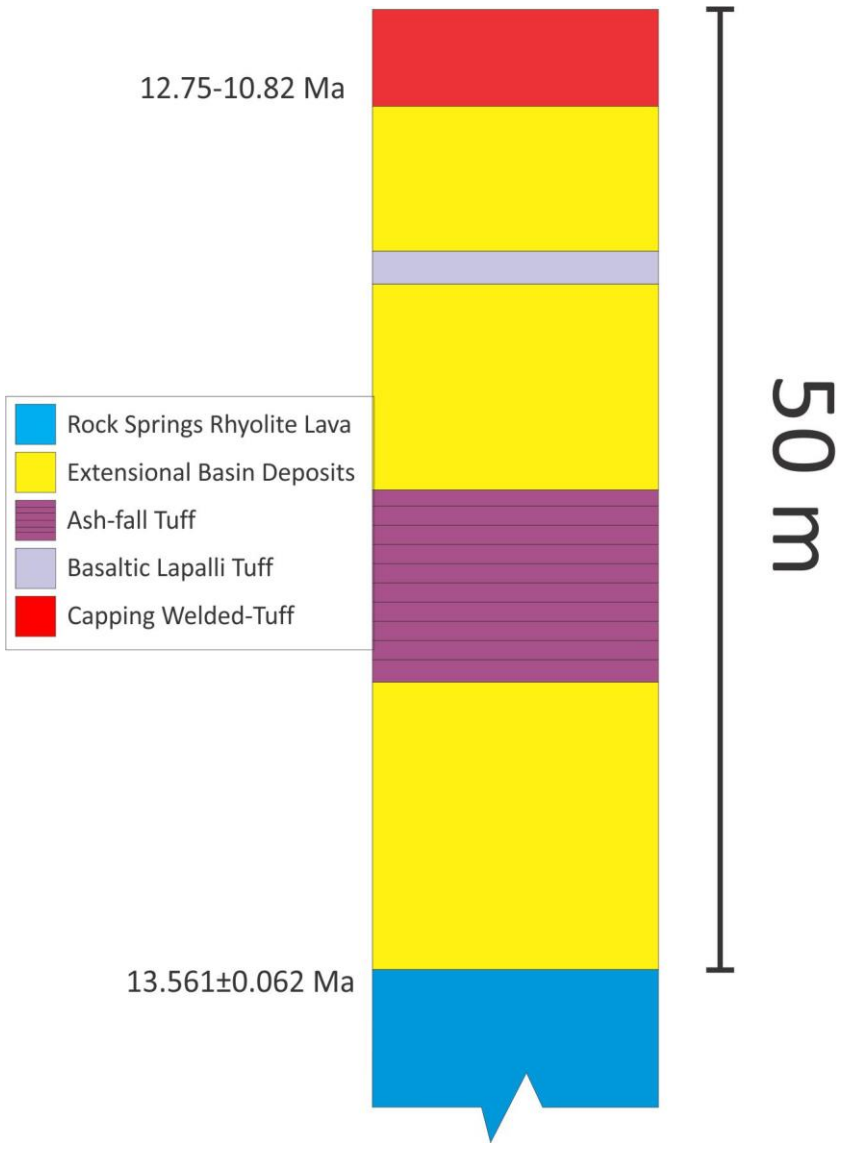

Figure 7.12: Stratigraphic section of the Rock Springs Formation created on informal stratigraphic units. The Rock Springs Rhyolite lava (MB11-1) and the Rock Springs ash-flow tuff (AI13-1) were both used in constraining the basin extension.

7.3 Eastern Jarbidge Rhyolite of this study vs. Previously Studied Jarbidge Rhyolite.

The physical volcanology of my samples (explained earlier in the thesis) as well as those previously studied by Brueseke et al. (2014) suggests that the Jarbidge Rhyolite in this study are indeed lavas and/or domes. In my samples, as well as Brueseke et al. (2014), there were no pyroclastic textures found during field work at the outcrop scale or in the petrographic analyses of thin sections. The mirrored indications of lavas between the two studies include: [1] no macro- or microscopic pyroclastic textures, including in the vitrophyre (AI13-3); [2] lobate morphologies (AI13-4); and [3] autobreccias (AI13-3). The upper vitrophyre units were also found in contact with lithoidal rhyolite units at site AI12-2 and there was vitrophyre (carapace) breccia. These are both found in younger Bruneau-Jarbidge eruptive center lavas (Bonnichsen and Kauffman, 1987). The ramping involved in sites AI12-2 and AI13-5 further confirms this interpretation. Brueseke et al. (2014) also found carapace breccia, crumble breccia, macro-scale flowbands, and sheet/columnar jointing. Although these secondary textures are not exclusive to lavas and in fact can be found in many rhemorphic ash-flow tuffs, when taken in tandem with the primary textures numbered above, they show that the Jarbidge Rhyolite reported here are indeed rhyolite lavas, consistent with the interpretation of Brueseke et al. (2014). This textural description is the first step in comparing the similarities to my own eastern Jarbidge Rhyolite units with those of the "main body" Jarbidge Rhyolite units studied by Brueseke et al. (2014) in the west of Elko County, NV.

The mineralogy of the eastern Jarbidge Rhyolite samples are closely related to that of the samples studied by Brueseke et al. (2014). Table 5 contains the modal averages of the rhyolites from this study as well as the Jarbidge Rhyolite studied by Brueseke et al. (2014). Total phenocryst abundances in my samples range from 20% to 40%. The Rock Springs Rhyolite has a phenocryst abundance of 20% , while in Brueseke et al. (2014) the range for the Jarbidge Rhyolite units is from 20-40%.

Table 5: Modal Average of Rhyolite Samples

	Phenocryst Totals	Quartz	Sanidine	Plagioclase	Pyroxene	Zircon
Jarbidge Rhyolite (This Study)	34%	20.5%	7.15%	5.25%	<1%	<1%
Jarbidge Rhyolite (Brueseke et al., 2014)	30%	11.2%	9.6%	7.0%	<1%	<1%
Rock Springs Rhyolite (This study)	20%	15%	4%	3%		

The samples in this study also exhibit a variety of textures indicative of complex petrogenetic processes; such textures are also seen in the Jarbidge Rhyolite from the main western bodies. These include ocelli; inclusion rims; embayments; sieved, boxy, spongy, and skeletal crystals. Textures like these can indicate magma mixing or assimilation and melting of country rock (Stimac, 1992; Seaman, 2000; Streck, 2008) or the possibility of cumulates in the magma body (Brueseke et al., 2014; Ellis et al., 2014). The abundance of crystal clots within the samples supports the notion of cumulates in the subsurface magma bodies that were entrained into ascending and erupting magmas. Embayments are characteristic textures of crystals forming via decompression melting (Donaldson and Henderson, 1988). Inclusions of sanidine or quartz in skeletal plagioclase crystals are possibly the result of the mixing of mafic and silicic magmas (Hibbard, 1981); however, there is no evidence in the geochemistry of the Jarbidge Rhyolite that suggests this type of mixing. Both the spongy and boxy cellular textures are due to dissolution (Streck, 2008) and according to Wood and Huppert (2003), dissolution and resorption of crystals can be due to the thermal evolution of under-plating mafic material. The Rock Springs Rhyolite exhibits all of these textures as well as the wormy intergrowth texture between quartz and plagioclase known as myrmekite.

Physical volcanology and mineralogy suggest that the Jarbidge Rhyolite volcanism in this study (eastern Jarbidge Rhyolite) is both physically and chemically similar to that studied by Brueseke et al. (2014). Geochemical data provide further evidence for this interpretation. Figure 7.13 shows that samples from both studies are metaluminous to slightly peraluminous rhyolites.

A-type rhyolites are classified by Whalen et al. (1987) and Patino Douce (1997) as having a high FeO/MgO and $(Na_2O+K_2O)/Al_2O_3$ ratios as well as low Al and Ca contents compared to calc-alkaline silicic magmas. A-type rhyolites, as well as most A-type granites, are interpreted as having originated in shallow (<15 km) quartzo-feldspathic, usually calc-alkaline, crust. As discussed by Brueseke et al. (2014), Jarbidge Rhyolite lavas are characterized by Rb/Nb ratios between ~5-11. These values are similar to that of the average upper continental crust (7±2) as reported by Rudnick and Gao (2003). My Jarbidge Rhyolite samples have Rb/Nb ratios of ~5 to 9, which are consistent with the results of Brueseke et al. (2014) and like that study, suggest the involvement of evolved crust in the petrogenesis of the studied Jarbidge Rhyolite. However, Figure 7.14 shows that the Brueseke et al. (2014) Jarbidge Rhyolite samples on average (~8) have slightly higher Rb/Nb ratios than my studied eastern samples (~6). Both of these averages are within the range of standard deviation as reported by Rudnick and Gao (2003), however samples studied by Brueseke et al. (2014) report Rb/Nb ratios outside of the standard deviation ($1\sigma=2$) value (Rudnick and Gao, 2003). This is an indication of possible change in involvement of evolved crust that influenced each cluster of Jarbidge Rhyolite differently. The involvement of a mafic component would lower the Rb/Nb ratio, thus indicating that my Jarbidge Rhyolite might have a higher mafic component involved in the source material. There could be a difference in melting the Archean mid-upper crust or upper-crustal bodies of Mesozoic granitoid (Brueseke et al., 2014) or there could be a change in the involvement of the mafic interplating that I discussed earlier from McCurry and Rodgers (2009) model. Indeed, numerous studies the compositional variability of crustal lithologies across the Great Basin region, including Cretaceous granitoids, Archean crust, middle Proterozoic plutons, Jurassic plutons, shelf/slope domain sediments, etc. (Bennet et al., 1987, Foster et al., 2006; Miller et al., 2012). Foster et al. (2006) confirms that, specifically in Nevada, three different lower crustal lithologies exist: Grouse Creek (Archean), >2.5 Ga; Mojave (Proterozoic), 2.0-1.7 Ga; Phanerozoic accreted terranes (Proterozoic). Elko County, NV overlies the Grouse Creek block. This block was most likely originally part of the Wyoming craton, but has since been detached and reworked by multiple metamorphic events.

Other trace and major elements plotted against wt. % silica (Figure 7.14) show that my Jarbidge Rhyolite units plot within the range of Jarbidge Rhyolite studied by Brueseke et al. (2014). An interesting feature shown by the Jarbidge Rhyolite is that barium decreases with

increasing SiO_2. Barium is a LILE (large-ion lithophile) and generally increases in concentration with silica content (Ure and Berrow, 1982). However, there are studies of highly evolved granites containing very low concentrations of barium (<200 mg kg-1) (Plant et al., 1980). Plagioclase and potassium feldspar fractionation will cause barium concentrations to decrease in magmas.

Aside from the Rb/Sr, and Na_2O plot, the Rock Springs Rhyolite plots within or near the range of Jarbidge Rhyolite, consistent with a petrogenetic relationship between the two. However, more work is needed to confirm this interpretation, particularly given that the unusually high Rb/Sr and Na_2O values suggest that this rhyolite is more evolved that the Jarbidge Rhyolite. Plotting against a multi-element diagram (Figure 7.15), we can see that Jarbidge Rhyolite units all show a similar trend. Although the Rock Springs Rhyolite has the same general pattern, it has negative Ba, Sr, and Ti anomalies (e.g., more feldspar and oxide fractionation). This again points to a more evolved version of the Jarbidge Rhyolite.

The barium concentration groups introduced earlier are still apparent when data from both my and the Brueseke et. al (2014) study are combined (Figure 7.16). Samples with low Ba exhibit low CaO, TiO_2, Sr, Zr, and P_2O_5, and high Rb, U, and R/Nb values. There is no apparent geographical factor that determines these groupings, so another explanation must be sought for these differences R/Nb vs Ba in particular shows considerable variation around the boundary between the two groups. As stated early Rb/Nb values according to Rudnick and Gao (2003) are indicative of crustal sourcing for magmas. There is a positive trend between the Ba concentration and the Rb/Nb values: as Ba concentrations increase, Rb/Nb values decrease, however the amount of overlap suggests a possibility of two semi-subparallel arrays. Higher values of Rb/Nb indicate upper crustal sourcing, while lower values indicate probable lower crustal sourcing or the addition of a mafic component (e.g., Central Snake River Plain rhyolites). According to Rudnick and Gao (2003), the average Rb/Nb value for the upper continental crust is ~7, The majority of the samples below the Ba=1000 ppm line have a Rb/Nb value above 7, while the majority of the samples about the barium division fall below Rb/Nb=7. This indicates either a change in magma crustal source or the same source, but a change in the interaction between the crust and magma (e.g., a change in the mafic component or different crust material [Archean, Proterozoic plutons, etc.]).

The Wells and West Wendover samples are located over 100-km apart from any other Jarbidge Rhyolite lava and form very distinctive dome-lava complexes, with easily mappable areal extents. Geochronology demonstrates that these units are different ages (15.25 Ma vs. 13.69 Ma). This indicates that both the Wells and West Wendover samples are distinct and have local eruptive loci. Similarly, the little Goose Creek Jarbidge Rhyolite are likely discrete bodies; however, they could potentially have been sourced from the same or multiple magma bodies at depth.

The chemistry of my Jarbidge Rhyolite in the east of Elko County, NV and that of the western "main body" of Jarbidge Rhyolite studied by Brueseke et al. (2014) shows that they are indeed similarly sourced lavas. The Rock Springs Rhyolite also falls within this grouping and it is inferred through multi-element and Harker diagrams that it could possibly be a more evolved version of the Jarbidge Rhyolite.

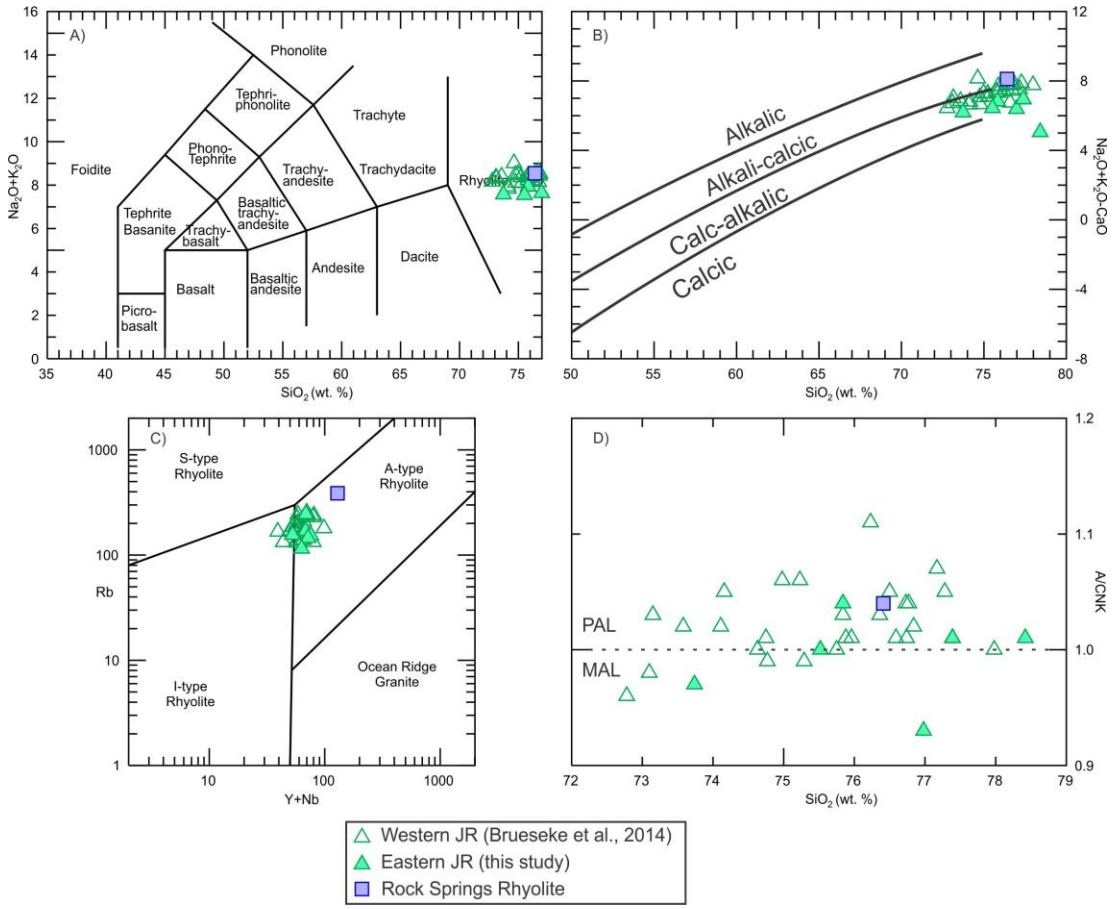

Figure 7.13: Major and trace element comparisons of eastern and western Jarbidge Rhyolite. (A) Total alkalis vs. silica diagram showing that all samples plot as rhyolite (Lebas et al., 1986). (B) MALI diagram; the western Jarbidge Rhyolite and the eastern Jarbidge Rhyolite plot as calc-alkalic (Frost et al., 2001). (C) Rb vs Y+Nb discrimination diagram (Pierce et al. 1984); all plot as A-type rhyolite. (D) SiO2 vs A/CNK; all samples are metaluminous (MAL) to slightly peraluminous (PAL).

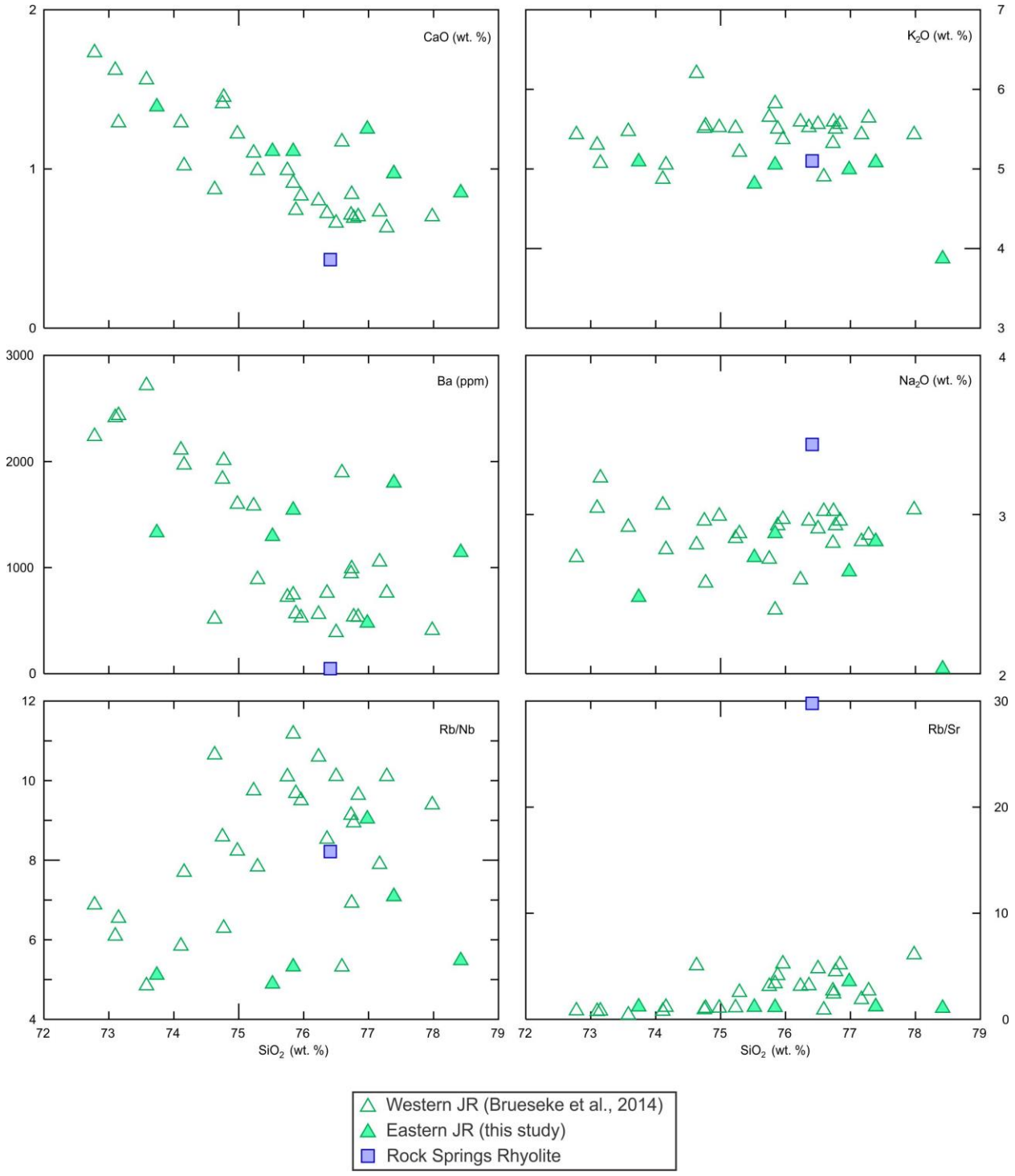

Figure 7.14: Harker diagrams for all rhyolite lavas. The sample with low Na_2O and K_2O is MB11-2. SiO2 and other major element oxides are measured in wt. %. Ba is measured in ppm.

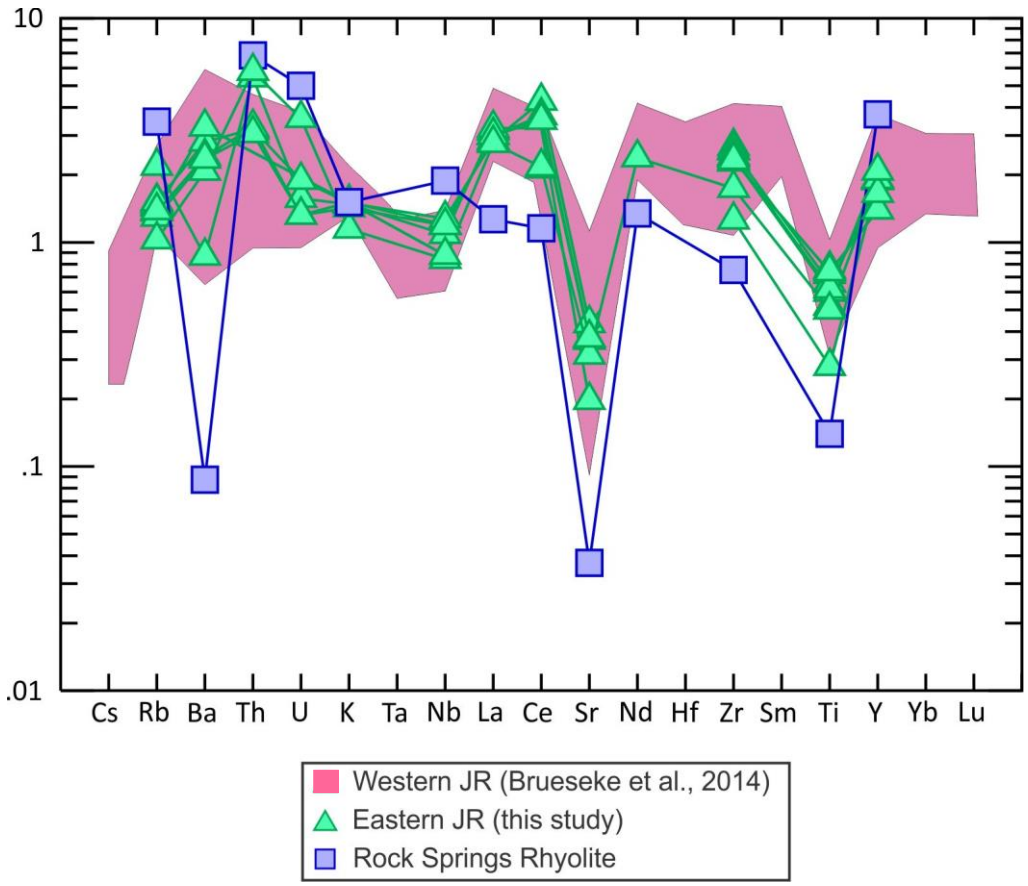

Figure 7.15: multi-element diagram normalized to average upper continental crust of Taylor and McLennan (1985). Rock Springs has low Ba, Sr, and Ti anomalies, while still holding the same general pattern as the Jarbidge Rhyolite. The pink field represents the Western Jaridge Rhyolite studied by Brueseke et al. (2014).

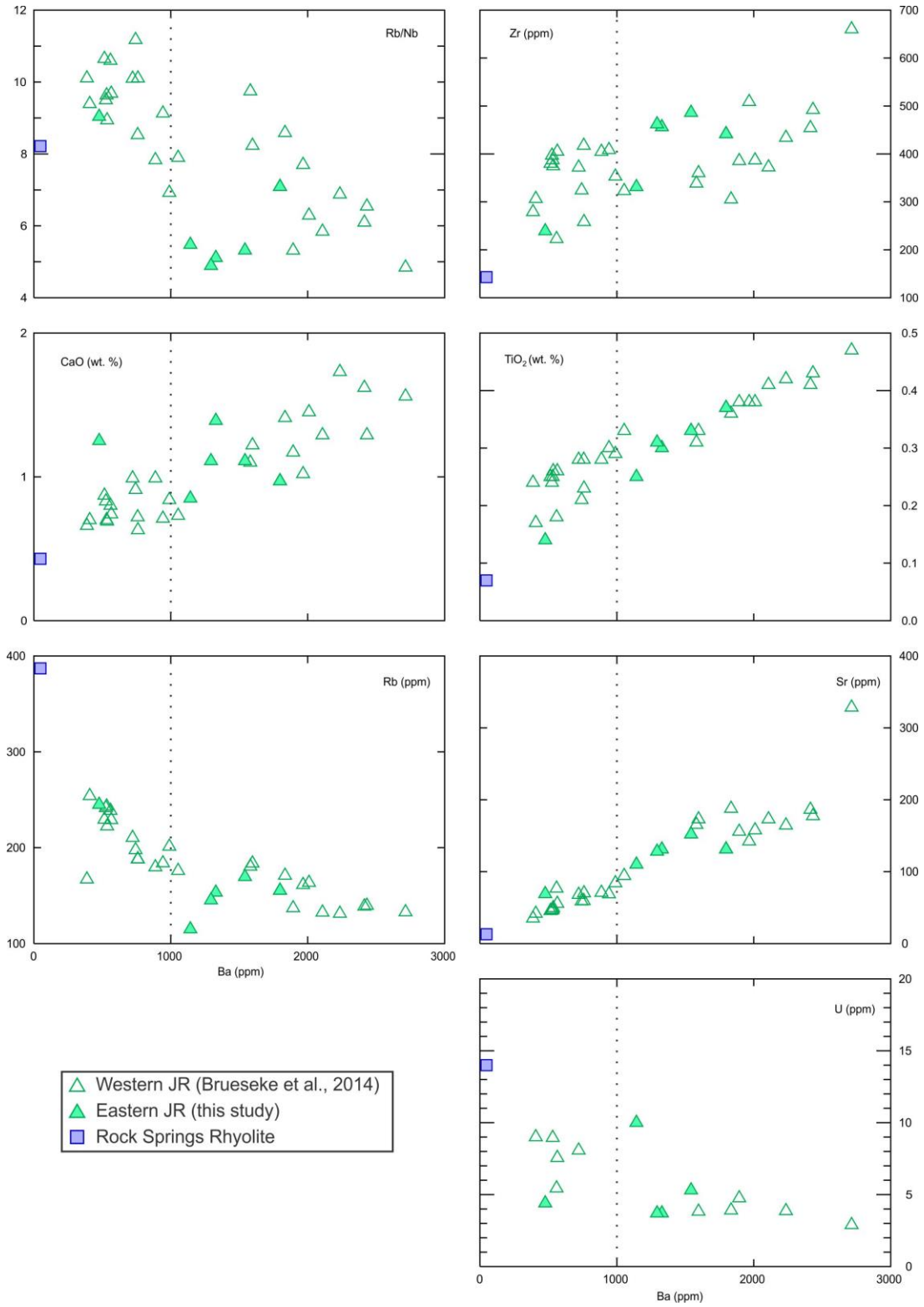

Figure 7.16: Barium plots that indicate a clear difference between the high and low barium groups. The dashed line represents a barium division at 1000 pm.

7.3.1 Geochronology

The $^{40}Ar/^{39}Ar$ geochronology from this study indicates that Jarbidge Rhyolite (and Rock Springs) volcanism was active in the region from 15.25 to 13.56 Ma. Previous data from Brueseke et al. (2014) indicates the "main body" Jarbidge Rhyolite has an age of ~16.1 to 15.0 Ma. Coupling these data, as well as older studies on eastern Nevada/Utah border (Henry, 2008; McKee, 1976; Mueller and Snoke, 1993; Evernden et al. 1964; Compton 1983; Hart and Carlson, 1985; Evans and Brown, 1981) with that from my own study, an eastward younging trend discussed by Brueseke et al. (2014) is evident. In work by McKee et al. (1976), K-Ar ages (16.8 to 15.4 Ma) were determined for the Jarbidge Rhyolite in the vicinity of the Jarbidge Mountains region. Henry (2008) has published an $^{40}Ar/^{39}Ar$ age for a Jarbidge Rhyolite flow just south of Bull Run Basin that yields an age of 16.2 Ma. There have been few studies of Miocene rhyolite volcanic geochronology in the northeast corner of Elko County, east of samples collected on the lavas studied by Brueseke et al. (2014). Mueller and Snoke (1993) dated a string of Jarbidge Rhyolite-like rocks at the northern end of the East Humboldt Range (e.g., near Wells, NV) referred to as the Willow Creek Rhyolite, which were found to range from 14.8 to 13.4 Ma via K-Ar geochronology. This study's determined ages for the Willow Creek Rhyolite are younger than my own dates for the Willow Creek Rhyolite (15.25±0.08), which is most likely due to the inherent inaccuracies associated with K-Ar dating. This can be seen in the relative uncertainties of the two sets of data: K-Ar (2σ=1.4), $Ar/^{39}Ar$ (2σ=0.08), where this study's $Ar/^{39}Ar$ standard deviation is over an order of magnitude less than that of the K-Ar data set. McKee et al. (1976) analyzed a tridymite rhyolite from near West Wendover, NV (e.g., my West Wendover sample) via K-Ar geochronology, which yielded an age of 11.6 Ma.

Further east of my samples, on the Utah/Nevada border, work done in the Grouse Creek Mountains on the Salt Lake Formation (Humboldt Formation) and local Cenozoic geology has identified crystal-rich (e.g., smoky quartz-phyric) rhyolites similar to the Jarbidge Rhyolite, which have been dated by Compton (1983) to be 11.7± 0.4 Ma. A thick rhyolite vitrophyre in Grouse Creek has been dated by Evans and Brown (1981) by K-Ar geochronology to be 12.2 Ma. New $^{40}Ar/^{39}Ar$ work done on rocks exposed east of my samples in Pole Creek, Dairy Valley, and Toms Cabin Spring (Grouse Creek region, Utah; Miller et al., 2013) reveal similar ages from petrographically similar rhyolites (e.g., to the Jarbidge Rhyolite) that also fit the eastward-younging age progressive trend of 12.92±0.08 to 11.93±0.04 Ma.

This younging trend of my own data combined with the previous K-Ar and $^{40}Ar/^{39}Ar$ ages to the west and east of my study site (Figure 7.17) (Evernden et al. 1964; McKee, 1976; Compton

1983; Evans and Brown, 1981; Hart and Carlson, 1985; Mueller and Snoke, 1993; Utah G.S. et al., 2013; Henry, 2008; Brueseke et al., 2014) indicates that the effusive rhyolite magmatism in northeastern Nevada and northwestern Utah is coeval with Miocene Basin and Range extension that has been suggested to result from the collapse of the Nevadaplano across northeastern Nevada (Perkins, 1995; Rodgers et al., 2002; Best et al., 2009; Brueseke et al., 2014).

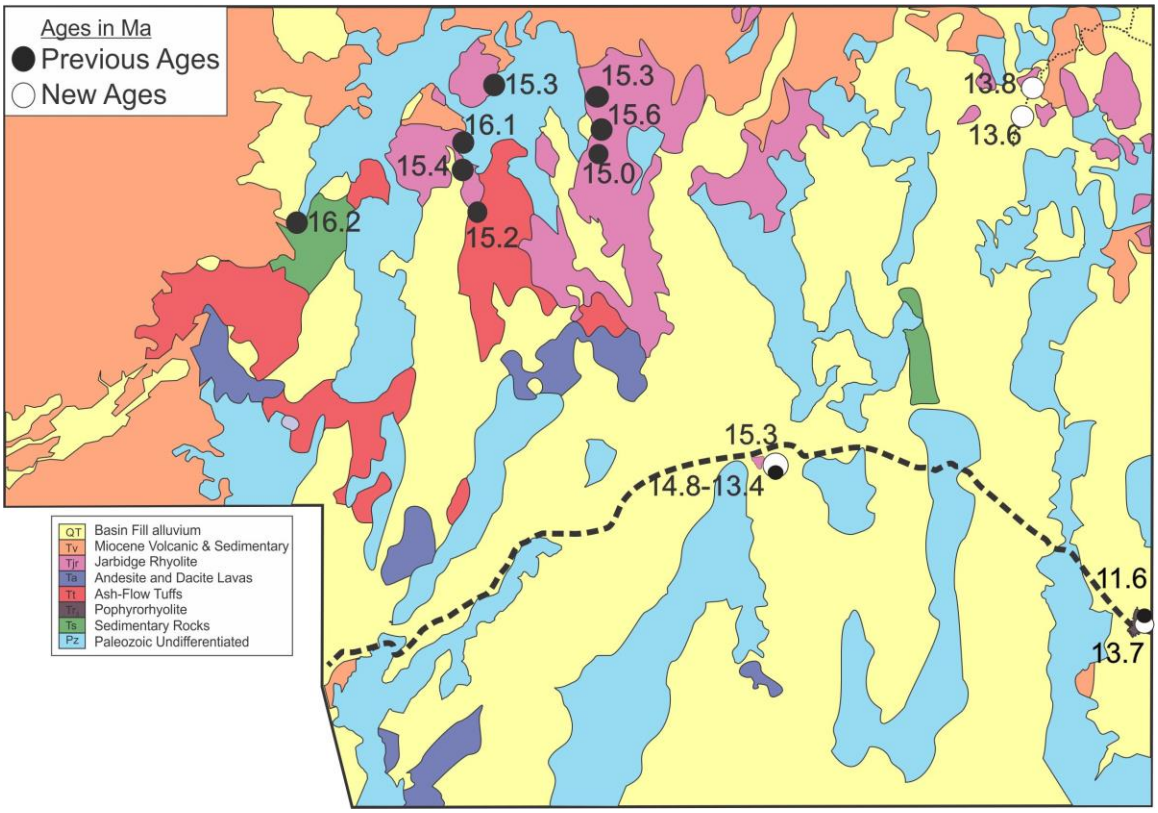

Figure 7.17: A simplified version of Coats (1987) geological map. The white dots are the new geochronology via $^{40}Ar/^{39}Ar$. The black dots represent $^{40}Ar/^{39}Ar$ data from Brueseke et al. (2014), Henry (2008), as well as K-Ar and $^{40}Ar/^{39}Ar$ data from McKee (1976) and Mueller and Snoke (1993).

7.3.2 Regional Comparison with Snake River Plain silicic volcanism

Several lava units from the Bruneau-Jarbidge eruptive center (central Snake River Plain) (Bonnichsen 1982, 2008) have been chosen to compare to the Jarbidge Rhyolite volcanism. These volcanics were chosen based on their geographical and temporal relationship to the Jarbidge Rhyolite volcanism. Using major and trace element geochemistry, distinct groupings can be formed to distinguish Bruneau-Jarbidge effusive felsic magmatism from the Jarbidge Rhyolite magmatism (Figure 7.18). The source differences between the Jarbidge Rhyolite and central Snake River Plain felsic magmas become apparent when you plot the Rb/Nb ratios for these rhyolites. The central Snake River Plain rhyolites all range from 2 to 4, which indicates the probability of a hybrid source consisting of: [1] a mafic component (low Rb/high Nb) and [2] a felsic crust (McCurry and Christiansen, 2008; Brueseke et al., 2014). This mafic component is underplated basalt/gabbro that stalls out in the crust, hybridizing and lowering the values of Rb/Nb. This differs from the Jarbidge Rhyolite , which show a range of Rb/Nb ratios of 5 to 9, inferring an upper crustal source with a minor mafic component as discussed earlier (Figure 7.18); this source difference is consistent with the results (Rb/Nb= 5-11) of Brueseke et al. (2014).

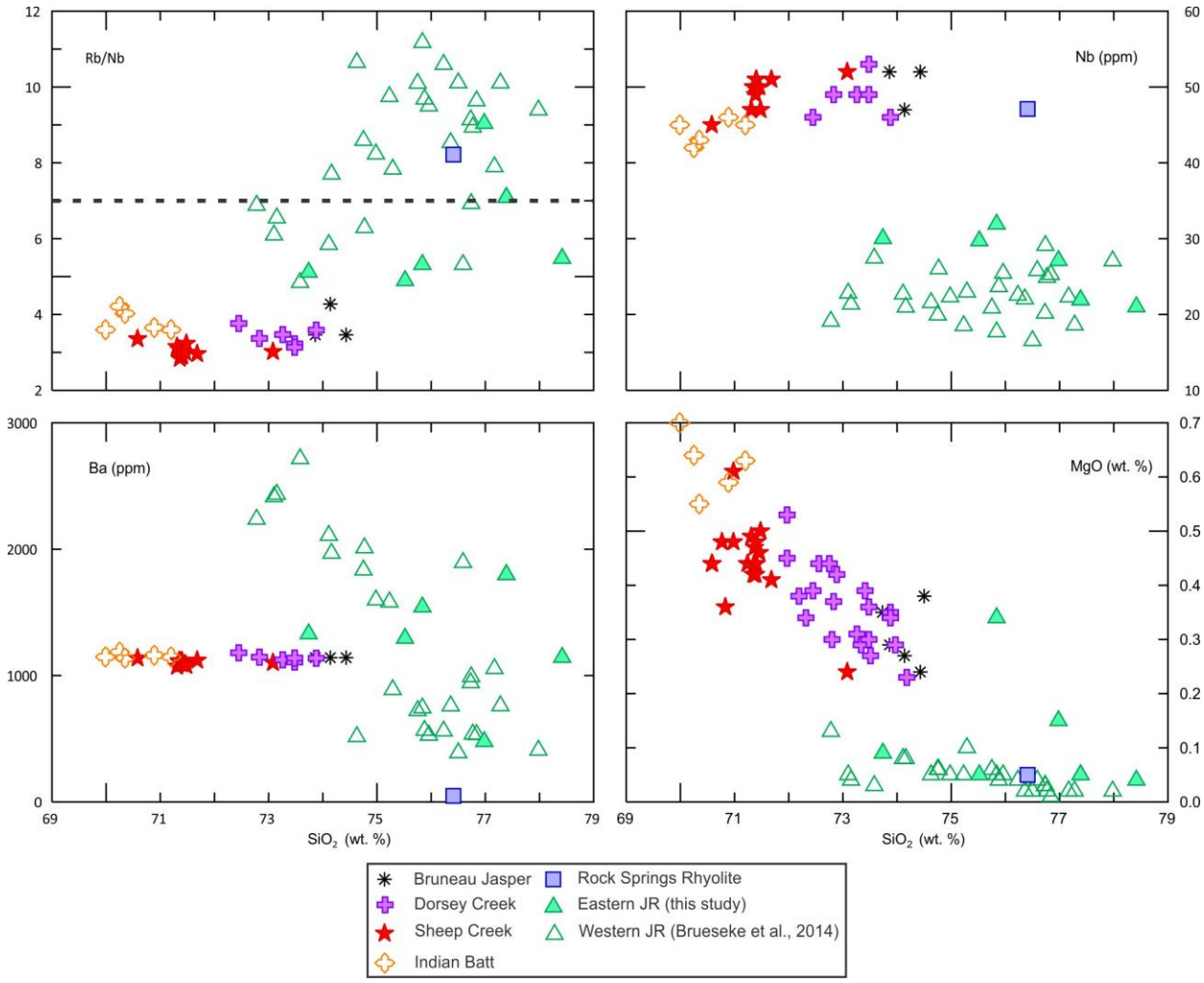

Figure 7.18: Harker diagrams showing distinct groups for the Jarbidge Rhyolite and Miocene central Snake River Plains Rhyolite lavas from the Bruneau-Jarbidge eruptive center. The black dashed line represents the average value of Rb/Nb (~7) for the upper continental crust as determined by Rudnick and Gao (2003).

7.4 Regional tectonomagmatic significance of Jarbidge Rhyolite volcanism

Combining the discussion points above it is clear that some of my samples (AI12-6; AI13-2,3,4; MB11-1,2; JC-09-22) studied in the northeastern portion of Nevada are indeed Jarbidge Rhyolite lavas. We can also see from the regional and new geochronology that these samples, which are to the east of the samples studied by Brueseke et al. (2014), on average are ~ two million years younger. Using these data as well as the geochronology discussed above, there

is a clear younging trend of Miocene effusive rhyolite magmatism that extends well into Utah. Comparing the trend of all the Jarbidge Rhyolite units studied thus far to the two major coeval tectonomagmatic trends of the region (i.e. the Yellowstone hotspot "path" and Basin and Range extension) (Figure 7.19), we can see that the age of magmatism of the Jarbidge Rhyolite follows the same northeastern trend, although, like the extension, for locations along the same lines of longitude, it precedes the Yellowstone hotspot in every location by a few million years. In Figure 7.20, I use a diagram created by Rodgers et al. (1990, 2002) and modified by Brueseke et al. (2014) to compare the distance from Jackson Hole, WY to both ages measured for the extension and ages for each large silicic eruptive center of the Yellowstone hotspot (Rodgers et al., 1990, 2002; and references within). Including the same information for the sampled Jarbidge Rhyolite and Rock Springs Rhyolite in this study, coupled with the previous work of Brueseke et al. (2014) shows us that the effusive rhyolite magmatism of northeastern Nevada occurred coeval with the extension of the Basin and Range at both locations and predated voluminous caldera-forming felsic eruptions of the Yellowstone hotspot at a given location. Using this interpretation of a younging trend of Jarbidge Rhyolite magmatism that is coeval to the timing of "modern" Basin and Range extension as well as the conclusion that Jarbidge Rhyolite is distinctly different and separate from the lavas sourced from the Yellowstone hotspot, my data supports the interpretation of Brueseke et al. (2014) that Jarbidge Rhyolite magmatism was most likely directly related to lithospheric extension due to Basin and Range extension and was not caused by the passage of the Yellowstone hotspot.

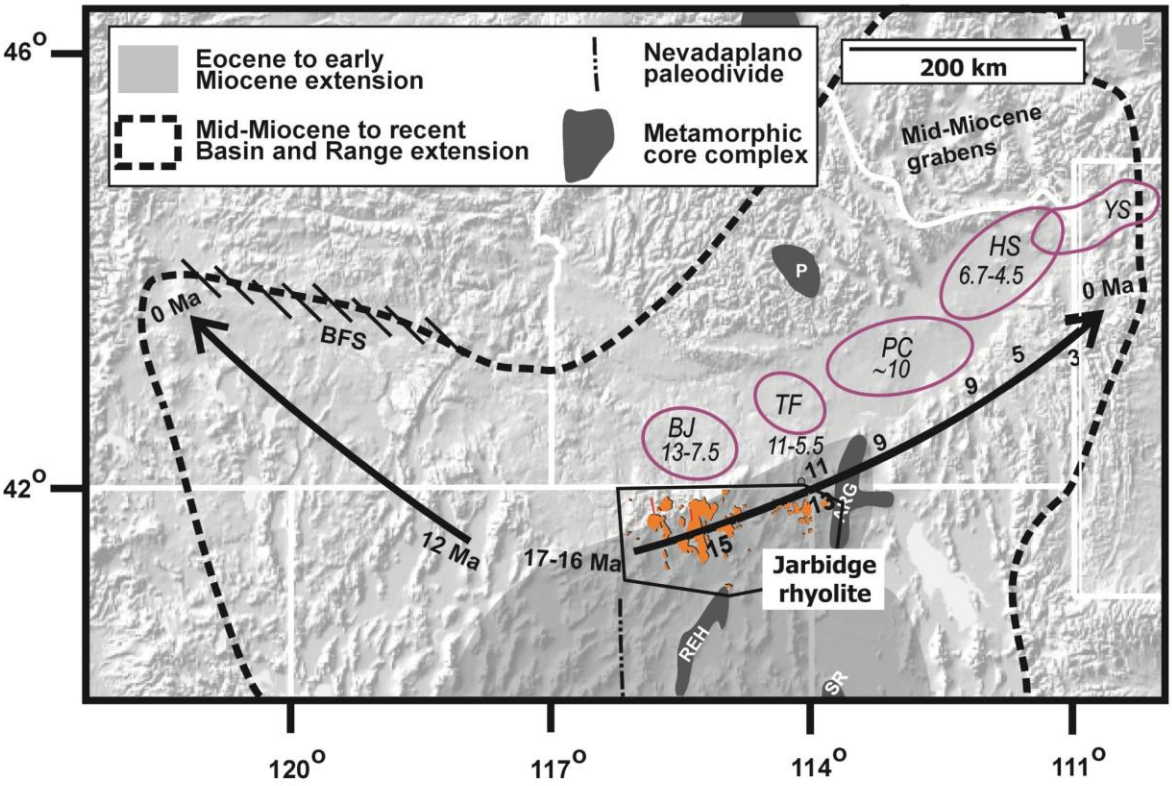

Figure 7.19: ***Adapted from Brueseke et al. (2014)*****. Basin and Range extension is represented as black arrows (Rodgers et al., 2002; Colgan et al., 2006; Scarberry et al., 2009; Sears et al., 2009), with the current extent outlined as dashed black lines. Associated ages are labeled in millions of years. The orange polygons represent Jarbidge Rhyolite magmatism. Purple ovals are eruptive centers associated with the Yellowstone hotspot. Abbreviation are: BJ, Bruneau-Jarbidge; TF, Twin Falls; PC, Picabo; HS, Heise; YS, Yellowstone; P, Pioneer Mountains; ARG, Albion-Raft River-Grouse Creek; REH, Ruby-East Humboldt; SR, BFS, Brothers fault zone.**

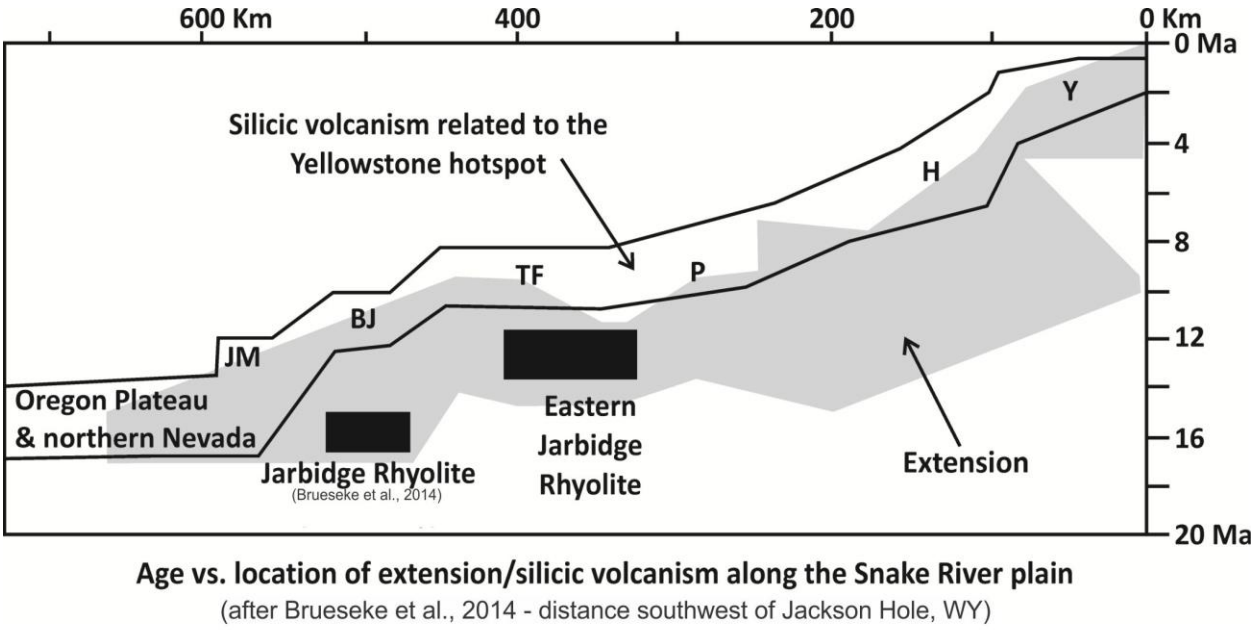

Figure 7.20: ***Adapted from Rodgers et al. (1990; 2002) and Brueseke et al. (2014).*** **Distance from Jackson Hole WY (X-axis) vs. age (in millions of years; Y-axis). The grey area represents timing of extension. The black boxes represent my samples (Eastern Jarbidge Rhyolite) and the main bodies studied by Brueseke et al. (2014). The eastern field originally defined by Brueseke et al. (2014) has extended further to the east via my own samples. The abbreviations are eruptive centers related to the Yellowstone hotspot (JM: Juniper Mountain, BJ: Bruneau-Jarbidge, TF: Twin Falls, P: Picabo, H: Heise, Y, Yellowstone).**

Chapter 8 - Summary

Using the physical, petrographical, geochemical, and geochronological data from various sites around northeastern NV, including more detailed reconnaissance work in the little Goose Creek region, I have been able to correlate previously unstudied geological units that were initially mapped by Coats (1987) as Tertiary basalts (Tb), Tertiary ash-flow tuffs (Tts), Tertiary phenorhyolites (Tr_3), and Jarbidge Rhyolite (Tjr). The Tertiary basalts have been correlated to the *ca*. 7.26±0.06 Ma (William et al., 1999) Snake River olivine tholeiites studied by McCurry et al. (unpub.) in the Cassia Mountains, ID. The Tertiary ash-flow tuffs were divided into two sub-groups based on their geochemistry: a lower-silica group (Goose Creek) and a higher-silica group (RS/CoR). The Goose Creek ash-flow tuffs show an affinity towards the Twin Falls eruptive center, extending the range of the known maximum extent line of the Twin Falls ash-flow tuffs. The higher-silica group tentatively correlates to outflow from the Bruneau Jarbidge eruptive center, specifically the Cougar Point Tuff. If correct, this would extend the range of the known outflow for the Cougar Point Tuff to well into south-central portion of Idaho as well as further southeast into Nevada. This correlation combined with geochronological and stratigraphic data on the Rock Springs ash-flow tuff and associated sediments allowed me to constrain basin extension in the Rock Springs area to a maximum range of 13.56 to 10.82 Ma, as well as the duration of local extension to 0.8 to 3.8 m.y. This is similar to other extensional basin ages obtained for work in other studies performed in similar locations (Trapper Creek and western Utah; Perkins et al. 1995; Rodgers et al., 2002; Miller et al., 2012). I have shown that the eastern Jarbidge Rhyolite lavas sampled in this study, as well as the Rock Springs Rhyolite, are chemically similar to the western Jarbidge Rhyolite studied by Brueseke et al. (2014). Furthermore, I have placed temporal constraints on these rhyolites, which provide more robust ages than the sparse earlier K-Ar dates and confirms an eastward time-transgressive Miocene trend. This "trend" mimics that of the Basin and Range extension towards the edges of the modern Basin and Range province. This Although this Miocene magmatism and extension follows a generally similar eastward trend as the major caldera forming eruptions related to the Yellowstone hotspot, it predates Snake River Plain eruptive events by a few million years (for locations along the same lines of longitude), suggesting a relationship between the Miocene

felsic magmatism of northeastern Nevada and likely northwestern Utah and Basin and Range extension.

Chapter 9 - Suggestion for Future Work

Detailed mapping of individual Jarbidge Rhyolite "map units" from the outcrops in little Goose Creek area will help to further define and constrain the Jarbidge Rhyolite. This field mapping will definitively show that the bodies I have defined as domes and lavas in the little Goose Creek area are in fact just that, as well as the extent of these individual flows. REE data from the eastern Jarbidge Rhyolite units as well as more $^{40}Ar/^{39}Ar$ geochronology on these bodies can help depict individual flows, separate distinct eruptive loci, and provide the timing of these eruptions relative to each other (as stated earlier, some of this geochronology is currently being undertaken). Isotopic data on the Jarbidge Rhyolite would help to confirm the interpretations about the crustal involvement. A detailed analysis including mapping and descriptions of the Dry Gulch Jarbidge Rhyolite and the associated lava lobes can be used to help explain lobe formations in felsic lavas and potentially shed light on the interaction between felsic lavas and water bodies.

Detailed mapping of all the ash-flow units will help in the correlation of local basin extension in the area, as many of these ash-flows are capping units above the basin deposition (liken to the Rock Springs ash-flow). Mapping will also help further refine eruptive volumes associated with individual pyroclastic eruptions, as well as total volumes produced from the Bruneau-Jarbidge and Twin Falls eruptive centers. Given these tuffs represent outflow related to some of the largest volcanic eruptions documented on earth, fully understanding the individual and cumulative volume of magmas erupted from these systems is critical to understanding the petrologic evolution and volcanic hazards of these types of systems. In places where the tuffs are intercalated with sedimentary strata, more $^{40}Ar/^{39}Ar$ geochronology should be used to solidify the ages of these tuffs to help in determining the age of basin formation in the area.

References

Andrews, Graham D. M., Michael J. Branney, Bill Bonnichsen, and Michael Mccurry., 2008,"Rhyolitic Ignimbrites in the Rogerson Graben, Southern Snake River Plain Volcanic Province: Volcanic Stratigraphy, Eruption History and Basin Evolution." *Bulletin of Volcanology* 70.3 269-91.

Armstrong, R. L., W. P. Leeman, and H. E. Malde. "K-Ar Dating, Quaternary and Neogene Volcanic Rocks of the Snake River Plain, Idaho." *American Journal of Science* 275.3 (1975): 225-51. Print.

Bennett, Victoria C., and Donald J. Depaolo. "Proterozoic Crustal History of the Western United States as Determined by Neodymium Isotopic Mapping."Geological Society of America Bulletin 99.5 (1987): 674. Print.

Bernt, J.D., 1998, Volcanism, tectonic evolution and gold-silver vein formation in the Jarbidge Mountains, Elko County, Nevada. Geological Society of Nevada Meeting Abstract.

Best, Myron G., Deborah L. Barr, Eric H. Christiansen, Sherman Gromme, Alan L. Deino, and David G. Tingey. 2009. "The Great Basin Altoplano during the Middle Cenozoic Ignimbrite Flareup: Insights from Volcanic Rocks." *International Geology Review* 51.7-8: 589-633. Print

Best, M. G., S. Gromme, A. L. Deino, E. H. Christiansen, G. L. Hart, and D. G. Tingey. "The 36-18 Ma Central Nevada Ignimbrite Field and Calderas, Great Basin, USA: Multicyclic Super-eruptions." Geosphere 9.6 (2013): 1562-636. Print.

Bonnichsen, B., 1982, Rhyolite lava flows in the Bruneau-Jarbidge eruptive center, Southwestern Idaho. In: Bonnichsen, B. and Breckenridge, R.M., eds., Idaho Bureau of Mines and Geology Bulletin 26, p. 283-320.

Bonnichsen, B., and Citron, G., 1982, The Cougar Point Tuff, Southwestern Idaho and Vicinity. In: Bonnichsen, B. and Breckenridge, R.M., eds., Idaho Bureau of Mines and Geology Bulletin 26, p. 255–281.

Bonnichsen, B. and Kaufman, D.F., 1987, Physical features of rhyolite lava flows in the Snake River Plain volcanic province, Southwestern Idaho. In: J.H. Fink (Editor), The emplacement of silicic domes and lava flows. Geological Society of America Special paper 212, Pgs. 119-145.

Bonnichsen, Bill, and M.M. Godchaux, 2002, Late Miocene, Pliocene, and Pleistocene geology of southwestern Idaho with emphasis on basalts in the Bruneau-Jarbidge, Twin Falls, and western Snake River Plain regions, *in* Bill Bonnichsen, C.M. White, and Michael McCurry, eds., Tectonic and Magmatic Evolution of the Snake River Plain Volcanic Province:Idaho Geological Survey Bulletin 30, p. 233-312.

Bonnichsen, B., Leeman, W.P., Honjo N., McIntosh, W.C., and Godchaux, M.M., 2008, Miocene silicic volcanism in southwestern Idaho: geochronology, geochemistry, and evolution of the central Snake River Plain: Bulletin of Volcanology, v. 70, p. 315-342.

Brueseke, M.E., Callicoat, J.S., Hames, W., and Larson, P.B, 2014. Voluminous mid-Miocene rhyolite volcanism in northeastern Nevada: the Jarbidge Rhyolite and its significance to the Cenozoic evolution of the northern Great Basin (U.S.A.):*Geological Society of America Bulletin*.

Branney, M.J., Bonnichsen, B., Andrews, G.D.M., Ellis, B., Barry, T.L., & McCurry, M., 2008, "Snake River (SR)-type" volcanism at the Yellostone hotspot track: distinctive products from unusual, high-temperature silicic super-eruptions. Bulletin of Volcanology v. 70, p. 293-314.Brueseke, M.E., and Hart, W.K., 2008, Geology and petrology of the mid-Miocene Santa Rosa-Calico volcanic field, northern Nevada: *Nevada Bureau of Mines and Geology Bulletin 113*.

Brueseke, M.E., Hart, W.K., and M.T. Heizler, 2008, Diverse mid-Miocene silicic volcanism associated with the Yellowstone-Newberry thermal anomaly: *Bulletin of Volcanology*.

Burchfiel, B. C., Darrel S. Cowan, and Gregorg A. Davis., 1992, "Tectonic Overview of the Cordilleran Orogen in the Western United States." *The Geology of North America* G-3: 407-79. Print.

Callicoat, J.S., 2010, Significance of Mid-Miocene volcanism in northeast Nevada: petrographic, chemical, isotopic, and temporal importance of the Jarbidge Rhyolite: Kansas State University, Manhattan, Kansas.

Camp, V.E. and Ross, M.E., 2004, Mantle dynamics and genesis of mafic magmatism in the intermontane Pacific Northwest: Journal of Geophysical Research, v. 109, B08204 DOI:10.1029/2003JB00283

Carlson, R.W. and Hart, W.K., 1987, Crustal Genesis on the Oregon Plateau: *Journal of Geophysical Research*. Coats, Robert Roy, 1987, Geology of Elko County, Nevada. Reno, NV, *Nevada Bureau of Mines and Geology, University of Nevada-Reno*

Christiansen, E.H., Sheridan, M.F., and Burt, D.M., 1986, The geology and geochemistry of Cenozoic topaz rhyolites from the Western United States. *Geological Society of America Special Paper* 205.

Christiansen, R.L., Fougler, G.R., and Evans, J.R., 2002, Upper-mantle origin of the Yellowstone hotpot. Geological Society Upper-mantle origin of the Yellowstone hotpot: Geological Society of America Bulletin, v. 114, p. 1245-1256.

Christiansen, E.H. and McCurry, M., 2008, Contrasting origins of Cenozoic silicic volcanic rocks from the western Cordillera of the United States: Bulletin of Volcanology v. 70, p. 251-267.

Coats, R. R., R. C. Green, and L. Y. Marks., 1977, "Mineral Resouces of the Jarbidge Wilderness and Adjacent Areas, Elko County, Nevada." *Geological Survey Bulletin 1439*

Coats, R.R., 1987, Geology of Elko County, Nevada: Nevada Bureau of Mines and Geology Bulletin 101, 112 p.

Coble, M.A., and Mahood, G.A., 2012, Location of initial impingement of the Yellowstone plume defined by widespread silicic volcanism contemporaneous with Columbia River Basalts, Geology, doi: 10.1130/G32692.1.

Colgan, Joseph P., David A. John, Christopher D. Henry, and Robert J. Fleck, 2008, Large-magnitude Miocene Extension of the Eocene Caetano Caldera, Shoshone and Toiyabe Ranges, Nevada: *Geosphere*.

Colgan, J.P. and Henry, C.D., 2009, Rapid middle Miocene collapse of the Mesozoic orogenic plateau in north-central Nevada: *International Geology Review.*

Compton, R.R., 1983, Displaced Miocene rocks on the west flank of the Raft River-Grouse Creek core complex, Utah, in Miller, D.M., Todd, V.R., and Howard, K.A., eds., Tectonic and stratigraphic studies in the eastern Great Basin: Geological Society of America Memoir 157, p. 271–279.

Coney, P.J., 1987, The regional tectonic setting and possible causes of Cenozoic extension in the North American Cordillera, *in* Coward, M.P., Dewey, J.F., and Hancock, P.L., eds., Continental extensional tectonics: Geological Society of London Special Publication 28, p. 177-186.

Coney, Peter J., and Tekla A. Harms., 1984, "Cordilleran Metamorphic Core Complexes: Cenozoic Extensional Relics of Mesozoic Compression." *Geology*: 550-54.

Crafford, A. Elizabeth Jones., 2008, "Paleozoic Tectonic Domains of Nevada: An Interpretive Discussion to Accompany the Geologic Map of Nevada." *Geosphere* 4.1: 260. Print.

Dickinson, W.R., 1997, Tectonic implications of Cenozoic volcanism in coastal California: Geological Society of America Bulletin, v. 109 p. 936-954.

Donaldson, C. H., and Henderson, C. M. B., 1988, "A New Interpretation of Round Embayments in Quartz Crystals." *Mineralogical Magazine* 52.364: 27-33.

Dorsey, Becky., 2007, "Review of Cordilleran Tectonics." Blue Mountains Seminar. Apr. Web. <http://pages.uoregon.edu/rdorsey/BM/Cord_Tect_UIUC.pdf>.

Ellis, Ben S., Olivier Bachmann, and John A. Wolff. "Cumulate Fragments in Silicic Ignimbrites: The Case of the Snake River Plain." *Geoogy* 42.8 (2014): n. pag.

Ellis, B.S., Barry, T.L., Branney, M.J., Wolff, J.A., Bindeman, I., Wilson, R., and Bonnichsen, B., 2010, Petrologic constraints on the development of a large-volume, high temperature,

silicic magma system: the Twin Falls eruptive centre, central Snake River Plain: Lithos, doi:10.1016/j.lithos.2010.09.008.

Ellis, Ben S., M. J. Branney, T. L. Barry, D. Barfod, I. Bindeman, J. A. Wolff, and B. Bonnichsen. 2012 "Geochemical Correlation of Three Large-volume Ignimbrites from the Yellowstone Hotspot Track, Idaho, USA." *Bulletin of Volcanology* 74.1: 261-77. Print.

Evans, S.H., Jr., and Brown, F.H., 1981, Summary of potassium-argon dating—1981: Contract report by Department of Geology and Geophysics, University of Utah, Salt Lake City, prepared for U.S. Department of Energy, Division of Geothermal Energy, Contract No. DE-AC08-80ID12079, 35 p.

Foster, D.A., Vogl, J.J., Mueller, P.A., Mogk, 1044 D.W., and Wooden, J.L., 2006, Proterozoic evolution of the western margin of the Wyoming craton: Implications for the tectonic and magmatic evolution of the northern Rocky Mountains: Canadian Journal of Earth Sciences, v. 43,

Fouch, M.J., 2012, The Yellowstone Hotspot: Plume or Not?: Geology, v. 40, doi:10.1130/focus052012.1.

Frost, R.B., Barnes, C.G., Collings, W.J., Arculus, R.J., Ellis, D.J. & Frost, C.D., 2001, A geochemical classification for granitic rocks. Journal of Petrology, v. 42, No. 11, p. 2033-2048

Hawkesworth, C. J. "Time Scales of Crystal Fractionation in Magma Chambers--Integrating Physical, Isotopic and Geochemical Perspectives." Journal of Petrology 41.7 (2000): 991-1006. Print.

Henry, Chris, Allen McGrew, Joseph Colgan, Arthur Snoke, and Matthew Brueseke, 2011, Timing, Distribution, Amount, and Style of Cenozoic Extension in the Northern Great Basin:GSA Field Guide 21.

Henry, Christopher D., 2008, "Ash-flow Tuffs and Paleovalleys in Northeastern Nevada: Implications for Eocene Paleogeography and Extension in the Sevier Hinterland, Northern Great Basin." *Geosphere* 4.1: 1-35.

Hibbard, M.J., 1981, The magma mixing origin of mantled feldspars. Contributions to Mineral Petrology, v. 76, p. 158-170.

Hughes, S.S., P.H. Wetmore, and J.L. Casper, 2002, Evolution of Quaternary tholeiitic basalt eruptive centers on the eastern Snake River Plain, Idaho, *in* Bill Bonnichsen, C.M. White, and Michael McCurry, eds., Tectonic and Magmatic Evolution of the Snake River Plain Volcanic Province: Idaho Geological Survey Bulletin 30.

Humphreys, Eugene, Erin Hessler, Kenneth Dueker, G. Lang Farmer, Eric Erslev, and Tanya Atwater., 2003, "How Laramide-Age Hydration of North American Lithosphere by the

Farallon Slab Controlled Subsequent Activity in the Western United States." *International Geology Review* 45: 575-95.

James, D.E., Fouch, M.J., Carlson, R.W., and Roth, J.W., 2011, Slab fragmentation, edge flow, and the origin of the Yellowstone hotspot track: Earth and Planetary Science Letters, v. 311, p. 124-135.

Johnson, C. M., 1991, Large-scale crust formation and lithosphere modification beneath middle to late Cenozoic calderas and volcanic fields, western North America, *J. Geophys. Res., 96*, 13485-13507

Le Bas, M.J., Le Maitre, R.W., Streckeisen, A. & Zanettin, B., 1986, Chemical classification of volcanic rocks based on total alkali-silica diagram, v. 27, No. 3, p. 745-750.

Leeman, W. P., and C. J. Vitaliano. "Petrology of McKinney Basalt, Snake River Plain, Idaho." Geological Society of America Bulletin 87.12 (1976): 1777. Print.

Leeman, William P. "Olivine Tholeiite Basalts of the Snake River Plain, Idaho." Cenozoic Geology of Idaho: Idaho Bureau of Mines and Geology Bulletin 26 (1982): 181-91.

Leeman, W.P., 1982, Rhyolites of the Snake River Plain-Yellowstone Plateau province, Idaho and Wyoming: A summary of petrogenetic models, in Bonnichsen, B. and Breckenridge, E.M., eds., Idaho Bureau of Mines and Geology Bulletin 26, p. 203-212.

Livaccari, Richard F., 1991, "Role of Crustal Thickening and Extensional Collapse in the Tectonic Evolution of the Sevier-Laramide Orogeny, Western United States." *Geology* 19.11: 1104. Print

Ludwig, K., 2012, User‟s manual for Isoplot 3.75: A geochronological tool kit for Microsoft excel, Berkley geochronology center, Special Publication No. 5.

Manley, C.R., 1996, In situ formation of welded tuff-like textures in the carapace of a voluminous silicic lava flow, Owyhee County, SW Idaho: Bulletin of Volcanology v. 57, 1143 p. 672-686.

Manley, C.R., and McIntosh, W.C., 2002, The Juniper Mountain volcanic center, Owyhee County, southwestern Idaho: Age relations and physical volcanology, *in* Bonnichsen, B., White, C.M., and McCurry, M. eds., Tectonic and magmatic evolution of the

Mertzman, S. A., 2000, K-Ar results from the southern Oregon - northern California Cascade Range. Oregon Geology, V. 62, no. 4, pp. 99-122.

McCurry, Mike, A.M. Watkins, J.L. Parker, Karen Wright, and S.S.Hughes, 1996, Preliminary volcanological constraints for sources of high-grade, rheomorphic ignimbrites of the Cassia Mountains: Implications for the evolution of the Twin Falls volcanic center: Northwest Geology, v. 26, p. 81-91.

McCurry M, Hughes SS (2002) Cassia Mountains, southern margin of eastern Snake River Plain, Idaho, unpublished data

McCurry, Michael, and David W. Rodgers, 2009, Mass Transfer along the Yellowstone Hotspot Track I: Petrologic Constraints on the Volume of Mantle-derived Magma: *Journal of Volcanology and Geothermal Research*.

McKee, Edwin H., and Andrew L. Tarshis., 1976, "Summary of Radiometric Ages of Tertiary Volcanic and Selected Plutonic Rocks in Nevada. Part V: Northeastern Nevada." *Isochron-west*: 15-27.

Miller, David M., John E. Repetski, and Anita G. Harris., 1991, "East-Trending Paleozoic Continental Magin near Wendover, Utah." Paleozoic Paleography o the Western United States I

Miller, David M., Donald L. Clark, Michael L. Wells, Charles G. Oviatt, Tracey J. Felger, and Victoria R. Todd., 2012, "Progress Report Geologic Map of the Grouse Creek 30' X 60' Quadrangle and Utah Part of the Jackpot 30' X 60' Quadrangle, Box Elder County, Utah, and Cassia County, Idaho (Year 3 of 4)." *USGS Open-File Report* : n. pag.

Morgan, Lisa A., David J. Doherty, and William P. Leeman., 1984, "Ignimbrites Of The Eastern Snake River Plain: Evidence For Major Caldera-Forming Eruptions." *Journal of Geophysical Research* 89.B10 8665-678.

Neal, Clive R., and Lawrence A. Taylor, 1989, "A Negative Ce Anomaly in a Peridotite Xenolith: Evidence for Crustal Recycling into the Mantle or Mantle Metasomatism?" Gochimica Et Cosmochimica Acta 53.5: 1035-040.

Patino Douce, A. E., 1997, Generation of metaluminous A-type granites by shallow melting of calc-alkaline granitioids, Geology, v. 25, no. 8, p. 743-746.

Perkins, M.E., Nash, W.P., Brown, F.H., and Fleck, R.J., 1995, Fallout tuffs of Trapper Creek, Idaho - A record of Miocene explosive volcanism in the Snake River Plain volcanic province: Geological Society of America Bulletin, v. 107, p. 1484–1506.

Pierce, K.L., and Morgan, L.A., 1992, The track of the Yellowstone hot spot: Volcanism, faulting, and uplift, *in* Link, P.K., Kuntz, M.A, Platt, L.B., eds., Regional Geology of Eastern Idaho and Western Wyoming: Geological Society of America Memoir 179, p. 1-8 53.

Robinson Roberts, Laura N., and Mark A. Kirschbaum., 1995, "Paleogeography of the Late Cretaceous of the Western Interior of Middle North America--- Coal Distribution and Sediment Accumulation." *U.S. Geological Survey Professional Paper 1561*

Rodgers, D.W., Ore, H.T., Bobo, R.T., McQuarrie, N, and Zentner, N, 2002, Extension and subsidence of the eastern Snake River Plain, Idaho, in Bill Bonnichsen, C.M. White, and Michael McCurry, eds., Tectonic and Magmatic Evolution of the Snake River Plain Volcanic Province: Idaho Geological Survey Bulletin 30, p. 121-155.

Rudnick, R.L. and Gao, S., 2003, Composition of the continental crust: Treatise on Geochemistry, chapter 3, p. 1-64.

Seaman, S.J., 2000, Crystal clusters, feldspar glomerocryst, and magma envelopes in the Atascosa lookout lava flow, Southern Arizona, USA: Recorders of magmatic events, Journal of Petrology, v. 41, No. 5, p. 693-716.

Sharp, Robert P. "The Miocene Humboldt Formation in Northeastern Nevada." *The Journal of Geology* 47.2 (1939): 133-60. Print.

Shervais, J. W., D. R. Schmitt, D. Nielson, J. P. Evans, E. H. Christiansen, L. Morgan, W. C. Pat Shanks, A. A. Prokopenko, T. Lachmar, L. M. Liberty, D. D. Blackwell, J. M. Glen, L. D. Champion, K. E. Potter, and J. A. Kessler. "First Results from HOTSPOT: The Snake River Plain Scientific Drilling Project, Idaho, U.S.A." Scientific Drilling 15 (2013): 36-45. Print.

Snoke, A, W,, K. A. Howard, A. J. McGrew, B. R. Burton, C. G. Barns, M. T. Peters, and J. E. Wright. "The Grand Tour of the Ruby-East Humboldt Metamorphic Core Complex, Northeastern Nevada." *Brigham Young Universtiy Geological Studies* 42 (1997): 225-69.

Steckler, Michael S., Nicola Piana Agostinetti, Charles K. Wilson, Pamela Roselli, Leonardo Seeber, Alessandro Amato, and Arthur Lerner-Lam., 2008, "Crustal Structure in the Southern Apennines from Teleseismic Receiver Functions." *Geology* 36.2: 155. Print.

Thompson, R.N., Morrison, M.A., Dickin, A.P., Hendry, G.L., 1983. Continental flood basalts…arachnids rule OK. In: Hawkesworth, C.J., Norry, M.J. (Eds.), Continental Basalts and Mantle Xenoliths: Shiva, pp. 158–185.

United States. National Park Service. "Nearby Attractions." *National Parks Service*. U.S. Department of the Interior, 27 Apr. 2014. Web. 01 May 2014.

Utah Geological Survey and Nevada Isotope Geochronology Laboratory, 2013, 40Ar/39Ar geochronology results for the Cotton Thomas Basin, Dairy Valley, Dry Canyon Mountain, Goshen, Judd Mountain, Peplin Flats, Pole Creek, and Toms Cabin Spring quadrangles, Utah: Utah Geological Survey Open-File Report 614, variously paginated, also available online, <http://geology.utah.gov/online/ofr/ofr-614.pdf>.

Wallace, Alan R., Michael E. Perkins, and Robert J. Fleck., 2008, "Late Cenozoic Paleogeographic Evolution of Northeastern Nevada: Evidence from the Sedimentary Basins." *Geoshpere* 4.1: 36-74. Print.

Wiliams, P.L., Mytton, J.W., and Morgan, W.A., 1999, Geologic map of the Stricker 3 quadrangle, Idaho and Nevada: U.S. Geologicl Survey, Geolgical Investigations Series Map I-2633, scale 1:48,000

Whalen J.B., Currie, K.L. & Chappell, B.W., 1987, A-type granites: geochemical characteristics, discrimination and petrogenesis. Contributions to Mineralogy and Petrology, v. 95, p. 407-419.

Wright, James E., and Arthur W. Snoke. "Tertiary Magmatism and Mylonitization in the Ruby-East Humboldt Metamorphic Core Complex, Northeastern Nevada: U-Pb Geochronology and Sr, Nd, and Pb Isotope Geochemistry." *Geological Society of America Bulletin* 105.7 (1993): 935-52.

Wright KE, McCurry M, Hughes SS, 2002, Petrology and geochemistry of the Miocene tuff of McMullen Creek, central Snake River Plain. In: Bonnichsen B, McCurry M, White CM (eds) Tectonic and magmatic evolution of the Snake River Plain volcanic province. Idaho Geol Surv Bull 30:177–194

Appendix A-Sample Location and Description

Samples are listed in the order they were collected. Northing and Easting correspond to UTM Zone 11T (unless specified otherwise) and NAD 27 CONUS.. Sample locations, descriptions, petrographic descriptions (minerals are listed in order of decreasing abundances) and selected samples for point counting are listed for all collected samples relevant to the Jarbidge Rhyolite.

Sample ID: JC-09-22 **Map Type:** Tjr

Northing: 4548547 **Easting:** 0666387

Description: Phyric lithoidal rhyolite outcrop below crest of hills. Phyric phases are medium grained and include rounded, corroded smoky quartz, sanidine, altered plagioclase and oxidized mafics. In thin section the sample is holocrystalline with a devitrified groundmass. Phenocryst phases include anhedral skeletal sanidine with plagioclase inclusions; anhedral, embayed quartz; an-subhedral, boxy plagioclase; anhedral altered mafics; anhedral, fractured garnets; and subhedral oxides (magnetite and ilmenite). Groundmass phases include: euhedral oxides (magnetite and ilmenite); subhedral zircon; and euhedral apatite.

Mode: Crystallinity (36.1), sanidine (89), quartz (125), plagioclase (31), pyroxenes (1), garnets (1), oxides (6), groundmass (GM)(448).

^{40}Ar/^{39}Ar Dating: 15.249±0.040 Ma

Sample ID: MB11-1 **Map Type:Tr_3**

Northing: 718284 Easting: 4622241

Description: Phyric lithoidal rhyolite outcrop at Rock Spring, Nevada. Phyric phases are fine-medium grained and include quartz, sanidine. In thin section the sample is holocrystalline with a devitrified groundmass. Phenocryst phases include anhedral-subhedral spongy sanidine; euhedral to anhedral embayed and fractured quartz; euhedral to subhedral intergrown plagioclase, mymerkite texture; anhedral oxides (magnetite); and subhedral zircon as inclusions. Groundmass phases include sanidine and oxides.

Mode: Crystallinity (20%), sanidine (15), quartz (110), plagioclase (22), Garnet (2), groundmass (GM) (604).

^{40}Ar/^{39}Ar Dating: 13.561±0.031 Ma

Sample ID: MB11-2 **Map Type:** Tjr

Northing: 722175 Easting: 4630359

Description: Phyric lithoidal rhyolite outcrop. Phyric phases are medium grained and include rounded, corroded smoky quartz, sanidine, altered plagioclase, and oxidized mafics. In thin section the sample is holocrystalline with a devitrified groundmass. Phenocryst phases include subhedral patchy, spongy, and fractured sanidine with plagioclase inclusions; anhedral to subhedral patchy, spongy plagioclase; euhedral to subhedral embayed quartz; anhedral to euhedral highly altered orthopyroxene; euhedral to subhedral fractured garnet with inclusions. Groundmass phases include subhedral to anhedral sanidine; subhedral quartz; hydrothermally altered chalcedony; anhedral oxides.

Mode: Crystallinity (32%), sanidine (23), quartz (165), plagioclase (65), pyroxenes (9), oxide (2), groundmass (GM) (549).

Sample ID: MB11-3 **Map Type:** Tb

Northing: 723145 Easting: 4632840

Description:

In thin section the sample is holocrystalline with crystalline groundmass. Phenocryst include: two populations of plagioclase. The largest population is euhedral to subhedral contained in glomeroporphyritic cluster, euhedral to anhedral olivine fractured, subhedral orthopyroxene, and the groundmass population is sub-euhedral plagioclase, subhedral pyroxenes and oxides (magnetite).

Sample ID: AI12-1 **Map Type:** Tb

Northing: 0731940 **Easting:** 4640513

Description: Basaltic unit consisting of two layers: an upper oxidized and vesiculated layer and a lower, unaltered layer. In thin section the sample is

holocrystalline with crystalline groundmass. Phenocryst include: two populations of plagioclase by size fraction. The largest population is euhedral to subhedral zoned, and contained in glomeroporphyritic cluster, euhedral to anhedral olivine fractured, embayed, altered, subhedral to anhedral intergrown orthopyroxene, highly altered clinopyroxene into ilmenite and the groundmass population is sub-euhedral plagioclase, subhedral olivine, subhedral pyroxenes ,and oxides (magnetite).

Sample ID: AI12-3 **Map Type:** Tts

Northing: 0732560 **Easting:** 4643844

Description: A moderately welded ash-flow that has a fine groundmass. It contains obsidian shards. In thin section the sample is hypocrystalline with a glassy groundmass. Phenocryst phases include anhedral to subhedral skeletal, embayed, altered plagioclase; subhedral to anhedral zoned sanidine; anhedral embayed quartz; Anhedral zircons occur as inclusions.

Sample ID: AI12-4 **Map Type:** Tts

Northing: 07333533 **Easting:** 4643511

Description: A moderately welded ash-flow that has a fine groundmass. It contains obsidian shards. In thin section the sample is hypocrystalline with a glassy groundmass. Phenocryst phases include anhedral to subhedral embayed, altered plagioclase; subhedral to anhedral zoned, skeletal, clotting sanidine; anhedral-subhedral embayed quartz; anhedral magnetite. Anhedral-subhedral zircons occur as inclusions.

Sample ID: AI12-5 **Map Type:** Tts

Zone: 12T **Northing:** 0266346 **Easting:** 4675264

Description: A highly welded ash-flow that has a fine groundmass. It appears in massive blocky flows with laminations. In thin section the sample is hypocrystalline with a glassy groundmass. Phenocryst phases include anhedral to subhedral plagioclase; subhedral to anhedral zoned sanidine with inclusions; anhedral-subhedral quartz;

anhedral to subhedral zoned, fractured, rimming, lamellae clinopyroxene; altered subhedral orthopyroxene; subhedral zircon.

Sample ID: AI12-6 **Map Type:** Tjr

Northing: 0744556 **Easting:** 4514225

Description: Phyric lithoidal rhyolite outcrop outside of West Wendover, NV. Phyric phases are medium grained and include rounded, corroded smoky quartz, sanidine, altered plagioclase and highly oxidized mafics. In thin section the sample is holocrystalline with a devitrified groundmass. Phenocryst phases include anhedral to subhedral sieve, embayment, and fractured sanidine with plagioclase inclusions; anhedral to subhedral, embayed quartz; an-subhedral, skeletal plagioclase; anhedral altered Clinopyroxne; Euhedral zircon contained in inclusion. Groundmass phases include: euhedral oxides (magnetite); euhedral zircon; and euhedral apatite.

Mode: Crystallinity (31%), sanidine (57), quartz (130), plagioclase (15), pyroxenes (2), groundmass (GM)(448).

^{40}Ar/^{39}Ar Dating: 13.686±0.034 Ma

Sample ID: AI13-1 **Map Type:** Tts

Northing: 0717981 **Easting:** 4621998

Description: A highly welded ash-flow that has a fine groundmass. In thin section the sample is hypocrystalline with a glassy groundmass. Phenocryst phases include anhedral to subhedral skeletal, sieve altered plagioclase; subhedral spongy, embayment sanidine with inclusions; anhedral to subhedral embayed quartz; subhedral orthopyroxene; anhedral biotite.

Sample ID: AI13-2 **Map Type:** Tjr

Northing: 0722885 **Easting:** 4627038

Description: Phyric lithoidal rhyolite outcrop outside of. Phyric phases are medium grained and include rounded, corroded smoky quartz, sanidine, and altered plagioclase. In thin section the sample is holocrystalline with a devitrified

groundmass. Phenocryst phases include subhedral fractured and zoned sanidine with plagioclase inclusions; anhedral to subhedral, embayed, parallel fractured (filled with oxides and zircon) quartz; an-subhedral, sieve, clotting plagioclase; anhedral altered (septo-altermorph) clinopyroxne; Euhedral zircon contained in inclusion. Groundmass phases include: euhedral oxides (magnetite); euhedral zircon; and euhedral apatite.

Mode: Crystallinity (35%), sanidine (81), quartz (144), plagioclase (55), pyroxenes (2), groundmass (GM) (519).

Sample ID: AI13-3 **Map Type:** Tjr

Northing: 0722528 **Easting:** 4627231

Description: Phyric vitrophyric rhyolite outcrop outside of. Phyric phases are medium grained and include rounded, corroded smoky quartz, sanidine, and altered plagioclase. In thin section the sample is hypocrystalline with a glassy groundmass. Phenocryst phases include subhedral, clotting and fractured sanidine; euhedral, embayed quartz; subhedral, sieve, clotting skeletal plagioclase; anhedral-subhedral altered clinopyroxne; Euhedral zircon contained in inclusion.

Mode: Crystallinity (41%), sanidine (36), quartz (167), plagioclase (85), pyroxenes (21), groundmass (GM) (441).

Sample ID: AI13-4 **Map Type:** Tjr

Northing: 0727364 **Easting:** 4633146

Description: Phyric lithoidal rhyolite outcrop outside. Phyric phases are medium grained and include rounded, corroded smoky quartz, sanidine, and altered plagioclase. In thin section the sample is holocrystalline with a devitrified groundmass. Phenocryst phases include anhedral to euhedral parallel fracturing sanidine; subhedral, fractured and embayed quartz; subhedral, skeletal and clotting plagioclase; anhedral altered orthopyroxene; Euhedral zircon contained in inclusion. Groundmass phases include: euhedral oxides (magnetite); euhedral zircon; and euhedral apatite.

Mode: Crystallinity (32%), sanidine (21), quartz (120), plagioclase (11), pyroxnes (3),

oxides(5), groundmass (GM) (343).

Sample ID: AI13-5 **Map Type:** Tts

Northing: 0732212 **Easting:** 4644091

Description: A moderately welded vitrophyric ash-flow that has a fine groundmass. In thin section the sample is hypocrystalline with a glassy groundmass In thin section the sample is hypocrystalline with a glassy groundmass. Phenocryst phases include subhedral skeletal plagioclase; euhedral sanidine with inclusions; anhedral embayed quartz; euhedral to anhedral altered clinopyroxene with some carlsbad twinning. Subhedral zircon occurs as inclusions.

Appendix B - Geochemistry

The following data are presented as raw data. The symbol "-" indicates that element was not analyzed for the sample.

Major Element Results (wt. %)

Samples	JC-09-22	MB11-1	MB11-2	MB11-3	AI12-1	AI12-3	AI12-4
SiO_2	76.98	76.01	77.85	43.40	41.96	72.14	72.48
TiO2	0.37	0.07	0.25	4.37	4.28	0.38	0.38
Al2O3	11.92	12.42	9.09	13.20	12.74	12.01	11.98
Fe2O3	0.77	1.48	2.82	22.17	21.10	2.25	2.35
FeO	0.60	-	-	-	-	-	-
MnO	0.01	0.02	0.04	0.28	0.31	0.04	0.05
MgO	0.06	0.05	0.04	5.54	5.08	0.24	0.24
CaO	0.96	0.43	0.85	9.17	9.47	0.93	0.98
Na2O	2.82	3.42	2.02	2.81	2.71	1.65	1.75
K2O	5.05	5.07	3.84	0.62	0.45	6.16	6.41
P2O5	0.08	0.03	0.06	0.91	0.88	0.06	0.09
Total	100.00	98.99	96.84	102.46	98.98	95.86	96.71
LOI	0.33	0.64	2.72	-0.63	2.21	4.45	3.61

Samples	AI12-5	AI12-6	AI13-1	AI13-2	AI13-3	AI13-4	AI13-5
SiO_2	74.27	77.00	75.28	75.85	74.01	75.38	71.53
TiO2	0.42	0.14	0.27	0.33	0.30	0.31	0.36
Al2O3	12.15	11.17	11.83	12.73	11.85	11.73	11.96
Fe2O3	3.07	1.51	2.49	1.14	3.13	3.32	2.70
FeO	-	-	-	-	-	-	-
MnO	0.05	0.02	0.02	0.02	0.05	0.05	0.04
MgO	0.19	0.15	0.17	0.34	0.09	0.05	0.16
CaO	0.82	1.25	0.65	1.11	1.40	1.11	1.23
Na2O	3.09	2.64	2.95	2.88	2.49	2.73	1.91
K2O	5.05	4.99	5.22	5.05	5.11	4.80	6.25
P2O5	0.07	0.05	0.05	0.08	0.07	0.07	0.06
Total	99.18	98.92	98.93	99.53	98.50	99.55	96.20
LOI	0.90	1.11	1.30	0.48	1.86	0.27	3.55

Trace Element Results (ppm)

Samples	JC-09-22	MB11-1	MB11-2	MB11-3	AI12-1	AI12-3	AI12-4
Ba	1798	48	1143	647	306	1178	1174
Co	-	-	-	-	66	2	<1

Cr	4	3	3	8	76	1	4
Cu	4	3	2	53	8	7	10
Ga	21.9	27.0	15.0	27.0	20.4	20.8	20.3
Nb	19	47.1	21.0	28.4	28.0	55.7	54.0
Ni	-	3	2	46	35	3	4
Pb	-	65	26	5	<1	24	34
Rb	155	387	115	9	3.9	170	166
Sr	131	13	110	226	255	69	68
Sc	4.1	2.0	2.0	37.0	36.0	1.0	1.0
V	3	2	13	399	420	28	36
Y	31	82	42	67	48.1	63.6	63.1
Zn	74	45	59	213	181	64	62
Zr	441	143	33	272	269	580	558
U	-	14	10	<1	0.5	6.6	4.3
Ta	-	7	62	50	6.6	37	35.4
La	-	3	83	40	12	83	84
Ce	-	74	139	8	10	20	199
Nd	-	35	6	5	-	-	-

Samples	AI12-5	AI12-6	AI13-1	AI13-2	AI13-3	AI13-4	AI13-5
Ba	1179	477	945	1542	1329	1294	1293
Co	4	<1	2	<1	3	3	2
Cr	1	<1	2	8	5	4	3
Cu	10	4	10	5	10	8	5
Ga	21.1	20.9	23.1	22.9	21.0	20.8	20.7
Nb	56.2	27.1	50.4	31.9	30.0	29.7	48.0
Ni	2	2	3	3	4	2	3
Pb	21	45	30	41	27	35	21
Rb	170.5	244.9	187.2	169.6	153.3	145.2	186.0
Sr	73	69	55	152	131	128	63
Sc	1	1	1	1	1	1	1
V	36	24	29	30	32	24	35
Y	64.8	41.5	71.6	36.4	45.8	42.1	56.8
Zn	65	77	81	72	81	81	63
Zr	589	239	477	486	456	462	531
U	3.8	4.4	5.2	5.3	3.7	3.7	7.2
Ta	31.3	58.	42.4	34.3	34.9	32.7	34.4
La	85	97	90	85	90	90	78
Ce	203	207	198	273	235	224	211
Nd	-	-	-	-	-	-	-

Appendix C – Precision and Accuracy

A measure of the total analytical precision for XRF analysis performed June, 2011.

Each analysis listed below is a separate aliquot taken from a singular sample (F30) and prepared independently by Karen Mertzman at Franklin and Mertzman College, following the methods of Mertzman (2000). These 10 analyses represent all the errors that could accrue from weighing, mixing, preparation of the fusion glass disk and trace element briquette, and the actual peak and background measurements made by the PW2404 Panalytical, Inc. XRF vacuum spectrometer.

Speciman	F30/1	F30/2	F30/3	F30/4	F30/5	F30/6	F30/7	F30/8	F30/9	F30/10
SiO2	48.78	48.81	48.79	48.71	48.69	48.76	48.74	48.70	48.70	48.74
TiO2	2.40	2.40	2.40	2.40	2.40	2.40	2.40	2.40	2.40	2.40
Al2O3	12.92	12.96	12.94	12.91	12.90	12.91	12.93	12.93	12.92	12.93
Fe2O3T	13.32	13.30	13.31	13.30	13.29	13.30	13.29	13.30	13.29	13.29
MnO	0.178	0.176	0.177	0.176	0.176	0.176	0.176	0.176	0.177	0.177
MgO	10.350	10.372	10.351	10.355	10.364	10.370	10.376	10.358	10.364	10.356
CaO	9.693	9.682	9.670	9.681	9.684	9.683	9.681	9.679	9.689	9.679
Na2O	1.901	1.895	1.895	1.890	1.904	1.898	1.894	1.900	1.899	1.894
K2O	0.386	0.389	0.389	0.387	0.386	0.388	0.389	0.388	0.388	0.388
P2O5	0.264	0.266	0.269	0.265	0.264	0.264	0.265	0.266	0.266	0.264
Total	100.192	100.250	100.191	100.074	100.058	100.149	100.141	100.097	100.093	100.118
Rb	6.2	6.0	5.9	6.5	6.0	5.9	6.2	6.2	6.0	6.3
Sr	297	296	297	299	295	295	298	293	296	301
Y	27.2	27.4	28.0	27.3	27.8	28.1	27.4	27.9	27.7	27.9
Zr	135	136	134	135	134	135	134	134	134	135

V	307	310	307	313	314	310	315	304	303	317
Ni	243	245	243	243	243	243	246	245	245	245
Cr	633	671	650	669	635	638	657	665	648	647
Nb	10.8	11.2	11.8	12.2	11.7	11.2	11.6	11.3	11.3	11.7
Ga	16.2	16.3	16.5	16.5	16.4	16.6	16.5	16.4	16.6	16.5
Cu	133	132	133	133	132	132	132	133	134	133
Zn	106	106	105	105	105	106	106	106	107	106
Co	57	58	57	58	57	58	59	59	57	59
Ba	89	101	96	109	76	89	81	91	86	88
La	14	14	15	16	16	15	15	16	15	16
Ce	29	31	30	27	32	29	30	31	30	31
U	<0.5	0.9	1.1	1.7	<0.5	0.5	0.7	2.0	0.7	<0.5
Th	3.0	<0.5	2.2	<0.5	1.8	2.0	0.9	1.4	2.6	1.5
Sc	34	33	33	34	34	33	34	33	33	33
Pb	<1	<1	<1	<1	2	3	1	2	1	<1

A measure of the accuracy of the current XRF major and trace element calibration being utilized in F&M College X-ray laboratory using geochemical standard BHVO-2 performed June, 2011.

A singular glass fusion disk for the major elements and a singular sample powder / copolywax briquette were each analyzed 10 times and compiled in the table below. Also listed is the geochemical analysis of BHVO-2 that can be currently found at the USGS web site.

Specimen	BHVO-2	BHVO-2	BHVO-2	BHVO-2	BHVO-2	BHVO-2	BHVO-2	BHVO-2	BHVO-2	BHVO-2	BHVO-2 Accepted
SiO2	49.94	50.02	49.97	49.94	49.83	49.95	50.00	49.92	49.97	49.95	49.90
TiO2	2.72	2.73	2.73	2.72	2.72	2.73	2.73	2.73	2.73	2.72	2.73
Al2O3	13.63	13.66	13.66	13.65	13.61	13.62	13.65	13.62	13.64	13.66	13.50
Fe2O3T	12.43	12.45	12.41	12.42	12.40	12.43	12.42	12.42	12.43	12.43	12.30

MnO	0.165	0.165	0.165	0.165	0.165	0.165	0.164	0.166	0.165	0.165	0.165
MgO	7.299	7.292	7.285	7.294	7.291	7.309	7.304	7.290	7.289	7.290	7.230
CaO	11.473	11.482	11.485	11.490	11.473	11.505	11.491	11.486	11.488	11.479	11.400
Na2O	2.196	2.190	2.197	2.200	2.202	2.191	2.190	2.199	2.192	2.197	2.220
K2O	0.505	0.507	0.507	0.505	0.504	0.504	0.505	0.507	0.508	0.507	0.520
P2O5	0.265	0.267	0.267	0.266	0.267	0.266	0.266	0.268	0.268	0.266	0.270
Total	100.623	100.763	100.676	100.650	100.462	100.670	100.720	100.606	100.680	100.664	100.235
Rb	8.3	7.8	7.5	7.2	7.3	8.5	7.8	8.1	8.6	7.9	7.9
Sr	371	380	384	380	380	380	379	378	383	385	385
Y	26.0	25.9	25.9	25.6	25.7	25.4	26.1	25.3	25.5	25.2	25.2
Zr	167	169	165	170	166	164	167	168	164	168	168
V	327	331	328	328	323	325	324	326	324	327	327
Ni	122	122	123	122	122	122	123	121	121	123	123
Cr	312	327	310	319	312	322	331	342	324	314	314
Nb	16.5	17.6	16.8	17.0	17.9	17.0	16.5	16.8	17.2	16.9	16.9
Ga	17.8	17.7	18.1	18.1	17.7	17.8	17.8	17.9	17.9	17.9	17.9
Cu	128	126	130	128	130	127	128	120	121	122	122
Zn	91	92	91	92	92	92	92	91	91	91	91
Co	45	45	47	46	44	48	45	46	45	45	45
Ba	121	112	124	111	118	115	104	128	120	107	107
La	15	13	15	17	17	16	15	16	17	17	17
Ce	29	29	29	31	29	28	28	29	30	30	30
U	1.1	0.8	1.1	1.7	1.5	0.5	1.5	1.9	2.0	0.8	0.8
Th	<0.5	<0.5	1.3	<0.5	1.4	0.5	<0.5	<0.5	<0.5	1.8	1.8
Sc	34	34	35	34	33	33	34	33	33	34	34
Pb	1	1	1	<1	<1	2	1	1	2	1	1